A Comprehensive Numerical Study of the Effects of Adjacent Buildings on Near-Field Pollutant Dispersion

Mauricio Chávez Yáñez

A Thesis
In the Department
of
Building, Civil and Environmental Engineering

Presented in Partial Fulfillment of the Requirements
For the Degree of
Doctor of Philosophy (Building Engineering) at
Concordia University
Montreal, Quebec, Canada

August 2014

CONCORDIA UNIVERSITY

School of Graduate Studies

This is to certify that the thesis prepared

By: **Mauricio Chavez Yañez**

Entitled: **A Comprehensive Numerical Study of the Effects of Adjacent Buildings on Near-Field Pollutant Dispersion**

and submitted in partial fulfillment of the requirements for the degree of

Doctor of Philosophy (Building Engineering)

complies with the regulations of the University and meets the accepted standards with respect to originality and quality.
Signed by the final examining committee:

Dr. G. Gouw	Chair
Dr. Robert N. Meroney	External Examiner
Dr. M. Paraschivoiu	External to Program
Dr. R. Zmeureanu	Examiner
Dr. S. Li	Examiner
Dr. T. Stathopoulos	Thesis Co-Supervisor
Dr. Ali Bahloul	Thesis Co-Supervisor

Approved by _____
Dr. F. Haghighat, Graduate Program Director

September 5, 2014

_____
Dr. A. Asif, Dean
Faculty of Engineering and Computer Science

ABSTRACT

A Comprehensive Numerical Study of the Effects of Adjacent Buildings on Near-Field Pollutant Dispersion

Mauricio Chávez Yáñez

Concordia University, 2014

Air pollution is a major concern in industrialized countries. In dense urban areas, the most common sources of pollutants are the exhaust stacks, ventilators, and cooling towers located on top of buildings. Depending on wind characteristics and flow re-circulations induced by adjacent buildings, effluents can be transported toward fresh air intakes and contaminate indoor air causing health problem to the buildings' occupants. This particular urban pollution case is known as re-entrainment of pollutants. Unfortunately, the available dispersion models are not adapted to analyse such problems, since they were developed for an isolated building configuration. The present research aims to investigate pollutant aerodynamics and re-entrainment potential for non-isolated building configurations using Computational Fluid Dynamics (CFD) techniques.

To do so, the steady Reynolds-Averaged Navier-Stokes (RANS) approach was evaluated and compared with wind tunnel data and ASHRAE-2011 dispersion model results. The best numerical model possible was defined by performing a sensitivity analysis on the effect of meshing, turbulence model, convergence criteria and turbulent Schmidt number (Sc_t). For passive scalar transport, it was observed that RANS underestimates dilution when using the standard $Sc_t = 0.7$, perhaps due to the inherent incapacity of RANS in reproducing unsteadiness of flow. However, a sensitivity analysis showed that a better agreement is obtained with $Sc_t = 0.3$, which is within the range of values suggested in the literature.

Furthermore, a comparative performance evaluation of steady and unsteady approaches was carried out. Three unsteady modelling techniques were compared: unsteady Reynolds-Averaged Navier-Stokes (URANS), Detached Eddy Simulation (DES) and Large Eddy Simulation

(LES). The flow pattern within the wake of a two-building configuration was evaluated and dispersion of pollutants compared against wind tunnel data. The influence of meshing size, time step and inlet boundary conditions was discussed. URANS using the Realizable k-ε model, fails to reproduce unsteadiness, and dilution values converge to the same RANS results but DES captures well the unsteadiness of the flow. LES dilution predictions are not satisfactory in all locations, perhaps because the mesh used was not sufficiently refined near the walls. It was concluded that under these specified computing conditions, DES showed results closer to experimental data than all other approaches considered.

Finally, RANS was selected to perform a series of simulations for three non-isolated building configurations: a building located upstream of an emitting building, a building located downstream of an emitting building and an emitting building between two tall buildings. After performing a parametric analysis of geometric characteristics of adjacent buildings, a guideline for safe placement of intakes on buildings façades was proposed.

In line with the previous results, this thesis provides three relevant contributions. First, in terms of numerical simulation, the thesis contributes with insights concerning computational simulation for pollutant dispersion in urban areas. Second, additional information in terms of normalized dilution values, contours and streamlines for different building configurations (isolated and non-isolated) is given in order to better comprehend the pollutant dispersion in the urban environment. Third, the thesis offers a guideline with practical recommendations regarding safe placement of intakes to avoid pollutants re-ingestion. These results are also a source of data to code and standard writing bodies.

ACKNOWLEDGEMENTS

I would like to thank my supervisor, Dr. Stathopoulos, for his guidance and valuable support through all my PhD work. Dr. Stathopoulos has been a truly dedicated advisor and inspiring teacher.

I also thank Dr. Ali Bahloul for his supervision, permanent encouragement and support.

This work would not have been possible without the IRSST financial and technical support.

I would like to thank all the members of the evaluation committee; Dr. Li, Dr. Zmeureanu and Dr. Paraschivoiu who agreed to be part of this process. I would also like to dedicate a special acknowledgement to Dr. Meroney who kindly agreed to serve as external evaluator for this dissertation. I am extremely honoured. Your work and trajectory have been a precious source of inspiration for my research.

To my colleagues; Neetha, Eleni, Dimitris, Daniel, Bodhi, Ayman, Stratos, Hatem, many, many thanks to everyone for all those wonderful moments in the lab. A special thanks goes to Mohamed; thanks, my friend for all those rich discussions.

Thanks to my parents, Viola and Tomas, for their love. Thanks to Cami, Edu, Carmen Gloria, Luis and Anne for your permanent encouragement.

My infinite acknowledgement to my wife, Consuelo, my light, and to my children, Paloma, Manuel and Emilio. Thank you for your love ….all this is for you!

.

TABLE OF CONTENTS

LIST OF TABLES

LIST OF FIGURES

LIST OF NOMENCLATURE

Symbol	Definition	Units
Ce	Exhaust concentration	ppm
Cr	Receptor concentration	ppm
Dr	Dilution at roof level (Ce/Cr)	
D_N	Normalised dilution	
D_t	Turbulent mass diffusivity	m^2/s
H	Building height	m
H_b	Height of the emitting building b1	m
W_b	Width of the emitting building b1	m
L_b	Length of the emitting building b1	m
$TI_{u/v/w}(y)$	Turbulence intensity in x, y, z, direction at given y (m)	
k	Turbulent kinetic energy	m^2/s^2
k_s	Roughness height	m
K	Non-dimensional concentration	
M	Exhaust momentum ratio (V_e/ U_H)	
Q_e	Volumetric flow rate	m^3/s
Re	Reynolds number	
Re_b	Building Reynolds number	
Re_s	Stack Reynolds number	
Sc_t	Turbulent Schmidt number	
t	time	s
U,V,W	velocity vector in x, y, z, direction	m/s
x	streamwise coordinate	m

y	vertical coordinate	m
Y^+	Dimensionless wall distance	
z	lateral coordinate	m
z_o	Aerodynamic roughness length	m

Greek symbols	**Definition**	**Units**
α	Power law exponent	
ε	Turbulent dissipation rate	m^2/s^3
κ	von Karman constant	
ν_t	Turbulent viscosity	m^2/s
ρ_e	Density of exhaust	kg/m^3
ρ_a	Density of air	kg/m^3

Abbreviations

ABL	Atmospheric boundary layer
ADMS	Atmospheric Dispersion Modelling System
ASHRAE	American Society of Heating Refrigeration and Air conditioning Engineers
CFD	Computational Fluid Dynamics
DES	Detached Eddy Simulation
GC	Gas Chromatograph
GCI	Grid Convergence Index
LES	Large Eddy Simulation
RANS	Reynolds-Averaged Navier-Stokes
RLZ	Realizable k-ε

RNG	Renormalized Group k-ε
RSM	Reynolds Stress-Model
SGS	Subgrid scale
SKE	Standard k-ε
URANS	Unsteady Reynolds-Averaged Navier-Stokes

1. INTRODUCTION

1.1 Motivation

There is an increasing concern about the health hazards posed to urban occupants exposed to inhalation of fine and ultrafine particles, including microorganisms, dust and nano-technological products. Inhaling these particles causes an occupational hazard due to the elevated amount emitted to the atmosphere and working environment by vehicular traffic, industries, laboratories, hospitals and central cooling systems. The permanent growth of industrialized cities has led government organizations and scientists to engage into preventive and remedial initiatives to eliminate or reduce negative effects on people's health of this so-called urban air pollution.

The transport of pollutants within the built environment is influenced by many complex factors. Among others, the most relevant factors affecting pollutant dispersion are the wind conditions and the urban morphology (Britter and Hanna, 2003). The former refers to the wind speed and turbulence intensity. The higher the wind speed, the greater the mixture between fresh air and pollutants, and the lower the concentration of pollutants (or higher the dilution) that is detected in the wind stream. In turn, complex urban morphology enhances vortical structures in the wake of buildings (Panagioutou et al. 2013).

Indeed, these recirculation zones tend to trap pollutants increasing local concentration, which may be very critical if the building fresh air intakes are located in these contaminated zones increasing the possibility of having ingestion of pollutants. The phenomenon is categorized as small-scale urban pollution and is known as: exhaust re-entrainment, re-ingestion of pollutant or cross-contamination (Petersen et al. 2002). Figure 1-1 shows an example of this pollutant ingestion mechanism for a two-building configuration reproduced in a wind tunnel.

This urban pollution phenomenon is an episodic event, which means it occurs randomly when certain conditions, in particular wind direction, urban morphology and the relative source location are met. However, the state of art has not been sufficiently advanced to allow building engineers to apply appropriate design criteria to avoid such problems for new construction or help alleviate it for existing buildings. Thus, limited information and recommendations are available in the literature (Snyder, 1981, Schulman et al. 1993, Saathoff et al. 2009, Stathopoulos et al. 2004, 2008). To limit air indoor contamination caused by the ingestion of outdoor pollutants, a better

understanding of pollutant aerodynamics is needed. In this sense, this thesis aims at investigating the applicability of computational fluid dynamics to pollutant dispersion for complex building configuration.

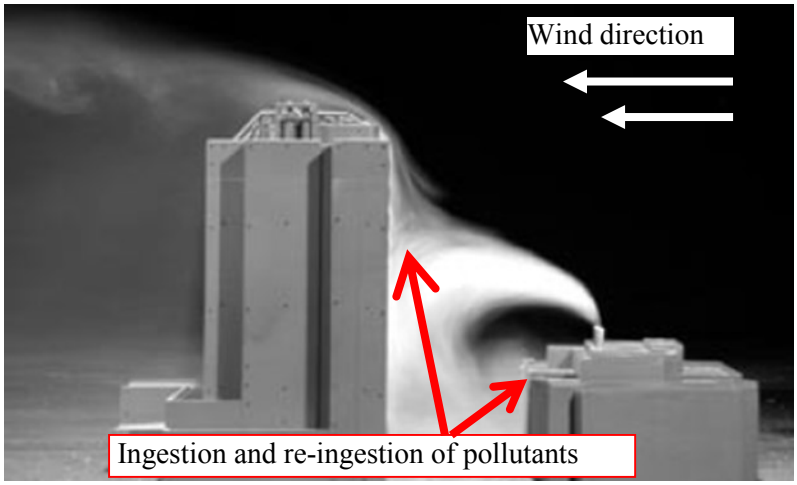

Figure 1-1. Recirculation zone in the wake of a building (from: http://www.epa.gov/lab21gov/pdf/bp_modeling_508.pdf)

Computational Fluids Dynamics (CFD) is a useful technique for dispersion simulations since it provides detailed information of flow patterns and concentration fields by solving the flow equations over the entire computational domain. Even though CFD is largely used for research, it needs to be treated with care since it can be a source of significant errors conditioning the suitability of simulation results. The current thesis includes a comprehensive review of most relevant computational parameters in order to ensure reliability of the results. It puts in perspective the advantages and the disadvantages of using CFD for parametric studies on pollutant dispersion in urban areas. The following section describes in detail the objectives of the thesis.

1.2 Objectives

The main objective of this thesis is to establish a reliable method to study the effect of adjacent buildings on the near-field dispersion of effluents using the Computational Fluid Dynamics (CFD) approach. It should be noted that the "near-field" concept used in this study

involves the fluid mechanical interaction between two or three consecutive buildings corresponding to a small-scale of urban pollution problem.

The specific objectives are as follows:

- To improve the accuracy and reliability of steady CFD simulations to predict pollutant dispersion in urban areas. To this end, systematic comparisons with wind tunnel data were carried out. The comparisons allowed the identification of the necessary parameters and conditions that needed to be adjusted for the successful evaluation of CFD to resolve dispersion problems.
- To evaluate the applicability of unsteady approaches under an engineering perspective. This means considering reasonable meshing and time step size to optimise computing time and accuracy.
- To conduct a parametric study of dispersion for different building configurations focusing on the effect of adjacent buildings. The goal is to identify the dominant parameters affecting dispersion of pollutants in the vicinity of an emitting building. Three cases of non-isolated building configuration were examined:
    i. Buildings of different geometries placed upstream of the source;
    ii. Buildings of different geometries placed downstream of the source;
    iii. One building placed upstream and another building placed downstream of the source
- To produce a guideline for safe placement of intakes on buildings façades for small urban layout composed by two or three buildings.

1.3 Outline of the thesis

Following the introduction in the current Chapter, a detailed literature review is presented in Chapter 2, describing previous studies carried out in the area of near-field plume dispersion using CFD. Chapter 3 describes the experimental methodology. Chapter 4 describe the computational methodology. In Chapter 5 comparisons with tunnel measurements are made in

order to validate the numerical methodology. In Chapter 6 unsteady approaches are evaluated. In Chapter 7 an extensive parametric study is conducted, and a guideline to avoid re-ingestion is produced. Finally, summary, conclusions and recommendations for future work are presented in Chapter 8, followed by a list of references and appendices. The following figure displays the outline of the thesis, Figure 1-2.

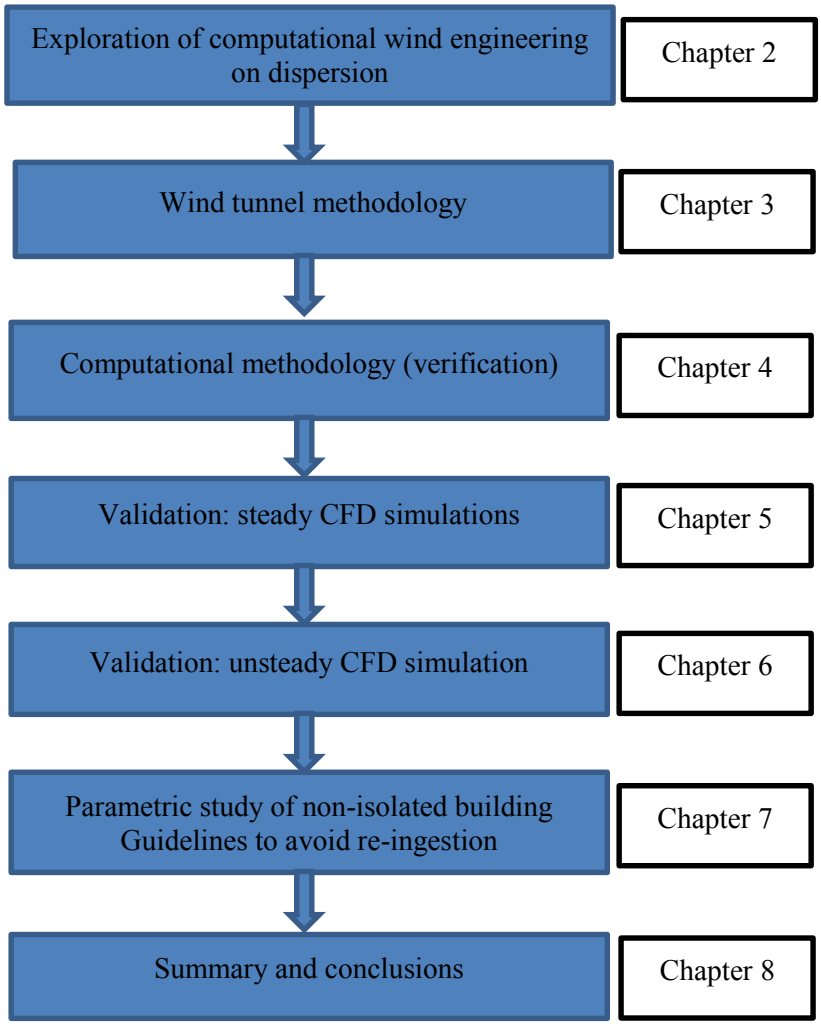

Figure 1-2. Outline of the thesis

2. LITERATURE REVIEW

2.1 General

The accurate prediction of pollutant dispersion in urban areas requires the understanding of urban aerodynamics. The extreme complexity of air flow in the city is conditioned by local geometry (building density, building heights distribution, street configuration, etc.) and local topology as well. For this reason, an accurate understanding of fluid mechanics applied on urban wind field is necessary for future improvements in models and methods (Cermak et al. 1995). Pollutant dispersion prediction has been addressed using mainly three methods: wind tunnel experiments, full scale modelling, semi empirical formulations and Computational Fluid Dynamics simulations (CFD). In this section a brief overview of the urban pollution issue followed by wind tunnel modelling, full scale studies and semi empirical formulations will be discussed. The last part of the section presents a detailed review of the CFD approach for pollutant dispersion studies.

2.2 Urban air pollution

Urban air pollution is a major concern since it has been proved to have the direct adverse effects on health. In 2013, the International Agency for Research on Cancer of the World Health Organization officially classified outdoor air pollution air as carcinogenic to humans (WHO, 2013). The air pollution in urban environments has many forms: pollution from routine activities (vehicles exhaust, industrial chimneys, etc), pollution from accidental or non-accidental release of hazardous materials –see Figure 2-1– (explosion, smoke from fire events, etc) and episodic urban pollution, which is related to re-entrainment or cross contamination from one building to an adjacent building.

Figure 2-1. Smoke in event of fire (source:
(www.wfis.uni.lodz.pl/edu/higher_wkshp_c_irwin_19oct.pdf)

The most effective strategy to cope the risk of intakes air contamination is generally through increasing filter effectiveness; however, it is possible to assist the risk management of episodic urban pollution by employing techniques capable of predicting the effect of a source of pollutants in the near-field environment. We understand here by "near field": the fluid mechanical interaction between a source within two or three consecutive buildings within the urban canopy layer –see Figure 2-2.

The most frequently used predictive techniques are; wind tunnel, empirical model and computational fluid dynamics (CFD) simulations. Full scale experiments are also used for dispersion studies, but since the tests are done on existing buildings, data is used for evaluation or to validate wind tunnel experiments or CFD simulations. The following is a literature review of techniques used for dispersion studies.

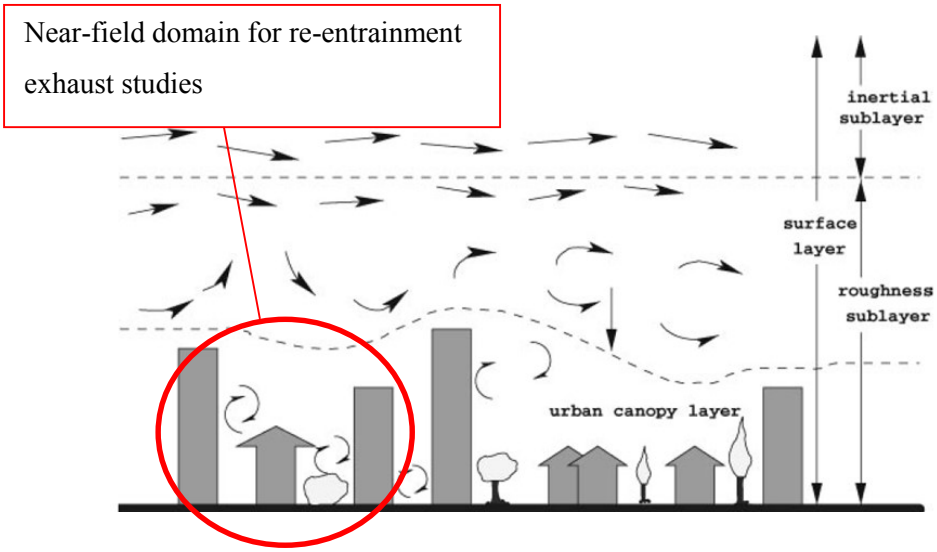

Figure 2-2. Urban air flow (Britter and Hanna, 2003)

2.2.1 Wind tunnel studies

Wind tunnel modelling has been largely used to study the flow characteristics associated with bodies that are completely immersed in a moving flow. The major advantage is the possibility to control the wind conditions and physical (model) configurations. This approach allows simulation of flow in complex building geometries including the effects of surrounding structures and local topology. Meroney (2004) defines wind tunnel or water tunnel as analog computers which have the advantage of "near infinitesimal" resolution and "near–infinite memory". Furthermore, this model approach employs "real fluids" with real properties and behaviour, where flow separation and recirculation are automatically taken into account without any kind of approximation. Although wind tunnel studies are useful in predicting plume dilutions, it may have some similarity constraints issues. The major disadvantage associated with wind tunnel modelling are time and financial limitations (Blocken et al. 2008). Figure 2-3 shows the boundary layer wind tunnel at Concordia University, where the experimental part of the thesis was conducted.

Figure 2-3. Front view section of the Boundary Layer Wind tunnel at Concordia University, Montreal, Canada

2.2.2 Full scale studies

Full-scale testing avoids difficulties and assumptions encountered in wind tunnel concerning similarities. Its major advantage is that it provides data from real atmospheric wind and real layout complexity. The measurements are valuable information which is used to validate wind tunnel of computational modelling. The major disadvantages are related with cost and time related to carry out field studies. In addition, there is also the uncontrollable nature and variation of wind and weather conditions, which can affect the duration and accuracy of the research (Blocken et al. 2008). Figure 2-4 shows a field pollutant dispersion test carried out at Concordia University.

Figure 2-4. Roof of BE building, Concordia University, Montreal

2.2.3 Empirical models

The Gaussian model is a mathematical (normal) distribution of pollutant concentration emitted from stacks in the vertical and crosswind directions. It is the basic workhorse for dispersion, and it is the one most commonly used because: 1) it produces results that agree well with experimental data, 2) it is fairly easy to use and 3) it is consistent with the random nature of turbulence (Hanna, 1982). This model does not consider site-specific geometries that may substantially alter plume behavior; thus this approach is not applicable for complex buildings or locations where other buildings are nearby, which is the case in urban areas.

Currently, the American Society of Heating, Refrigerating and Air Conditioning Engineers (ASHRAE, 2011) develops standards for designers dealing with the design and maintenance of indoor environments (http://www.ashrae.org). The ASHRAE Applications Handbook, Chapter 45, gives guidelines for determining plume dilutions for an isolated building – i.e., without considering the effects of adjacent buildings. A geometric stack design method for estimating minimum stack height to avoid plume entrainment in the flow recirculation zones of a building and its rooftop structures is proposed in ASHRAE (2011). Figure 2-5 is used to explain this method.

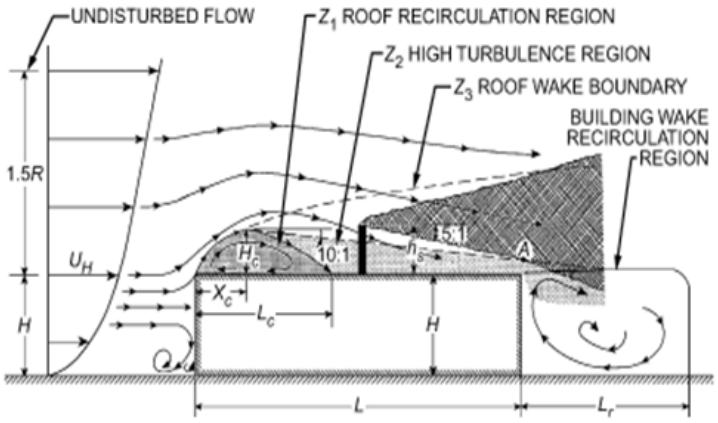

Figure 2-5. Design procedure for required stack height to avoid contamination [from Wilson (1979)]

In ASHRAE (ASHRAE, 2011), dimensions of the recirculation zones are expressed in terms of the scaling length, R, which is defined as:

$$R = B_S^{0.67} B_L^{0.33} \qquad (2-1)$$

where B_S is the smaller of upwind face dimension (height or width) and B_L is the larger of these dimensions (m). The dimensions of flow re-circulation zones that form on the building are:

$$H_c = 0.22\ R \qquad (2-2)$$

$$X_c = 0.5\ R \qquad (2-3)$$

$$L_c = 0.9\ R \qquad (2-4)$$

Where H_c is the maximum height of the recirculation zone at the roof, X_c the distance from the leading edge to H_c and L_c the length of the roof recirculation zone. The wind recirculation cavity L_r id defined as: $L_r = R$.

These formulations are useful in estimating the minimum stack height necessary for the plume to just avoid the recirculation zone. The design method assumes that the boundary of the high turbulence region is defined by a line with a slope of 10:1 extending from the top of the

leading edge separation bubble. The location of the plume relative to the recirculation zones is determined by taking into account the plume rise due to exhaust momentum and assuming a conical plume with a slope of 5:1 (ASHRAE, 2011).

To quantify the dilution of pollutant at specific location from the source in the along wind direction, ASHRAE proposes the following Gaussian distribution:

$$D_r(x) = \frac{4U_H\sigma_y\sigma_z}{V_e{d_e}^2}\ exp\left(\frac{\xi^2}{2\sigma_z}\right) \qquad (2-5)$$

where U_H is the wind velocity at the building height, $\sigma_{y,z}$ are lateral spreading coefficients, V_e the exhaust velocity, d_e the stack diameter, and ξ the vertical plume separation ($\xi = h_{plume} - h_{top}$). More details about this model can be found in ASHRAE-2011.

2.2.4 Computational wind engineering for dispersion studies

Computational Fluid Dynamics (CFD) is the analysis of fluid flow, heat, mass transfer and associated phenomena such as chemical reactions by solving a subset of the Navier Stokes equations at finite grid locations. It provides results of the flow features at every point in space simultaneously (see Figure 2-6). In urban wind engineering, CFD has emerged as a promising technology due to the flexibility to model complex geometries such as cities with dense high-rise buildings. CFD is not intrinsically limited by similitude constraints (as wind tunnel), and therefore it should be possible to numerically simulate all aspects of pollutant dispersion and its interactions with the surroundings (Meroney, 2004). Even though, CFD offers some advantages compared with methods previously mentioned, it requires specific care in order to provide reliable results. A number of parameters such as grid size, discretization scheme, choice of turbulence model, boundary conditions must be verified and validated by systematic comparison with experimental data or other high accuracy methods (Blocken et al. 2008).

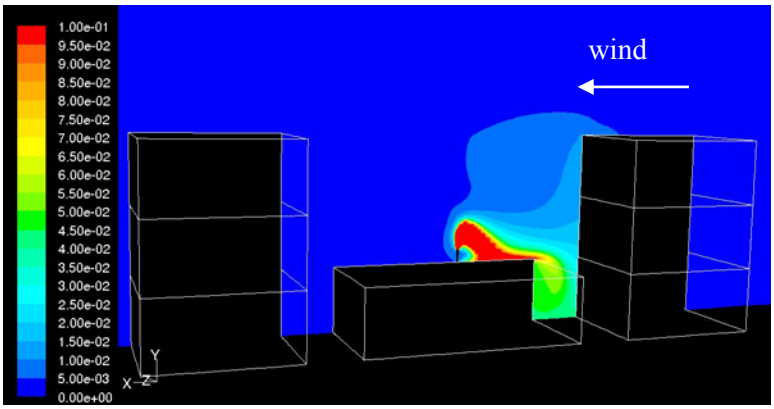

Figure 2-6. CFD modelling example

Since the seventies, computational wind engineering, as a branch of computational fluid dynamics, has been promoted to simulate the airflow around buildings. However, applications of CFD to air pollution aerodynamics started with prediction of wind flow and mass transport over an isolated cubic or other simple-shaped model. The isolated cubic building is a textbook case; it is used as a benchmarking process to compare different approaches and methods for dispersion prediction. The following is a review of studies involving near-field flow and transport of pollutants.

One of the first studies involving the complexity of flow field around a bluff body (representing an isolated building) and the relative performance of various turbulence models were conducted by Murakami and Mochida (1988). In this study, velocity distribution from three-dimensional steady state simulations of flow around a cubic model were compared with wind tunnel results to examine the accuracy of the Standard k-ε turbulence model. The distribution of turbulent kinetic energy (k) was examined, and it was found that the level of the production of k around the windward corner was significantly overestimated. The study suggested the modification of the turbulence production and dissipation expressions in the k-ε model. An expanded article by Murakami and Mochida (1989) reached identical conclusions but also included flow around a building complex.

In a subsequent study, Murakami (1993) showed that flow fields around bluff bodies are characterized by complex distributions of the strain-rate tensor, which is highly anisotropic and

changes significantly depending on the relative position of the bluff body. He revealed that the overestimation of turbulent kinetic energy, produced by the Standard k-ε model, is improved using the unsteady Large Eddy Simulation (LES). He concluded that one of the most distinct differences between Standard k-ε and LES is the production term of turbulent kinetic energy. He concluded that LES has a great potential in flow prediction around buildings.

Brzoska et al. (1997) using a fourth-order accurate finite element code, compared wind tunnel measurement with Standard k-ε model simulation of releases from a stack located within the recirculation zone behind the building. The purpose of this work was to quantify the effect of stack velocity on the concentration in the recirculation. The study verified that pollutant mass in the recirculation zone decreases considerably at high stack velocity. The fraction captured will depend on the wind speed and its profile, the building size and shape, as well as the discharge characteristics. The paper presented a strategy for estimating the fraction of pollutant captured by the recirculation for the case of a discharge within the wake. Finally, as previous researchers found, the authors confirmed that Standard k-ε model yields large values of turbulent kinetic energy at the front corner of the building, which results in reduction or elimination of the recirculation zone on the top of the building due to the excessive diffusion. In the recirculation zone behind the building, the turbulent kinetic energy is underestimated changing separation and reattachment of streamlines resulting in a larger recirculation cavity.

In a similar study, Meroney et al. (1999) examined the flow field and dispersion around several building shapes. The study compared the turbulent models Standard k-ε, Renormalization Group (RNG) k-ε and Reynold's Stress Model (RSM) incorporated in Fluent (a commercial CFD code) with wind tunnel measurements. The intent of these comparisons was to determine if relatively robust commercial software could be used to simulate properly wind engineering problems. It was observed that numerical simulation consistently over-predicts surface concentrations downwind of the source locations. The study considered these discrepancies as a consequence of the impossibility of Reynolds-averaged numerical model to replicate the intermittency of flow in recirculation zones visualized in the wind tunnel. Then, even if the concentration patterns were well reproduced, magnitudes were frequently an order-of-magnitude larger than those of wind tunnel measurements. Concerning pressure patterns, it was shown that numerical predictions were reasonably accurate and magnitudes were close enough to permit

engineering calculations. This suggests that mean pressure fields are less sensitive to numerical model details than other criteria. Finally, it was found that RSM turbulence models produced somewhat more realistic results than Standard k-ε or RNG models.

Flowe and Kumar (2000) performed a parametric study to determine the length of the recirculation cavity as a function of the ratio of building width to building height both in front of and in the rear of the building. The purpose of their study was to investigate the feasibility of using a three-dimensional k-ε numerical model as a means of modelling airflow past a building and stack geometry. The collected dispersive data were then used to determine new correlations between the ratio of building width to building height and the recirculation cavity size and average concentration in the rear recirculation cavity. They concluded that knowing the size and characteristics of the recirculation zone permits the development of improved Gaussian plume models.

Castro (2003) pointed out the fact that an isolated building, is a practical rarity because any site of interest generally contains a number of structures or, at least, has other buildings not far away from the one of interest and certainly within the expected range of influence. Additionally, surface pressures and local wind fields depend crucially on the characteristics of the upstream flow, so it is important to simulate the upstream boundary layer properly. This requires a careful match between the turbulent model parameters and the rough surface boundary conditions. The study also confirmed that Standard k-ε turbulence model is totally inadequate for flows around bluff bodies, because it always gives too much generation of turbulent kinetic energy just upstream of the impingement regions, resulting in inaccurate levels of surface pressures, particularly near the leading edges. The study proposed significant improvements by using appropriate 'fix-ups' to the k-ε or by using differential stress turbulence models, but it remains unclear to what extent the very strong suctions at leading edges and corners can be simulated. It should be noted that the use of more sophisticated turbulence models, generally requires the use of significantly finer grids and more accurate numerical schemes.

The discrepancies observed in the k-ε Reynolds-Averaged Navier-Stokes (RANS) model were examined by Cheng et al. (2003) who compared Standard k-ε model with LES model of a fully developed turbulent flow over a matrix of cubes (resembling an array of buildings). The

results of his investigation proved that both models give reasonably good qualitative results. For instance, flow structures including a horseshoe at the front face of the cube that wraps around the side wall, an arch-shaped vortex in the wake, and thin separation bubbles on the rooftop and side walls were observed. Quantitatively, the profiles of mean velocity were generally better represented by LES model. In fact, the k-ε RANS model produced a severe underestimation of the mean streamwise velocity component in the horseshoe vortex region just upstream of the lower part of the front face of the downstream cube. This, in turn, creates much thicker boundary layers on the side. The complex features of flow within and above the cubes array (e.g. vortex shedding, large separation zones, topology of reattachment lines bordering the recirculation regions, fine-scale flow structures near the side walls, etc.) are reproduced better with the LES model. Clearly, the advantages of LES model are quite evident compared with the k-ε RANS model; however the computational cost (run time) is also significantly higher. In Cheng et al's (2003) study, the computational cost associated with LES model is about 100 times greater than that incurred with the k-ε RANS model.

Liu and Ahmadi (2006) studied the particle transport, dispersion and deposition near a building using a Lagrangian particle tracking approach. The computational model accounted for the drag and lift forces acting on the particle, as well as the effect of Brownian force, in addition to the gravitational sedimentation effects. A point source of helium gas was chosen to serve as the contaminant source and the helium concentration in the plane behind the building and perpendicular to the direction of airflow was evaluated. The results showed that the deposition and dispersion of 0.01 and 1μm particle were similar. The gravitational force had a significant effect on the deposition rate of 10 μm particles. The comparison with the available data showed an agreement for the mean airflow and gas concentration.

Prediction of small water droplets transport from cooling tower has been studied by Meroney (2006, 2008). CFD predictions of a range of particle sizes in both isolated and complex urban environments were considered and compared with experimental data. In general, it was concluded that CFD predicts plume rise, surface concentration, plume centerline concentrations and surface drift deposition within of field experimental accuracy.

Olvera et al. (2008) studied the recirculation cavity behind a cubical building using a commercial CFD code and the RNG k-ε turbulence model. It was observed that plume buoyancy affects the size and shape of the cavity region of flow structure and concentrations within it. The article recommends including this effect in the downwash algorithm in order to improve the accuracy of modelling results for far-field concentration distributions. Indeed, this would be mandatory in accident assessments, where accurate predictions of short-term, near-field concentration fluctuations near source releases are required.

The inaccuracies of dispersion prediction associated to Standard k-ε models and the effects of turbulent Schmidt number (Sc_t) were analysed by Tominaga and Stathopoulos (2007). Sc_t is necessary to solve the transport mass equation in CFD prediction of dispersion with k-ε RANS model; it is defined as the ratio of turbulent momentum diffusivity (eddy viscosity) to the mass diffusivity ($Sc_t = \nu_t/D_t$). The paper emphasized on the issue that Sc_t has a significant effect on dispersion predictions since it appears in the turbulent diffusion hypothesis, which is used to estimate the turbulent mass flow. A smaller value of Sc_t tends to provide better predicted results on concentration distributions around an isolated building using Standard k-ε model. It was concluded that the systematic underestimation of turbulent diffusion of momentum by k-ε RANS model can be compensated using an appropriate smaller Sc_t. However, to pronounce a clear statement for the optimum Sc_t remains not possible due to the strong flow characteristic dependence of Sc_t.

Di Sabatino et al. (2007) verified the effect of Sc_t for flow within a small building arrangement and pollutant dispersion in street canyons. The study compared Standard k-ε model with the atmospheric dispersion model ADMS-Urban. Similarly, with previous researchers, it was found that the concentration in the street canyons is overestimated. The authors explained this overestimation as a consequence of the lower turbulent kinetic energy (k) levels obtained in CFD simulations near the buildings. Finally, it was also mentioned that dispersion can be artificially increased by lowering the Sc_t.

Tominaga and Stathopoulos (2009) tested different turbulent models for flow and dispersion around an isolated cubic building. Standard k-ε was again found to be inadequate for concentration prediction because it cannot reproduce the basics of flow structure, for instance

reverse flow on the roof. However, the RNG k-ε and Realizable models provided much better agreement with experimental data using $Sc_t = 0.3$. It was confirmed that the underestimation of turbulent diffusion for momentum can be compensated by small value of Sc_t.

In summary, the various research studies presented in this section show that many studies concerning pollutant dispersion in urban areas have been focused on the isolated building case. Some publications have found that, in general, CFD simulations show good agreement with experimental measurements in terms of flow pattern. However, using the steady state RANS model an underestimation of dispersion in the proximity of the source is always observed for the isolated building case. Some authors explained this underestimation as a consequence of the impossibility of RANS to replicate the intermittent nature of bluff body flow. This literature review also reveals that the underestimation of dispersion by RANS is a consequence of low turbulent momentum diffusion predicted near the building. To compensate for this underestimation, a calibration is possible by decreasing the value of Sc_t. However, it is clear that changes on Sc_t value cannot be generalized considering the particular flow characteristics of each case. Presently, a discussion about whether a Sc_t calibration is valid to improve pollutant dispersion is currently open as it can be found in various publications (Di Sabatino et al. 2007; Tominaga and Stathopoulos, 2007; Blocken et al. 2008; Chavez et al. 2011).

2.3 Summary

This chapter reviewed the extant publications related with flow and dispersion around buildings. Most of the researches considered here have focused on the isolated building which has become a benchmark to test different numerical approaches. In term of numerical performance, numbers of publication have revealed the difficulties of RANS, in particular the standard k-epsilon model to predict accurate dispersion in the wake of the building. In fact, the common problem of turbulence models is the underestimation of turbulent kinetic energy (k) in the wake which results in less diffusion with a subsequent overestimation of recirculation length. The origin of k underestimation is the impossibility of Reynolds-averaged numerical models to replicate the intermittences of flow in recirculation zones (e.g. the wake). Some researchers have found that RSM perform better than Standard k-epsilon or RNG.

To compensate for the diffusion underestimation, some researchers suggest modifying turbulent Schmidt number (Sc_t). Reducing Sc_t increases turbulent diffusion. The validity of this kind of "calibration" is presently under discussion, and no clear statement is so far available in the literature. Changing Sc_t influences only the diffusion mechanism and not the fluid dynamics (Tominaga and Stathopoulos, 2007, 2009; Di Sabatino et al. 2007, Blocken et al. 2008).

Only three building configurations have been considered for fundamental studies on flow and dispersion around buildings: the isolated building, the street canyon and the array of buildings. Only a few studies have considered two-building configuration (e.g. Gousseau et al. 2011, 2012; Lateb et al. 2010) but for fixed geometry. The current thesis explores the effect of adjacent buildings on dispersion of pollutant by focusing on the shape of buildings. Therefore, two-building configurations as well as three-building configurations are analysed in term of pollutant dispersion in the along wind direction.

3. EXPERIMENTAL METHODOLOGY

3.1 General

The current study is based mainly on CFD simulations; however it combines wind tunnel experiments, which were used for validation purposes. The methodology concerning wind flow modelling using wind tunnel is described in the present chapter as well as some aspects of pollutant dispersion modelling.

3.2 Wind tunnel setup

The Boundary Layer Wind Tunnel (BLWT) of Concordia University is an open circuit wind tunnel of 1.8 m square in section and 12.2 m in length. A thick atmospheric boundary layer was generated using spires, and coarse roughness elements. The roughness elements consisted of 5 cm cubes that were staggered and spaced about 6 cm from each other. A cobra probe, whose accuracy of measurement is generally within 0.5 m/s up to turbulence intensity values of about 30% (Hajra, 2012), was used to measure velocity and turbulence intensities. Table 3-1, summarizes the wind tunnel conditions.

Table 3-1. Boundary layer characteristics.

Boundary layer characteristic	**Value (wind tunnel scale)**
Friction velocity (U*)	1 m/s
Roughness length (Z_o)	3.5 mm
Gradient height (Z_g)	95 cm
Power law exponent (α)	0.31
Gradient velocity (V_g)	14.2 m/s
Turbulence length scale (L_u^x)	40 cm
Wind speed at building height (U_H)	6.2 m/s

3.3 Scaling considerations

For correct modelling of non-buoyant plume exhaust in the wind tunnel, the thesis considered Snyder's (1981) criteria:

a) Geometric similarity:

The geometry (shape) between full-scale and wind tunnel should be similar.

b) Building Reynolds Number (Re_b) > 11000

$Re_b = (\rho U_H D)/\mu$ where ρ and μ are the density and dynamic viscosity of air, U_H is the wind velocity at the building height in the wind tunnel and D is the significant obstruction dimension perpendicular to wind direction in wind tunnel scale. If the value of Re_b is sufficiently large (> 11000) the flow field becomes independent of Re_b.

c) Stack Reynolds Number (Re_s) > 2000

$Re_s = (\rho V_e D)/\mu$ where ρ and μ are the density and dynamic viscosity of air, V_e is the exhaust speed at the stack in the wind tunnel, and D is the internal diameter of the stack in wind tunnel scale. A value of 2000 is well established for the maintenance of turbulent flow in a pipe. A long pipe was considered underneath the model to ensure fully developed flow at the outlet.

d) Similarity of wind tunnel flow with atmospheric surface layer

The wind flow in the Boundary Layer wind tunnel represents an urban terrain with power law exponent of 0.31. This exponent yields the best approximation of the inlet velocity profile in the wind tunnel corresponding experiments. Roughness elements and spires were used to generate the desired terrain roughness. The model value of the longitudinal integral scale was 0.4m, which corresponds to a full-scale value of 80 m. The model roughness length of the upstream exposure was 0.0033m, which corresponds to a full-scale roughness length of 0.66m.

e) Equivalent stack momentum ratio

Exhaust momentum (M) is defined as $M = (\rho_e/\rho_a)(V_e/U_H)$ where ρ_e and ρ_a are density of exhaust gas and ambient air, V_e is the exhaust speed and U_H is the wind speed at the building

height. According to Snyder (1981) the value of "M" in the full scale and wind tunnel has to be equal for accurate simulation of tracer gas studies. Generally for non-buoyant plumes, the term (ρe/ρa) is omitted from the expression. For the present study the cylinder containing a mixture of SF_6 and Nitrogen had 10ppm concentration of SF_6 in it. This implies that the gas released from the stack in the wind tunnel is practically Nitrogen (density near to the ambient air).

For all cases analysed in this thesis a single wind direction perpendicular to the building face was considered. Dilution concentration measurements were carried out using receptors (4 upwind and 5 downwind the stack) located on the rooftop of b1 (emitting building) and spaced 0.025m apart and 0.125m from the lateral edges, as shown in Figure 3-1. For some cases receptors were also placed along the windward of a downstream building (case-dh4 in the forthcoming section). These extra receptors were located centrally, 0.025m apart starting at 0.075m from the ground. The stack location for all cases was 0.15m from the downwind edge of b1 and 0.125m from the lateral edges. The data used in this study were collected by Hajra (2012) and supplemental tests carried out by the author.

The buildings tested were made of timber on a 1:200 scale.

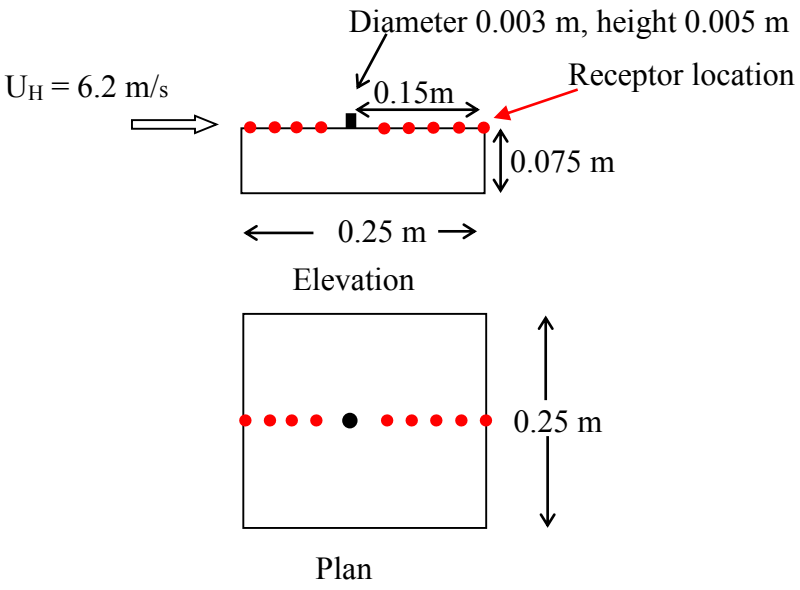

Figure 3-1. Plan view and elevation of the emitting building (b1)

3.4 Tracer gas for dispersion

Tracer gas consisting of a mixture of Sulphur hexafluoride (SF_6) and Nitrogen was released from a roof stack of an emitting b1. A multi-syringe pump was used to collect the gas samples to determine the concentration of effluents at various rooftop receptors of b1 described before. According to ASHRAE (2011), when the source and receptors lie in the same recirculation zone, as in the present study, concentration values obtained up to an averaging time of 2 minutes in the wind tunnel correspond to full-scale averaging time of one hour. For the present study the averaging time for collection of the samples in the experiments carried out in the wind tunnel was only 1 min, since the instrument is capable of measuring samples at the maximum averaging time of 1 min. This is not expected to affect the accuracy of the measurements, as discussed further in Stathopoulos et al., 2004. A Gas Chromatograph (GC) was used to assess the gas concentrations collected using the syringe samplers. Deviations in concentration measurements were usually within ± 10 % (Stathopoulos et al. 2008).

3.5 Visualisation

Real-world observations and laboratory visualization tests can facilitate the understanding of complex flow behaviour and dispersion of pollutant around buildings. The wind tunnel visualization via smoke release from the exhaust stack model defines the zones of interest and to optimize receptor locations for further analysis. Capturing the dispersion of pollutant can be used as a reference for qualitative validation of dispersion prediction obtained by CFD simulations.

Figure 3-2 shows corresponding snapshots for the most representative configurations on dispersion problem: an isolated emitting building and the effect of a building placed upstream of the emitting building.

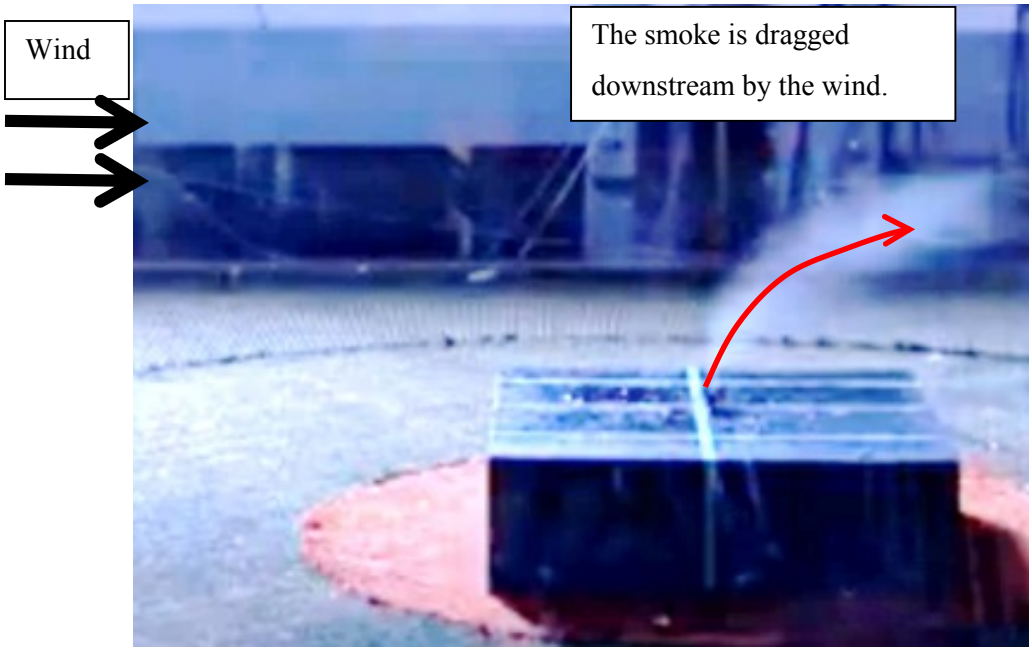

a) Isolated building

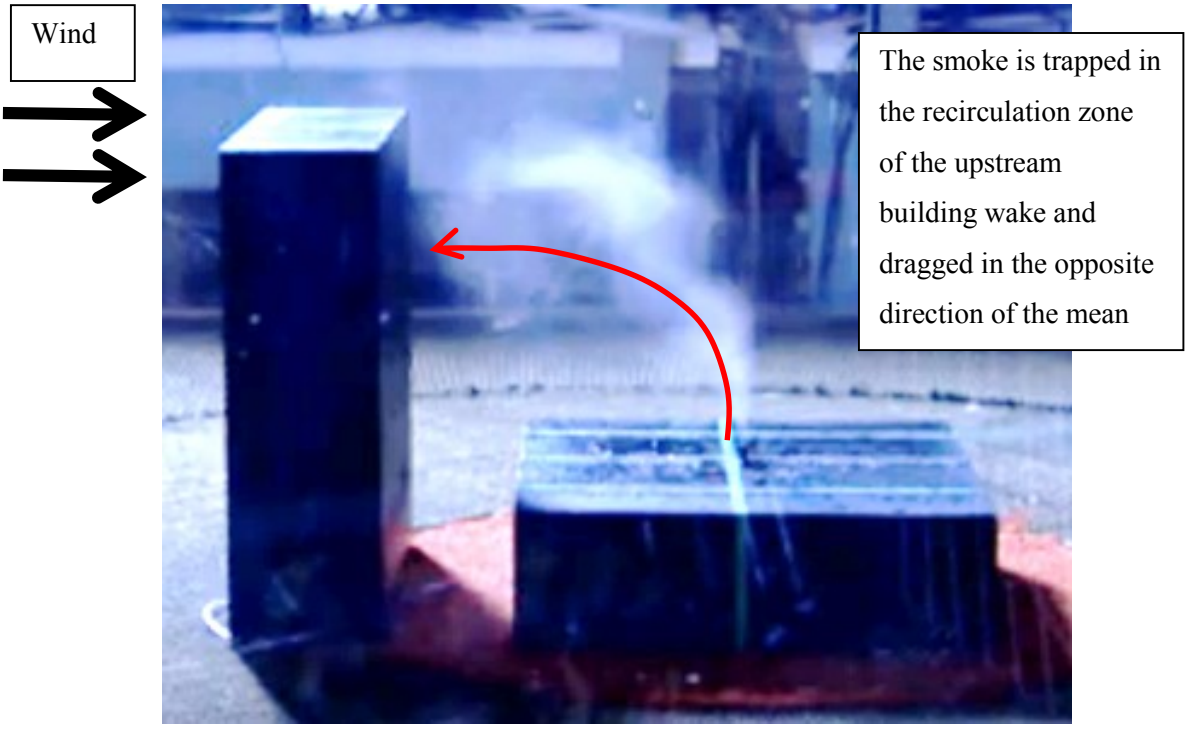

b) Effect of an upstream building

Figure 3-2. Wind tunnel visualization test of adjacent building effect.

The isolated building case (Figure 3-2 (a) shows the usual plume behaviour during pollutant dispersion modelling; the stack plume is dragged downstream by the wind reducing its concentration by mixing with the atmospheric clean air

Significant changes in plume behaviour and, consequently, on dispersion of pollutants can be noted when a taller building is placed upstream of the emitting building (Figure 3-2 (b)). In this case an upwind displacement of the plume is observed, caused by the swirl in the wake of the upstream building. Since the plume is dragged towards the upstream building, the pollutants tend to pollute the complete leeward façade of the same upstream building.

3.6 Normalized dilution definition

The pollutant released from stack is simulated with SF_6 for a particular exhaust momentum ratio, $M=V_e/U_H$ (where V_e is the exhaust velocity and U_H is the wind speed at b1 height). The dispersion of pollutants is analysed using the normalized dilution concept, which can be explained as follows: if a pollutant is discharged with a certain initial concentration, this concentration will be reduced as the pollutant travels within the atmosphere mixing with clean air. Then, dilution is defined as the ratio between the source concentration and the measured concentration at a specific point in the domain. Consequently, the lower the measured concentration the higher the dilution value will be.

The following formulation, suggested by Wilson (1979), was used to evaluate the normalized dilution, D_N:

$$D_N = \frac{D_r Q}{U_H H^2} \qquad (3-1)$$

where:

$D_r = C_e / C_r$ is the dimensionless concentration coefficient at the coordinate location (named also receptors);

C_e = contaminant mass fraction in exhaust (this study used 10 ppm of SF_6);

C_r = contaminant mass fraction at the coordinate location (ppm);

Q is the flow rate at the exhaust (m^3/s);

U_H is the wind speed at the isolated emitting building height (H), U_H = 6.2 m/s.

3.7 Summary

This Chapter detailed the wind tunnel setup for pollutant dispersion studies. It presented the emitting building, b1, from which pollutant would be injected into the atmosphere. A visualization test was shown to highlight the effect of an adjacent building. Concept of normalize dilution, D_N, was also presented which will be the key parameter used during this study for evaluating dispersion.

4. COMPUTATIONAL METHODOLOGY

4.1 General

The aim of the numerical prediction is to solve the governing set of partial differential equations that describe any kind of fluid flow, such as wind flow in the atmosphere. These equations are based on the fundamental laws of conservation of mass, mass species, and momentum (Navier-Stokes equations). In this research, computational fluid dynamic (CFD) simulation is used to solve the equations and predict flow and dispersion around buildings. In general, depending on how CFD solves the equations three approaches can be identified: Direct Numerical Simulation (DNS), Large Eddy Simulation (LES) and the Reynolds Averaged Navier-Stokes (RANS) equations, which uses turbulence models to close the equation system. In this research LES and RANS are examined. The current chapter is a review of theoretical background as well as elemental steps for performing a reliable CFD simulation. After reviewing the fundamental equations, a description of the physical model used, domain, meshing, boundary condition, dispersion mechanism and convergence criterion is provided. All the numerical simulations performed in this thesis were made using the commercial CFD code Fluent.

4.2 Governing equations

Turbulent flow is governed by the unsteady Navier-Stokes equations:

$$\frac{\partial u_i}{\partial x_i} = 0 \qquad (4-1)$$

$$\frac{\partial u_i}{\partial t} + \frac{\partial u_i u_j}{\partial x_j} = -\frac{1}{\rho}\frac{\partial p}{\partial x_j} + \frac{\partial}{\partial x_j}\left(\nu \frac{\partial u_i}{\partial x_i}\right) \qquad (4-2)$$

$$\frac{\partial c}{\partial t} + \frac{\partial c u_j}{\partial x_j} = \frac{\partial}{\partial x_j}\left(\frac{\nu}{Sc}\frac{\partial c}{\partial x_j}\right) \qquad (4-3)$$

These equations describe all the details of turbulent flow and dispersion. They can be solved numerically, but a prohibitive grid size needed for high Re problems makes this approach unviable for urban studies (Rodi, 1995).

4.2.1 RANS

The Reynolds Averaged Navier-Stokes equations can be derived by decomposing into the mean and fluctuating components about the mean, as indicated below. Capital letters represent the mean and the tick represents the fluctuations.

$$u_i = U_i + u_i' \qquad (4-4)$$

$$p = P + p' \qquad (4-5)$$

$$c = C + c' \qquad (4-6)$$

Introducing this decomposition into the original time dependant equation (4-1), (4-2), (4-3), leads to the averaged equation (or RANS equations):

$$\frac{\partial U_i}{\partial x_i} = 0 \qquad (4-7)$$

$$\frac{\partial U_i}{\partial t} + U_j \frac{\partial U_i}{\partial x_j} = -\frac{1}{\rho}\frac{\partial P}{\partial x_j} + \frac{\partial}{\partial x_j}\left(\nu \frac{\partial U_i}{\partial x_j} - \overline{u_i' u_j'}\right) \qquad (4-8)$$

$$\frac{\partial C}{\partial t} + U_j \frac{\partial C}{\partial x_j} = \frac{\partial}{\partial x_j}\left(\frac{\nu}{Sc}\frac{\partial C}{\partial x_j} - \overline{u_j' c'}\right) \qquad (4-9)$$

The additional terms, on the right hand side, represent the effect of turbulence (Reynolds stresses) and they have to be modelled in order to close the system. A common method employs the Boussinesq hypothesis to relate the Reynolds stresses to the mean velocity gradients (Fluent, 2009) by the turbulent viscosity μ_t which is not a fluid property, but depends on the structure of the turbulence (Rodi, 1995),

$$-\rho\overline{u_i' u_j'} = \mu_t\left(\frac{\partial u_i}{\partial x_j} + \frac{\partial u_j}{\partial x_i}\right) - \frac{2}{3}\left(\rho k + \mu_t \frac{\partial u_i}{\partial x_i}\right)\delta_{ij} \qquad (4-10)$$

The most common model for turbulence is the so-called $k-\varepsilon$ model which introduces two extra transport equations (for the turbulent kinetic energy, k and the dissipation rate, ε) and μ_t is

computed as a function of k and ε. In this study the following turbulence models are tested: the Standard k-epsilon (SKE), the Re-normalization group (RNG) and the Realizable (RLZ). The disadvantage of the Boussinesq hypothesis is that assumes μ_t as isotropic scalar. An alternative model which is not restricted to this condition is the Reynolds-stress-equation model (RSM) solving equations for the individual stresses. This approach is most suitable for highly anisotropic flow, as wake of building; however the computational cost is higher. RSM is tested and compared with the previous $k-\varepsilon$ in this study.

Details and mathematical formulation of all turbulence models can be found in Fluent (2009).

4.2.2 LES

LES separates turbulent flow into larges eddies and small eddies using a low-pass filter. The large eddies are explicitly solved while the small eddies are modelled using a subgrid-scale (SGS) model. The major assumption is that the flow in the subgrid-scale behaves as an isotropic flow. However, when the grid is sufficiently small the influence of the modelled scale is negligible at the large scale (Rodi, 1995). The development of the LES equations proceeds in fashion similar to the RANS equations. Instead of ensemble averaging, spatial filtering is performed (Philips, 2012) as shown below,

$$\frac{\partial \tilde{u}_i}{\partial x_i} = 0 \qquad (4-11)$$

$$\frac{\partial \tilde{u}_i}{\partial t} + \tilde{u}_j \frac{\partial \tilde{u}_i}{\partial x_j} = -\frac{1}{\rho}\frac{\partial \tilde{p}}{\partial x_j} + \frac{\partial}{\partial x_j}\left(\nu \frac{\partial \tilde{u}_i}{\partial x_j} - \tau_{ij}^R\right) \qquad (4-12)$$

$$\frac{\partial \tilde{c}}{\partial t} + \tilde{u}_j \frac{\partial \tilde{c}}{\partial x_j} = \frac{\partial}{\partial x_j}\left(\frac{\nu}{Sc}\frac{\partial \tilde{c}}{\partial x_j} - q_j\right) \qquad (4-13)$$

where the overbar denotes the filtering operator and the terms, on the right hand side the, the SGS components. In terms of computational cost, LES is in between of DNS and RANS, (Rodi, 1995) but almost 100 times more expensive than RANS calculations (Cheng et al. 2003).

4.2.3 DES (Hybrid RANS/LES)

In the DES approach, the unsteady RANS models are employed in the near-wall regions, while LES is used away from the wall (Fluent, 2009). The switching from one model to the other is realized according to mesh definition and not to the local turbulent properties (Lateb, 2013). The application of DES, may still require important computing resources; however is less than LES, but greater than RANS (Fluent, 2009).

4.3 Physical model representation

Since the present numerical simulation results are validated using wind tunnel data, it is crucial to numerically reproduce the wind tunnel as much as possible. In consequence, all the numerical models and parameters included in the present study have the same reduced scale as the wind tunnel. Thus, the current study was conducted considering a scaling of 1:200. The numerical building models are represented by simple shapes as cuboid and the computational domain as a parallelepiped as shown below in Figure 4-2.

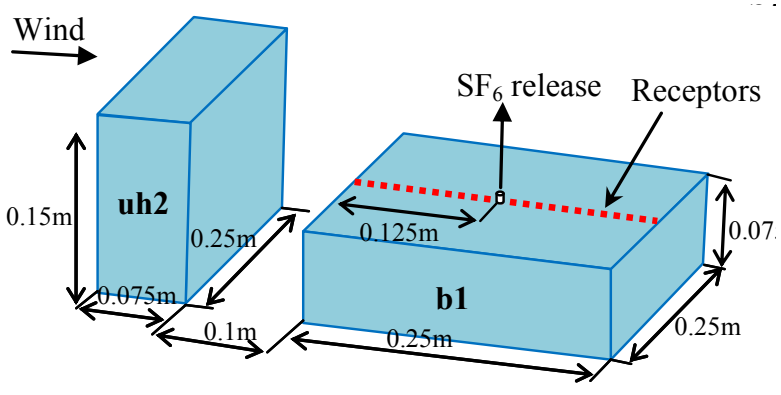

Figure 4-1. Schematic representation of non-isolated building

4.4 Domain

The computational domain is a parallelepiped. Based on recommendations proposed in COST Action (Franke et al. 2007), the dimensions of the computational domain are specified as follows: considering H as the height of the taller building in the model, the lateral and the top boundary was located 5H away from the building and the outlet boundary was 20H downwind from the building to allow flow development (Tominaga and Stathopoulos, 2009). For the inlet a distance of 3H is adopted in order to minimize the development of streamwise gradients, as discussed in Blocken et al. (2008).

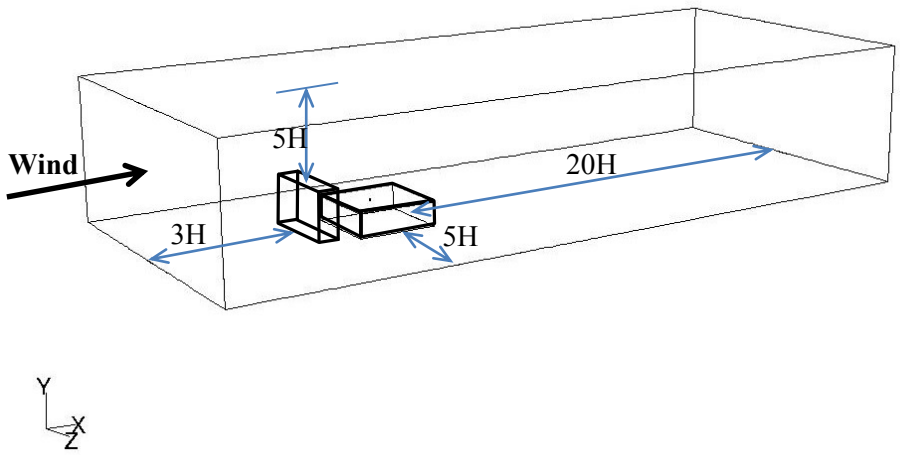

Figure 4-2. Domain size of numerical model

4.5 Meshing

The meshing analysis is conducted for one non-isolated building configuration shown in Figure 4-3. The meshing is constructed using the program Gambit, and the elements used were mainly hexahedra grids since it has been proved that this mesh style provides the best computational results (Hefny and Ooka, 2009). Near the stack and edges a concentration of mesh is defined and near all the vertical walls structured hexahedral elements are specified. The coarse mesh contains 10 elements at the circular section of the stack and 36 elements at each horizontal edge of b1. The expansion ratio between two consecutive cells is limited to 1.25 and the maximum cell length fixed to 0.075 m far away from the model. To build the consecutives medium and fine meshes a constant refinement coefficient of 1.5 in all edges of the buildings is defined. Finally, the

resulting three meshes are: coarse (624,893 cells), medium (1,460,520 cells) and fine (3,374,915 cells). The Enhanced Wall Treatment option, which provides consistent solutions for all y+ values (contrary to the default Wall Function that need y+ larger than 30) is used (Fluent, 2009). The general mesh aspect and details for the stack and corners is observed in Figure 4-3 and 4-4.

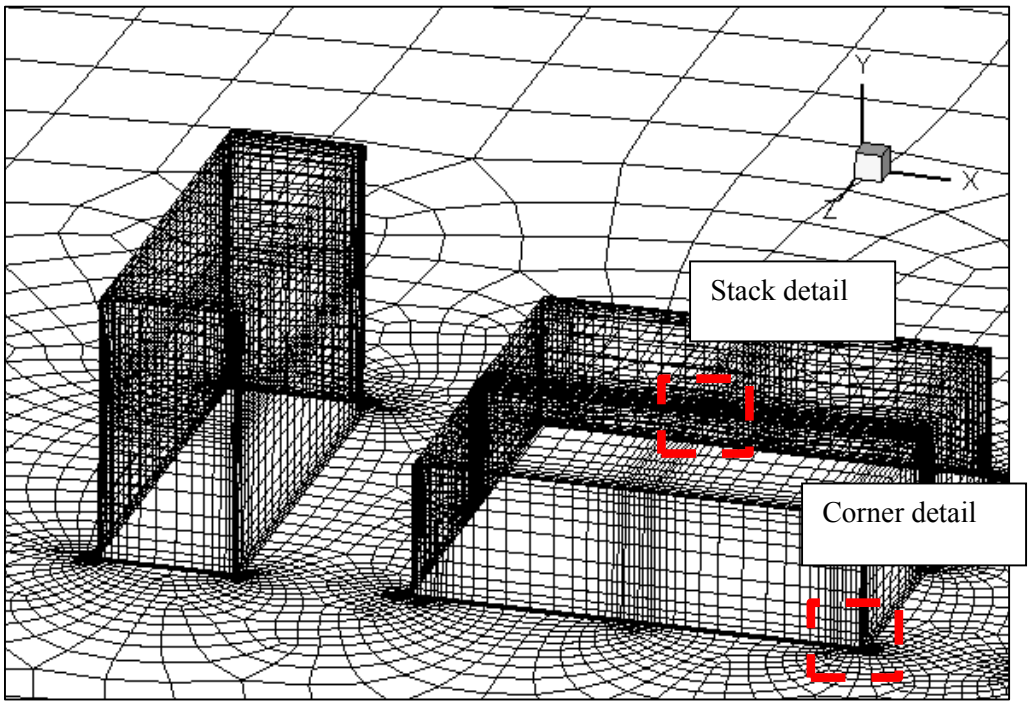

Figure 4-3. Coarse mesh (624,893 cells)

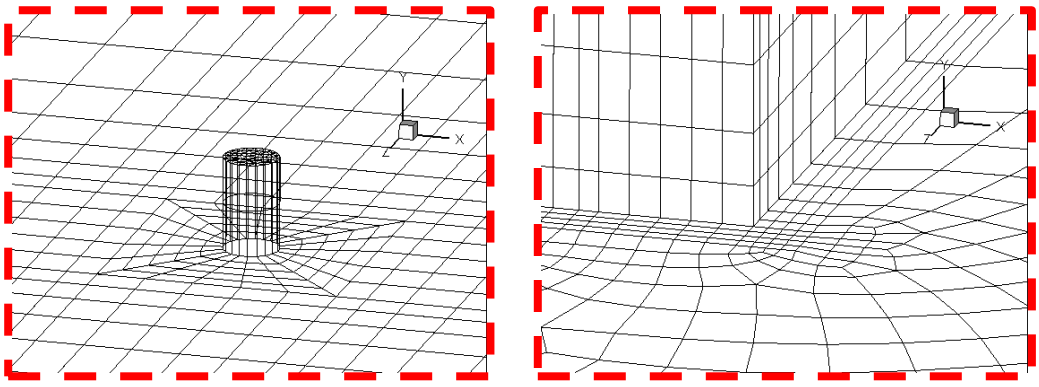

a) Stack detail **b) Corner detail**

Figure 4-4. Meshing details (a) stack, (b) and near corner detail

The grid independence is evaluated using the Grid Convergence Index (CGI) which is a measure indicating how a computed value, obtained with a specific mesh, is far from the asymptotic value (Roache, 1994). The asymptotic value is calculated using the Richardson extrapolation method (Richardson et al. 1927) as suggested by Franke et al. (2007). The method estimates an exact solution (f_{ex}) of a defined variable from a series of numerical results (f_k) obtained from consecutive high quality meshes indexed by k. In this case, the numerical variable observed is the normalized dilution, D_N. The basic assumption is that the extrapolated exact solution corresponds to the asymptotic value of D_N when the grid size tends to zero. The extrapolation is made from numerical solutions of three meshes having a constant mesh refinement using the following equation:

$$f_{ex} = f_1 + \frac{f_1 + f_2}{r^p - 1} \qquad (4-14)$$

In general, the index $k = 1$ denotes the fine, $k = 2$ the medium and $k = 3$ the coarse mesh. Then f_1 and f_2 are the solutions for fine and medium meshes respectively. The refinement ratio is introduced with the term r (= 1.5) and p is the order of accuracy that can be estimated by using the following equation:

$$p = \frac{ln\left(\frac{\varepsilon_{32}}{\varepsilon_{21}}\right)}{ln(r)} \qquad (4-15)$$

where, $\varepsilon_{i+1,i} = f_{i+1} - f_i$ $(4-16)$

To apply the Richardson method, the ratio of the solution changes from the results of the three meshes, $R = \frac{f_2 - f_1}{f_3 - f_2}$, should have monotonic convergence the following definition:

- Monotonic convergence; $0 < R < 1$

- Oscillatory convergence; $R < 0$

- Divergence; $R > 1$

To analyse the grid convergence, D_N prediction at three points in the space and for three meshes were observed. The selected points are directly above the stack within the wake of the upstream building. They have the following coordinates: Point-1 (1.1, 0.15, 0), Point-2 (1.1, 0.125, 0) and Point-3 (1.1, 0.1, 0). A representation of the spatial location these points are shown in Figure 4-5.

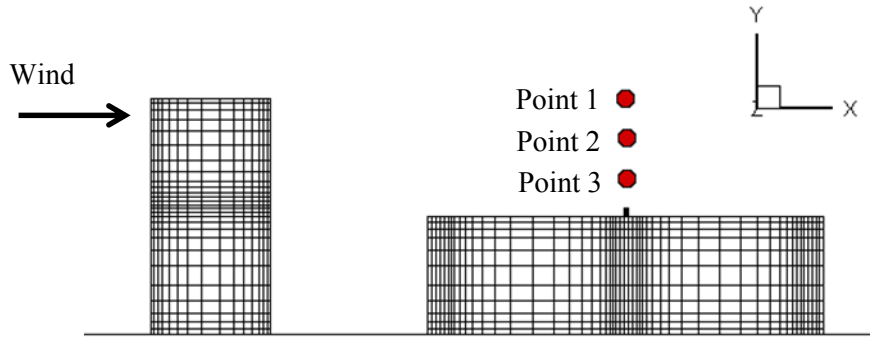

Figure 4-5. Location of three points to analyse grid convergence

The grid convergence study is a mathematical verification which gives an estimation of spatial discretization errors. As mentioned, GCI is used to carry out the current grid refinement analysis by providing an uniform measure of convergence based on estimated errors derived from the Richardson extrapolated asymptotic solution (Ali et al. 2009). This measure represents the resolution level and gives an idea of how much the solution approaches the exact solution. The GCI can be expressed as follows,

$$GCI_{i+1,i} = F_s \frac{|\varepsilon_{i+1,i}|}{f_1 \ (r^p - 1)} \qquad (4-17)$$

where F_s is a safety factor, here equal to 1.25 (Celik et al. 2006).

Table 4-1 shows the GCI value for each point as well as the value of R and p. It is observed that GCI monotonically decreases with mesh refinement in all points ($GCI_{21} < GCI_{32}$) indicating that grid dependence is successfully reduced by increasing grid size. For points 1 and 2 a smooth convergence toward the exact value is observed; however for point 3 a markedly difference is

noted between coarse and medium mesh. This difference is clearly observed in Figure 4-6 were D_N, normalized by the extrapolated D_N value, is plotted against mesh size. Point 3, which is closer to the stack, seems to be more sensitive to mesh refinement. Given that the medium mesh produces an acceptable error for a reasonable mesh size it was chosen for the remainder of the study.

Table 4-1. Order of accuracy and GCI for three points and three meshes

	ε_{32} (10^{-1})	ε_{21} (10^{-1})	R	p	GCI_{32} (%)	GCI_{21} (%)
P1: y = 0.15m	0.1861	0.945	0.51	1.67	9.45	4.98
P2: y = 0.125m	0.5350	0.268	0.50	1.71	6.91	3.55
P3: y = 0.10m	0.0810	0.007	0.09	5.96	7.63	0.72

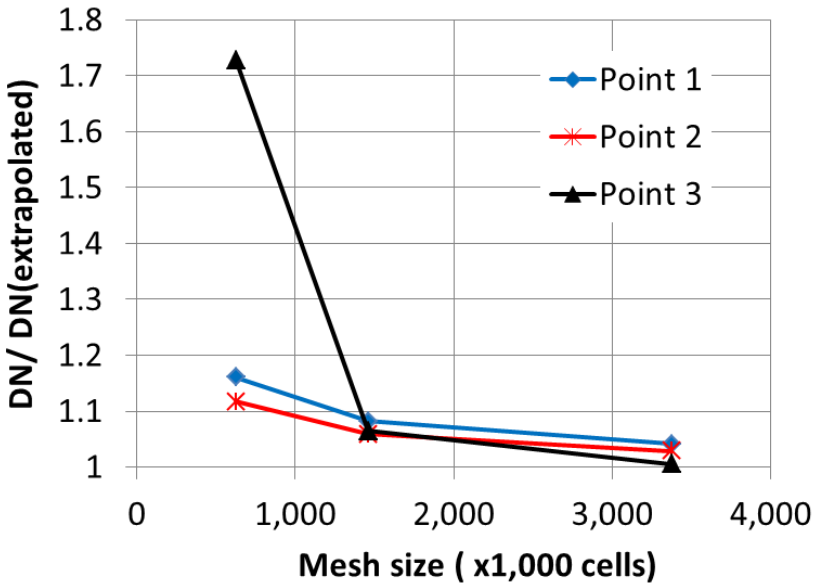

Figure 4-6. Comparison of D_N (normalized by the extrapolated value) for three meshes at three different locations, Point 1 (y = 0.15 m), Point 2 (y = 0.125 m) and Point 3 (y = 0.1 m) above the stack.

4.6 Boundary conditions

As mentioned before, numerical simulations are validated trough comparisons with wind tunnel results. In order to minimize the number of uncertainties, CFD boundary conditions are defined as similar as possible to the wind tunnel experimental setup. In others words, CFD simulations try to reproduce the wind tunnel, then all the parameters are adjusted to the wind tunnel scale. The following is a description of the boundary condition used all along the present study.

The bottom surface (i.e. ground) is a rigid plane with an aerodynamic roughness length y_o=0.0033 m (which corresponds to y_o=0.66 m at full scale). In FLUENT this roughness length is implemented by the sand-grain roughness height k_s (m), defined using the function developed by Blocken et al. (2007): $k_s=9.793y_0/Cs$, where Cs is a roughness constant. Considering the default value of Cs equal to 0.5, k_s should be specified as 0.0646. However, this value is limited to the distance of the centroid of the first cell to the bottom domain, as imposed by FLUENT. The effect of this limitation is translated to streamwise changes in the inlet vertical profile which would affect the accuracy of CFD simulations, an issue that has been discussed in previous works (Hargreaves and Wright, 2007; Norris and Richards, 2010; Parente et al., 2011a, 2011b). To reduce the effect of undesired inlet profile, the current study has adopted the minimization of upstream domain length criterion by specifying 3H (mentioned previously) as suggested by Blocken et al. (2007). This option is reasonable in the present case considering that the wind flow impinging the plume is more affected by the presence of the upstream building than the roughness length. At the outlet, an outflow (zero gradient) condition is specified to generate a fully developed flow. Building walls, top and sides of the domain are modelled as no slip walls.

The approaching mean velocity and turbulence intensity profiles measured in the wind tunnel are used to specify the inlet boundary layer at the CFD model are shown in Figure 4-7. Similar to the experiment, a power law exponent of 0.31 corresponding to urban terrain is used for the study. The velocity at the building b1 height (H = 0.075 m) is 6.2m/s.

$$U(y) = 6.2\left(\frac{y}{0.075}\right)^{0.31} \qquad (4-18)$$

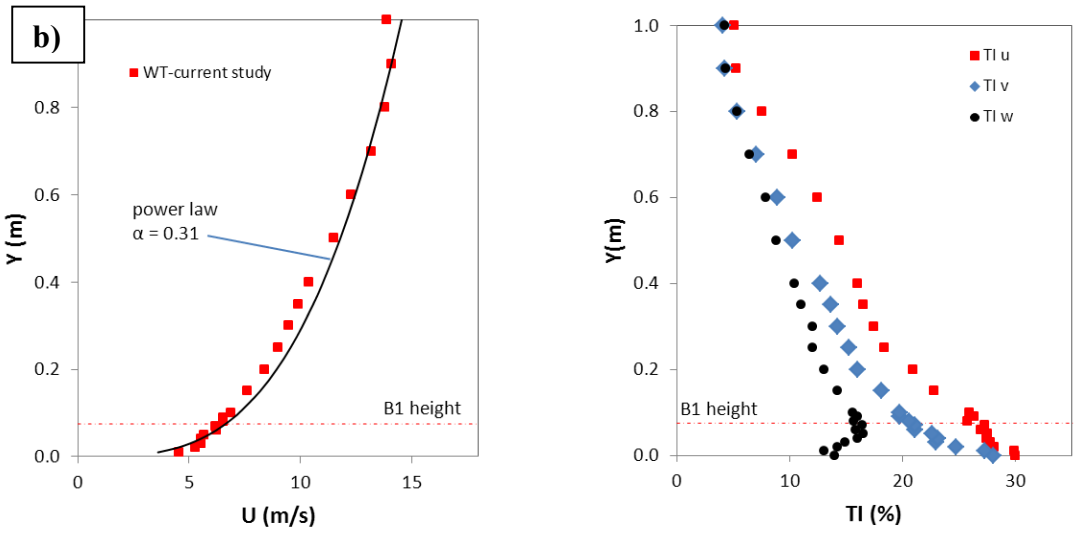

Figure 4-7. Atmospheric boundary layer profiles from wind tunnel. a) mean velocity, b) turbulence intensity.

When the flow enters the domain at an inlet, FLUENT requires specification of transported turbulence quantities: turbulent kinetic energy profile (k) and dissipation rate profile (ε). The measured turbulence intensity profiles are converted in k profile considering the three components of fluctuating velocities $\langle u' \rangle, \langle v' \rangle$ and $\langle w' \rangle$ assuming; $\langle u' \rangle = TI_u \, U/100$. Then, k is calculated using the following equation;

$$k = \frac{1}{2}(\langle u' \rangle^2 + \langle v' \rangle^2 + \langle w' \rangle^2) \qquad (4-19)$$

The dissipation rate profile (ε) was defined as $\varepsilon = u^{*3}/\kappa y$ where κ is the von Karman constant (0.42) and u* is the friction velocity obtained from the equation $u(y)/u^* = 1/\kappa(\ln(y/y_o)$ with roughness length y_o = 0.0033 m. At the model scale of 1:200, the equivalent full-scale roughness length is 0.66 m, which is at the low end of the expected range for an urban environment (0.5 m < y_o<1.5 m) (Stathopoulos et al. 2004). In order to introduce these turbulence parameters as well as the mean wind velocity profile at the inlet boundary of CFD model, a UDF was implemented. The boundary conditions are summarized in Figure 4-9.

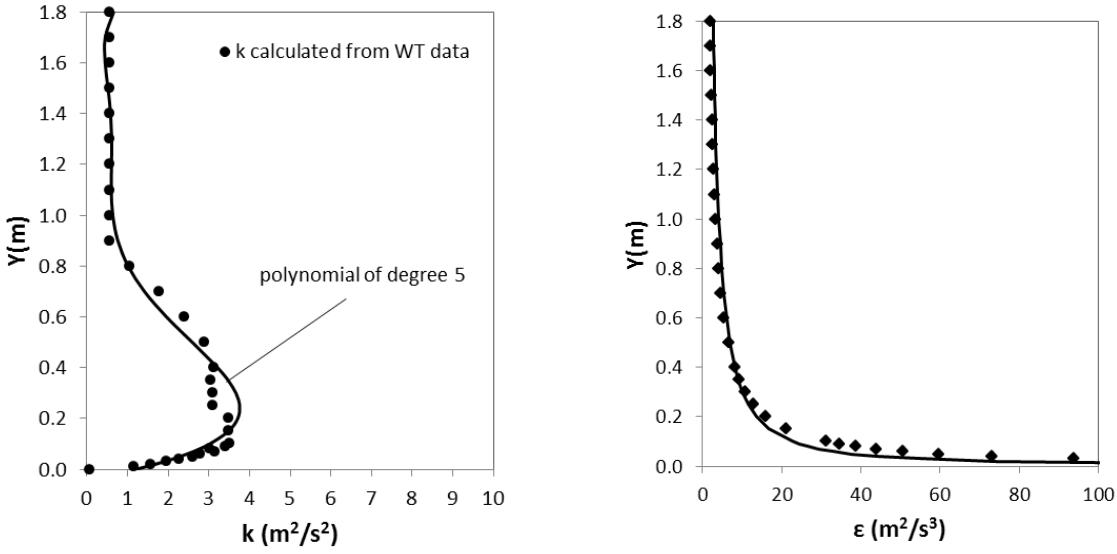

Figure 4-8. Turbulence kinetic energy and dissipation profiles calculated from wind tunnel data

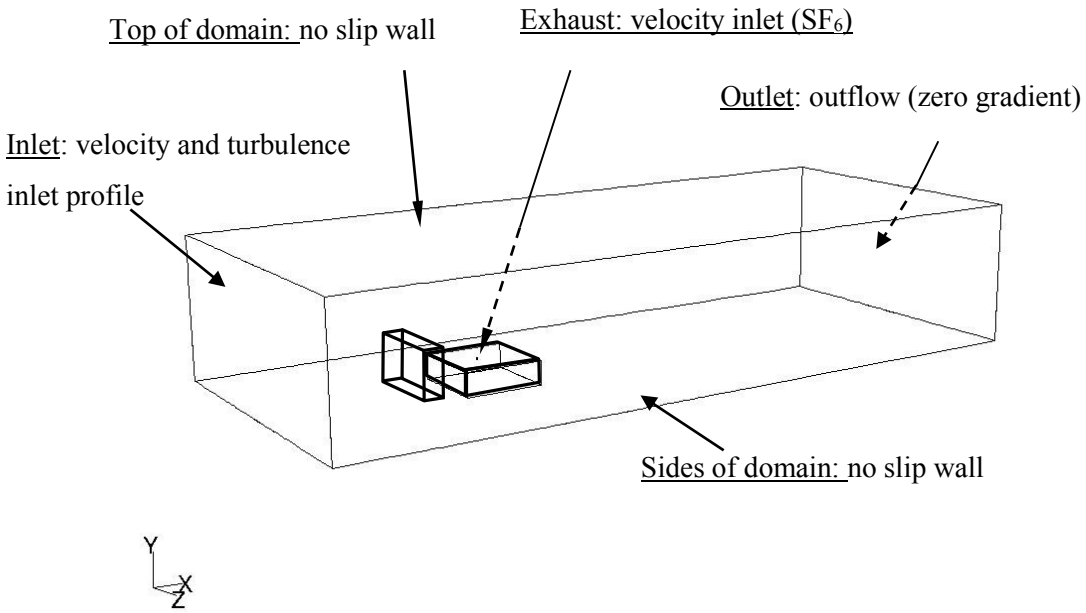

Figure 4-9. Boundary conditions of CFD model

4.7 Mass transport process

The transport of pollutants is a combination of two processes: dispersion and diffusion. The dispersion is the redistribution of species due to the difference in velocities along different streamlines. It refers to transport with the mean fluid flow. Diffusion is the process of spreading mass by gradients in species due to random motions around a center of mass. For a stack emissions, dispersal of pollutants is what happens along the rising plume centerline (mean flow) and diffusion is what happens perpendicular to the plume centerline due by turbulence effect. The latter mechanism is named turbulent mass diffusion. In the RANS approach the gradient diffusion hypothesis to estimate turbulent mass diffusion is used;

$$-\overline{u_i' c'} = D_t \frac{\partial c}{\partial x_i} \qquad (4-20)$$

where D_t is the turbulent mass diffusivity and $\frac{\partial c}{\partial x_i}$ the mean mass gradient. To determine D_t the turbulent Schmidt number (Sc_t) is needed, which is defined as the ratio of turbulent moment diffusivity (eddy viscosity) ν_t and the turbulent mass diffusivity D_t, ($Sc_t = \nu_t / D_t$).

In FLUENT Sc_t is considered constant in the all domain and it must be declared as input prior to any calculation or else the default value assumed is 0.7.

The value of Sc_t has important implications for dispersion simulations as observed in previous studies (Tominaga and Stathopoulos, 2007, 2009; Di Sabatino et al. 2007; Blocken et al. 2008). However, no definitive statement is available in the literature concerning the validity of manipulating the standard value for calibration purposes.

Schmidt numbers have been measured in the wind tunnel by various researchers in the past. Tracer experiments carried out by Koeltzsch (2000) have confirmed a strong dependence of height within the boundary layer affecting the value of Sc_t. However, negligible changes in Sc_t were found with a change in atmospheric stability (Flesch et al. 2002). The estimation of Sc_t at the height 0.075 m (emitting building height) using formulations proposed in previous studies is shown in Table 4-2.

These formulations are empirical equations based on experimental measurements. Rotta (1964) developed his equation based on temperature distribution within turbulent boundary layer; Pruitt et al., (1973) used field measurements of wet and dry bulb temperature; Dyer and Bradley (1982) also conducted field measurements to determine flux gradient relationship; Hogstrom (1996) used previous field data to develop a new set of equations and Koeltzsch (2000) performed turbulent measurements of a horizontal plate in a wind tunnel.

Table 4-2. Values of Sc_t in previous studies

Previous studies	Formulation	Value of Sc_t (y = 0.075m)
Rotta, 1964	$Pr_t = 0.9 - 0.4\ (y / \delta)^2$ δ : boundary layer thickness = 0.9m y : distance above the ground within the boundary layer Turbulent Prandtl number (Pr_t) considered similar to turbulent Schmidt number.	0.89
Pruitt et al., 1973	$Sc_t = \varphi_c / \varphi_m$, where $\varphi_m = (1 + 16\ (y / L))$ and $\varphi_c = 0.89\ (1 + 34\ (y / L))$ φ_m : momentum flux φ_c : mass flux L : Monin Obukhov length = 54200 y : same as previous	0.88
Dyer and Bradley, 1982	$Sc_t = \varphi_c / \varphi_m$, where $\varphi_m = 1 + 4.8\ (y / L)$ and $\varphi_c = 0.95 + 4.5\ (y / L)$ φ_m, φ_c, L and y same as previous	0.95
Hogstrom, 1996	$Sc_t = \varphi_c / \varphi_m$, where $\varphi_c = \varphi_m = 1 + 5.3\ (y / L)$ φ_m, φ_c, L and y same as previous	1
Koeltzsch, 2000	$Sct = \sum_{i=0}^{5} a_i \left(\frac{z}{\delta}\right)^i$, where a = (.0.226, 12.2, 46.2, 81, -67.9 and 21.5) δ and y same as previous	0.55

For computational urban environmental studies, the most common Sc_t values is 0.7 which was proposed by Spalding (1971); but a range from 0.2 to 1.3 according to the flow properties and

geometries are also used (Tominaga and Stathopoulos, 2007). As mentioned, the dependence of Sc_t on simulation of pollutant dispersion is relevant and hence the present work pays special attention to Sc_t values in Chapter 5.

4.8 Convergence criterion

The convergence criterion is generally based on the residuals of equations, which serve to designate how far the current solution is from the exact solution (Franke et al. 2007). Knowing that the exact solution is obtained after an infinite number of iterations, the convergence criterion becomes then the stopping criterion of the iterative process. The convergence criterion is a critical parameter that should be defined before and monitored during any CFD calculation. However, there is no clear consensus in the literature about the level of iterative convergence. For instance, the iterative convergence criterion for industrial applications is usually 10^{-3} and the suggested criterion for urban studies is 10^{-5} (Ramponi and Blocken, 2012; Franke et al. 2007). The current section explores the influence of residual definition for D_N prediction for three cases: an isolated and two different non-isolated building configurations.

Figure 4-10 shows clearly that a reduction of the convergence criterion from 10^{-5} shows almost no changes in the final solution. This means that keeping the standard criterion at 10^{-5} is sufficient for a converged solution for the case of an isolated building. In contrast, Figure 4-11 and 4-12, which correspond to different two-building configuration, show that convergence criterion reduction has an important effect on the final D_N value at roof level. Figure 4-13 shows that reducing the convergence criterion from 10^{-5} to $0.9x10^{-5}$ by adding close to 800 extra iterations, D_N varies by more than 500% from the previous value at the specific location x = 0.1m (indicated with a circle in Figure 4-11). A further reduction of the convergence criterion demonstrates that to obtain two consecutive variations of D_N by about 7%, a residual equal to $0.4x10^{-5}$ is required. The associated computational cost for reducing the convergence criterion from 10^{-5} to $0.4x10^{-5}$ is reflected on the 8,026 extra iterations needed to reach this level. In addition with residual criterion, it is suggested monitoring a variable in a point within the domain and verify that the variable is constant or oscillate around a constant value after stopping calculation (Franke et al. 2007).

In conclusion, in order to limit potential source of error on D_N prediction for not having enough iterations, the convergence criterion was fixed at $0.4x10^{-5}$, i.e. lower than the standard value of $1.0x10^{-5}$, for all the equations. From the observation of all the non-isolated building cases examined in the present study, about 27,000 iterations were sufficient to reach this level.

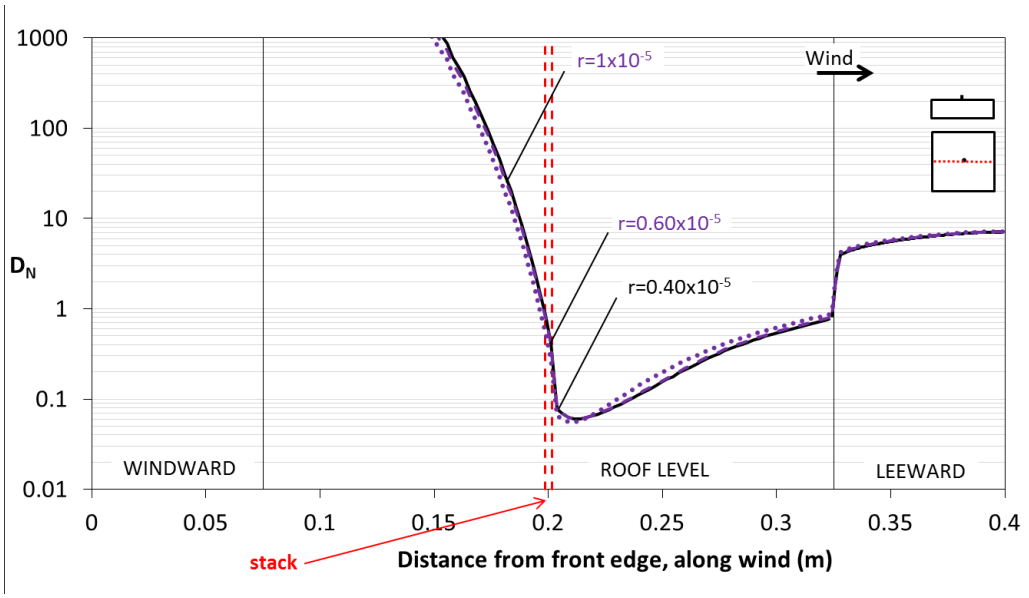

Figure 4-10. Residual effect on an isolated emitting building (b1)

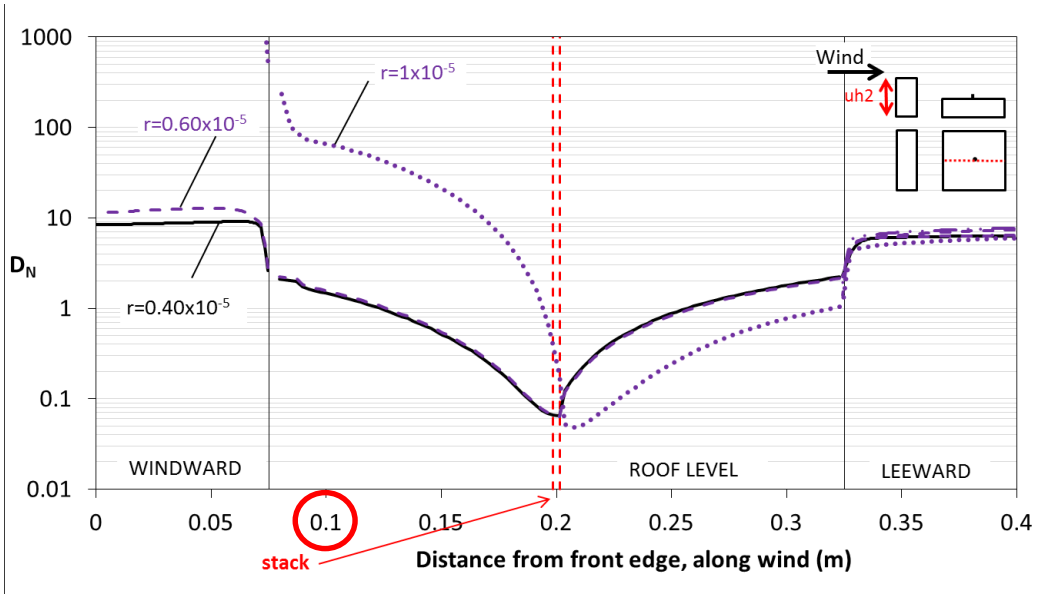

Figure 4-11. Residual effect on a non-isolated building (uh2 upstream of b1)

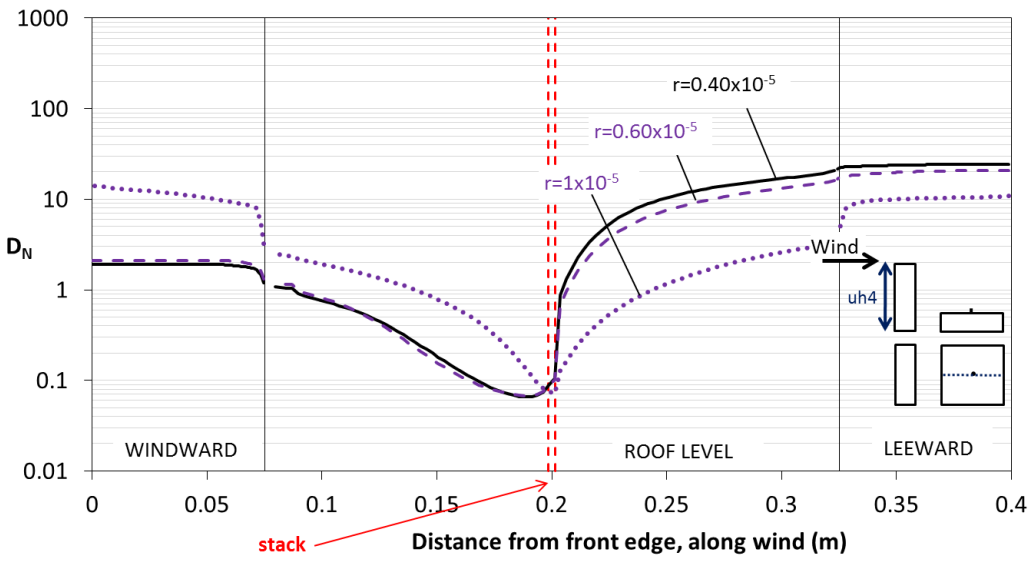

Figure 4-12. Residual effect on a non-isolated building (uh4 upstream of b1)

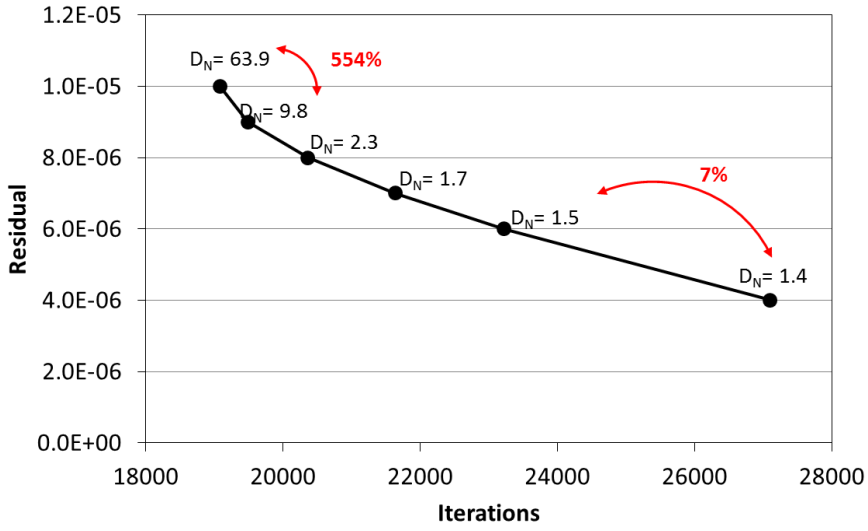

Figure 4-13. D_N at x=0.1m (see Figure 4-11) for different number of iterations when uh2 is located upstream of b1

4.9 Summary

The current chapter reviewed theoretical background as well as elementals steps for performing a reliable CFD simulation. Basic considerations concerning domain size, meshing characteristic, boundary condition and convergence criterion were discussed.

5. COMPARISON BETWEEN STEADY CFD, WIND TUNNEL AND ASHRAE MODEL

5.1 General

The current chapter presents steady CFD simulations and compares results with wind tunnel data for validation purposes. Before comparing, two important numerical considerations are evaluated: turbulence model and turbulent Schmidt number (Sc_t). The chapter is structured in three sections: (1) four turbulence models are tested in order to determine the appropriated approach for the current application; (2) the effect of Sc_t on dispersion of pollutants is analysed; and (3) three representative non-isolated building configurations are compared using steady CFD, wind tunnel and the ASHRAE prediction model to validate the numerical methodology.

5.2 Introduction

Currently, the techniques available to assess pollutant concentrations in the built environment include field measurements, wind tunnel tests, semi- empirical models such as ASHRAE-2011, and CFD simulations. Although wind tunnel and field studies are useful in predicting plume dilutions, time and financial constraints are two of the major disadvantages associated with them (Blocken et al. 2008). A study carried out by Hajra (2012) confirmed that most available semi-empirical models cannot be used for near-field pollutant dispersion problems since they were developed for isolated buildings and do not incorporate the effects of adjacent buildings. CFD has been used by various researchers to study flow and dispersion around isolated buildings, street canyons and array of buildings, but few studies have focused on the "near-field" concept where the fluid dynamic interactions between two or three adjacent buildings govern pollutant dispersion. The aim of the present chapter is to simulate pollutant dispersion for non-isolated building configurations focusing on two important numerical aspects: turbulence model and turbulent Schmidt number effect. The goal of the investigation is to evaluate the performance of RANS by systematic comparisons with tunnel data.

5.3 Methodology

Dispersion simulations for an isolated b1 and an upstream building named uh2 ($2H_b$ x W_b x L_b) a two-building configuration as shown in Figure 5-1 (a) and (b), respectively.) were performed using four different turbulence models, namely: Standard k-ε (SKE), Realizable k-ε (RLZ), Renormalized Group k-ε (RNG) and Reynolds Stress-Model (RSM). The results were compared with experimental data for an identical configuration.

For all simulations, all the transport equations (momentum, energy, turbulence variables and concentration) are discretized using second-order upwind scheme. The SIMPLE algorithm is used for pressure-velocity coupling.

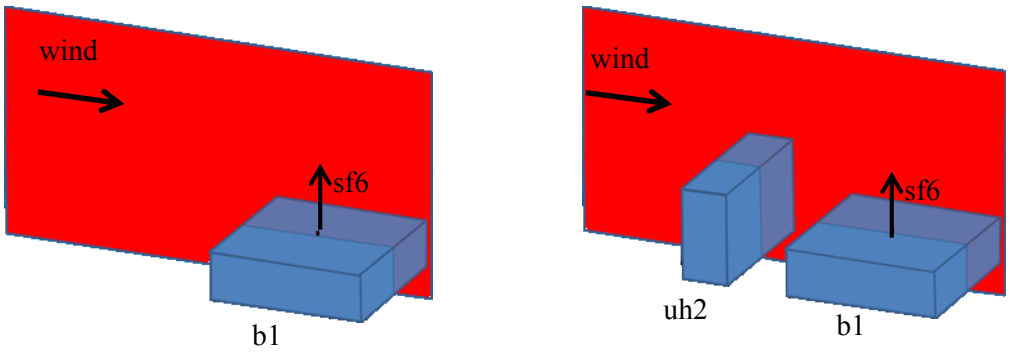

a) b1 Isolated b) uh2 upstream of b1

Figure 5-1. Schematic representation of isolated and a two-building configuration.

Figure 5-6 shows the comparison between CFD and experimental data for D_N prediction for an isolated emitting building. From the wind tunnel data, it is observed that D_N increases almost linearly for locations away from the stack in the wind stream direction. This phenomenon is expected since wind naturally tends to blow away pollutants and decrease concentration (increase dilution) from the source. It is noted that CFD follows the trend of wind tunnel data in the region downwind of the stack very well; however, the computed D_N values are underestimated by a constant factor. The underestimation can be probably associated to the inherent limitations of RANS to capture unsteadiness in a high turbulent regime. High turbulence is characterized by a

high mixing rate, which promotes dilution and this is exactly what is underestimated in the present CFD results. Additional comparisons when the stack is located in the front edge of the building have shown similar characteristics, i.e. an acceptable trend agreement and an underestimation of D_N values from CFD predictions (Appendix A). The region upwind the stack is characterized very high D_N value – no experimental data was obtained in this region. All cases were obtained using the standard value (default by Fluent) of $Sc_t = 0.7$.

5.4 Validation and sensitivity analysis

5.4.1 Turbulence model

A general view of computations in terms of streamlines and normalized dilution, D_N, field is analysed for all the turbulence models. Figure 5-2 and 5-3 show the streamlines and Figure 5-4 and 5-5 show D_N iso-contours in two plan views; vertical middle plane and horizontal plane at y = 0.08 m, which corresponds to the stack outlet location in the y direction.

In general, a two-building configuration induces low wind speed between buildings. These zones are also characterized by the presence of high vorticity as it can be noticed by the streamlines in Figure 5-2 and 5-3. The analysis of the figures brings the following remarks:

RNG shows a strong combination of backward and upward velocities in Figure 5-2 (b). This is correlated with the larger velocity magnitude field in the zone upwind of the stack plotted in Appendix B-(2). The effect of this strong backflow pattern is reflected in high dispersion (low dilution) towards the leeward of the upstream building, Figure 5-4 (b). In addition, RNG shows a predominant spreading in the vertical plane –mainly upwind– and very limited spreading in the lateral directions (see Figure 5-4 (b)). The wider plume observed in the horizontal plane –compared with the other models- is the resultant of high amount of pollutants trapped in the recirculation zone associated with the upwind separation on the sides of the upwind building.

SKE and RLZ show comparable streamlines (Figure 5-2 (a) and 5-3 (a)) and velocity field in the vertical and horizontal plan (Appendix B-(1) and (3)). In terms of dispersion, SKE shows the lowest spreading upwind the stack among all the models, Figure 5-4 (a). In addition, it shows

very high dilution (low concentration) in the space between both buildings near the ground. This is because almost no concentrations are ever convected into the vicinity of the separation streamlines. Moreover, pollutants are mainly dragged by the mean flow downwind the stack.

In general, RSM and RLZ show comparable flow pattern, except in the horizontal plan as observed in Appendix B-(3) and (4). In the horizontal plan, RSM is the only model that shows clear acceleration at the lateral corners of the upstream building. The consequence is a wider recirculation region in the horizontal plan.

In terms of turbulent kinetic energy (k) shown in Appendix-C, SKE shows the highest k at the windward wall of the upstream building, and the lowest k in the horizontal plane within the wake. This behaviour was expected since it is mentioned in the literature (e.g. Castro, 2003). RLZ, RNG and RSM show comparable k in the vertical plane. In horizontal plane within the wake, RLZ and RSM show comparable k results (Appendix C-(3) and (4). In dispersion studies, the accurate prediction of k is needed because the turbulent diffusivity governing dispersion mechanism it related to this variable (Gousseau et al. 2012).

In conclusion, for this case, it can be said that RNG promotes spreading of pollutants upwind the stack resulting in low dilution values (high concentration) in this zone compared with the others models. In contrast, SKE spreads pollutants mostly downwind from the stack, then very limited pollutants are found between both buildings. RLZ and RSM perform similarly; RLZ spreads more pollutants upwind the stack, and less in the lateral direction compared with RSM.

a) SKE

b) RNG

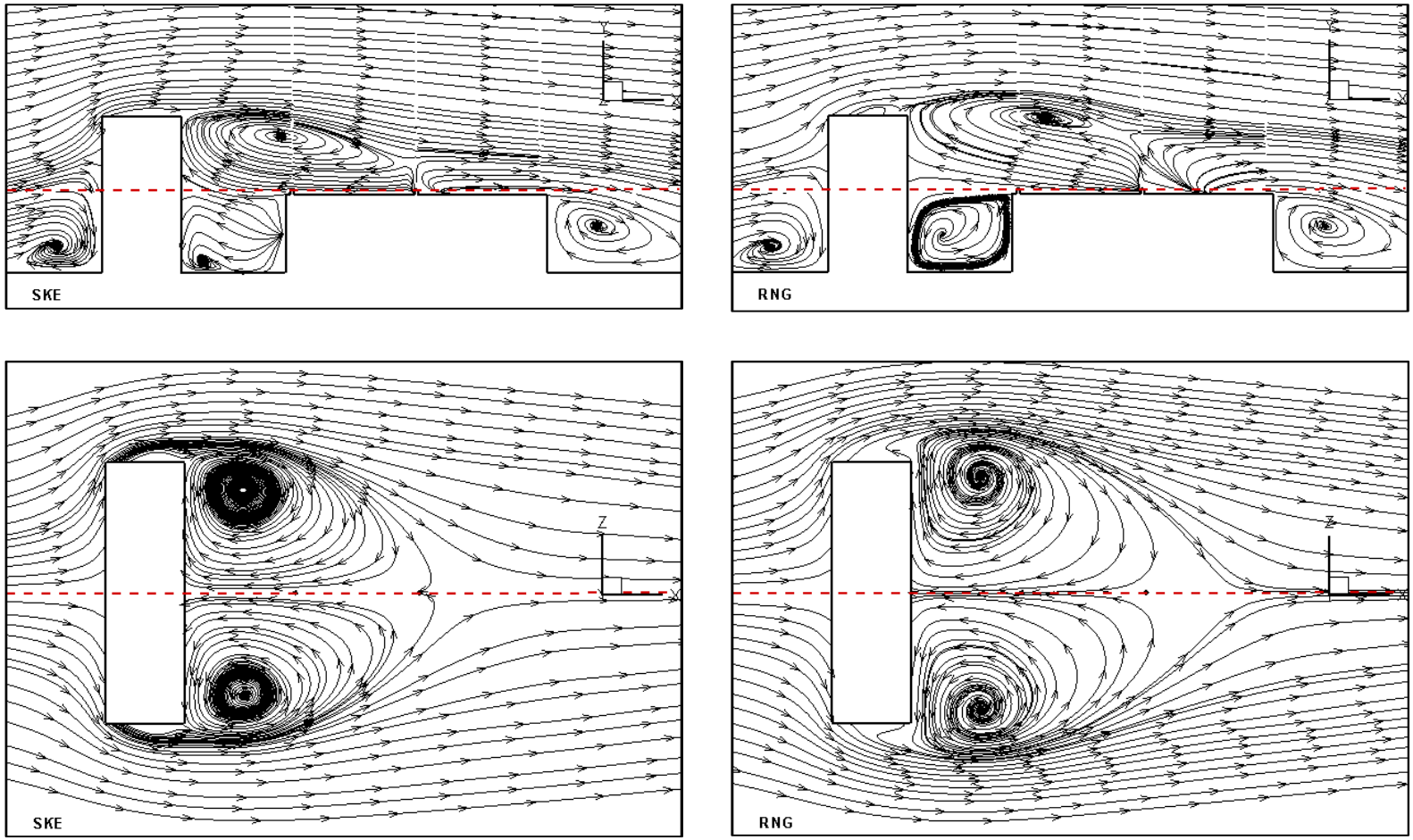

Figure 5-2 . Streamlines of vertical cross-section and plan view at height y = 0.08 m, (a) SKE and (b) RNG

a) RLZ

b) RSM

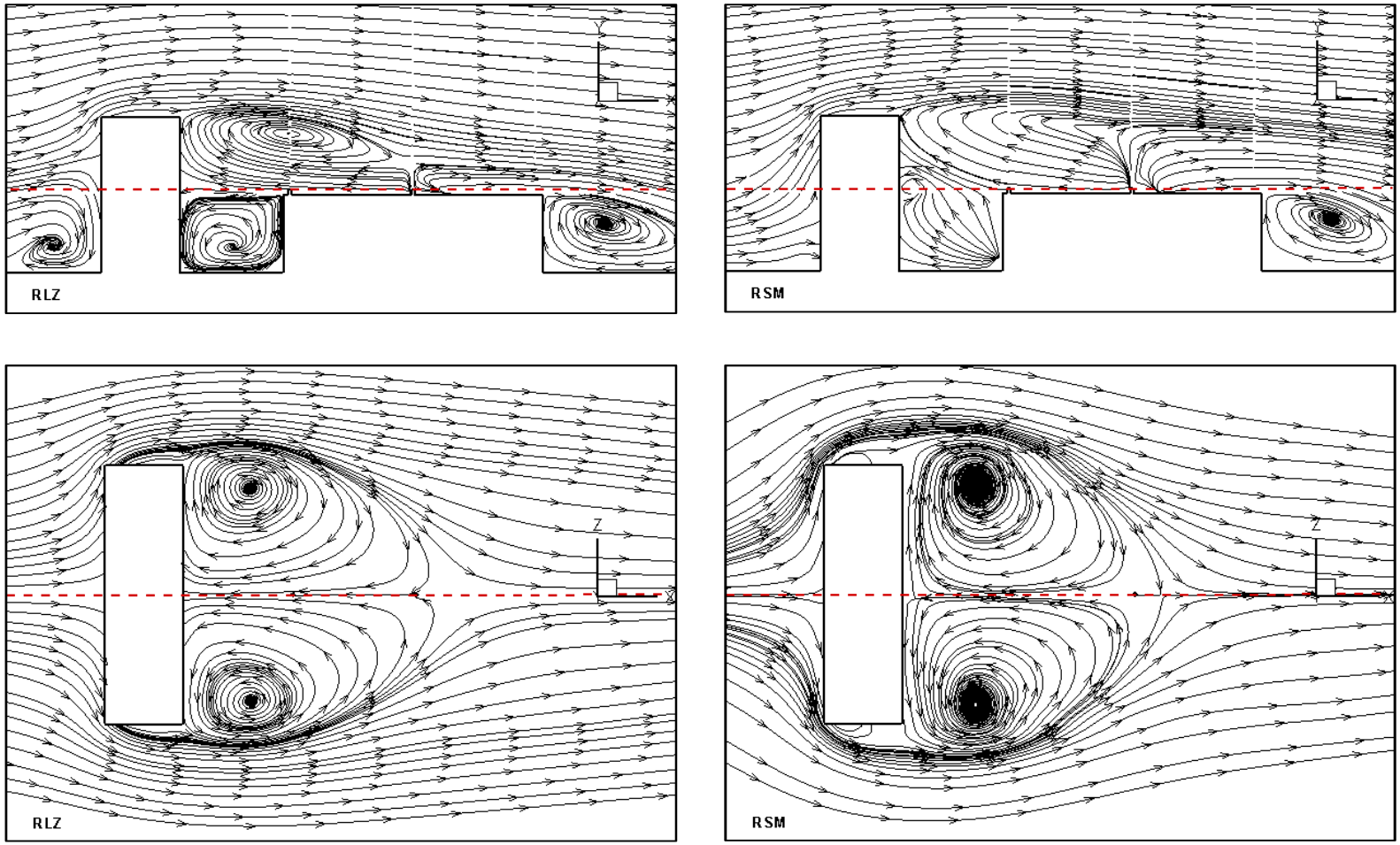

Figure 5-3. Streamlines of vertical cross-section and plan view at height y = 0.08 m, (a) RLZ and (b) RSM

a) SKE

b) RNG

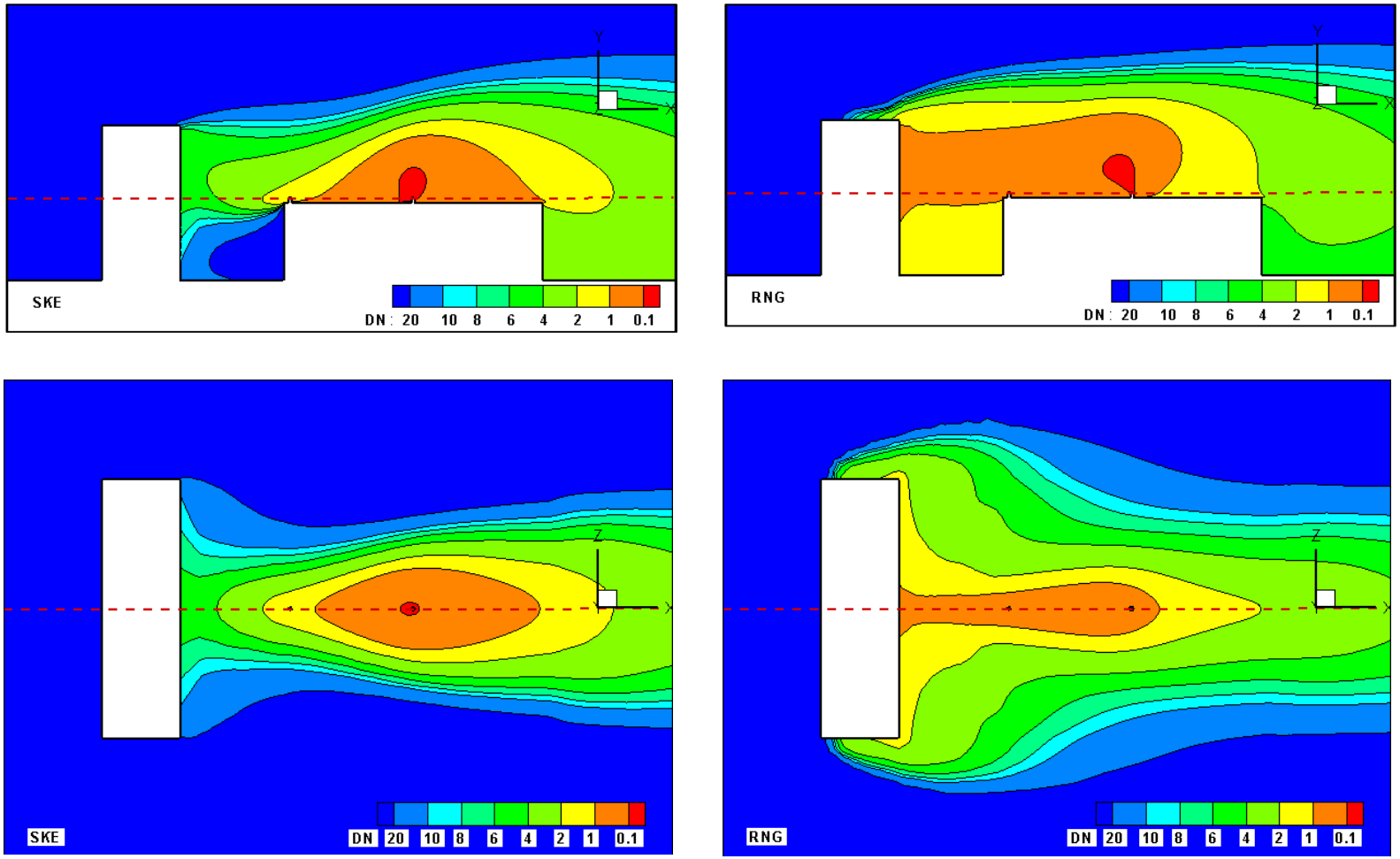

Figure 5-4. Contours of D_N of vertical cross-section and plan view at height y = 0.08 m, (a) SKE and (b) RNG. Using Sct = 0.7 and M=1.7

a) RLZ

b) RSM

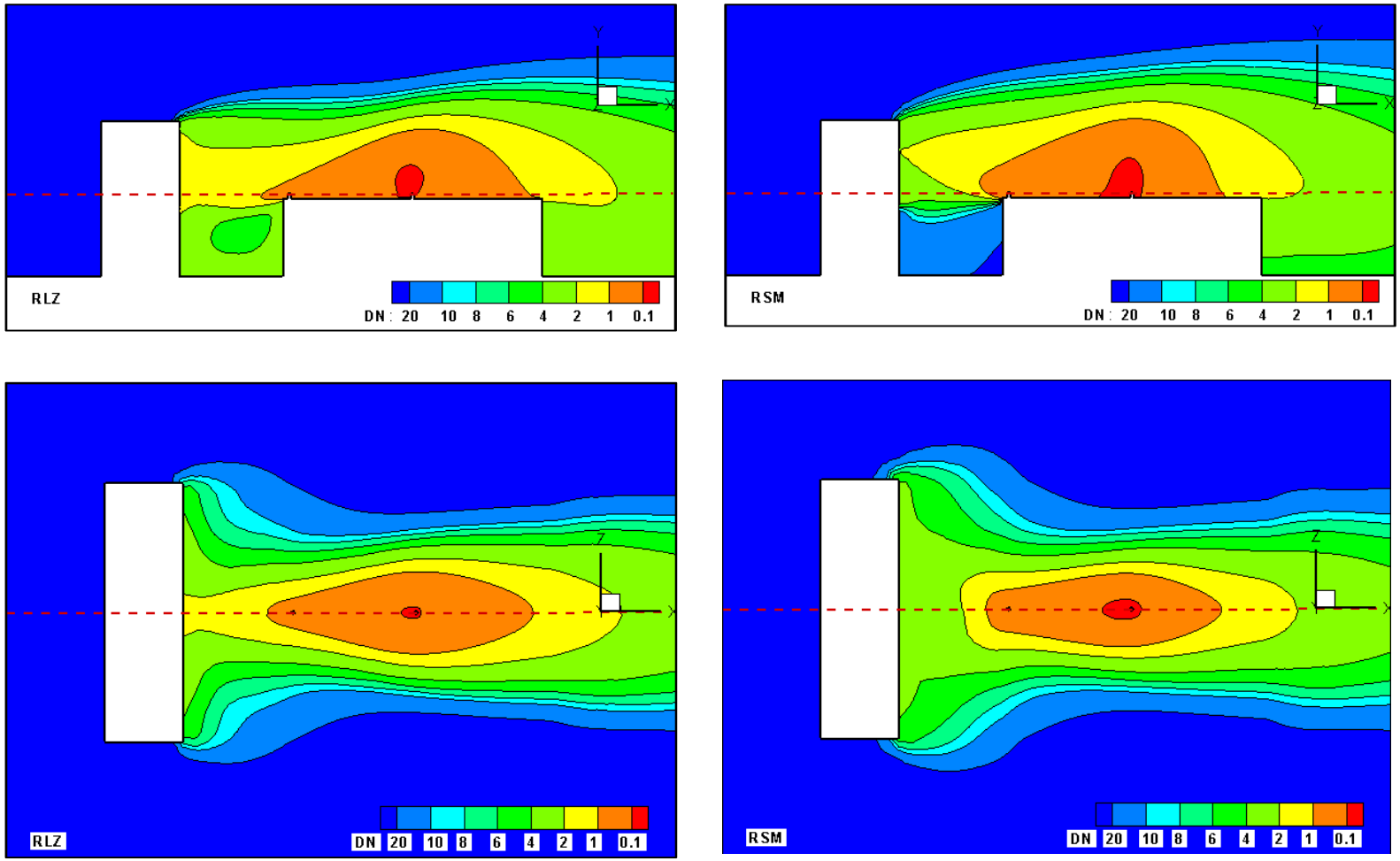

Figure 5-5. Contours of D_N of vertical cross-section and plan view at height y = 0.08 m, (a) RLZ and (b) RSM. Using Sct = 0.7 and M=1.7

To quantify the comparison between all turbulence models with wind tunnel data, Figures 5-6 and 5-7 present the predicted D_N along the central line of b1 for the isolated and non-isolated building configuration. For the isolated case, it is clearly observed that CFD predicts important lower dilutions than wind tunnel at all receptors for all the turbulence models. This is attributable to the underestimation of turbulent diffusion verified in previous studies involving dispersion around an isolated cube (Blocken et al. 2008, Tominaga and Stathopoulos 2009).

Figure 5-7 shows D_N prediction for a two-building configuration. In general, D_N prediction made by all turbulence models follows the trend of experimental data, except in the region close to the stack where no data is available. As the isolated case, an underestimation is perceived in all receptors; however, it is much less severe than the previous isolated case. Values of D_N obtained by SKE and RLZ show similar trends at roof level. RNG shows high D_N at the roof, but relative low D_N (high concentration) at the windward wall of b1. This is related with the strong backflow seen in previous streamlines and iso-contours.

To quantify the proximity of numerical solution to the experimental data, the variance for each turbulence model is calculated using wind tunnel at the reference. The results were: RMS = 0.21, RNG = 1.47, SKE = 1.42 and RLZ = 1.08. In consequence, RSM is indicated as the most accurate model for this case followed by RLZ.

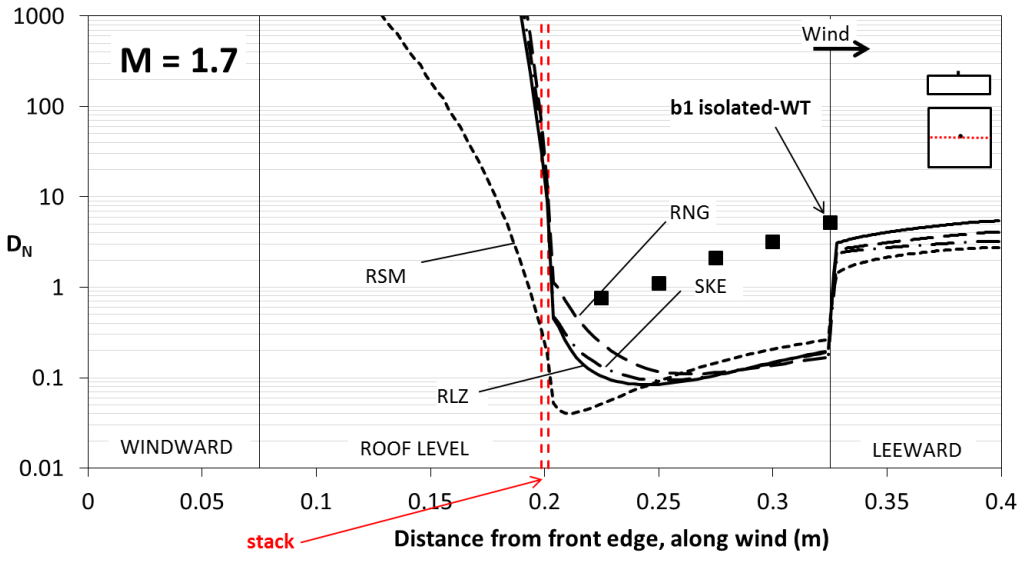

Figure 5-6. Turbulence model on an isolated emitting building (b1). Using Sc_t=0.7

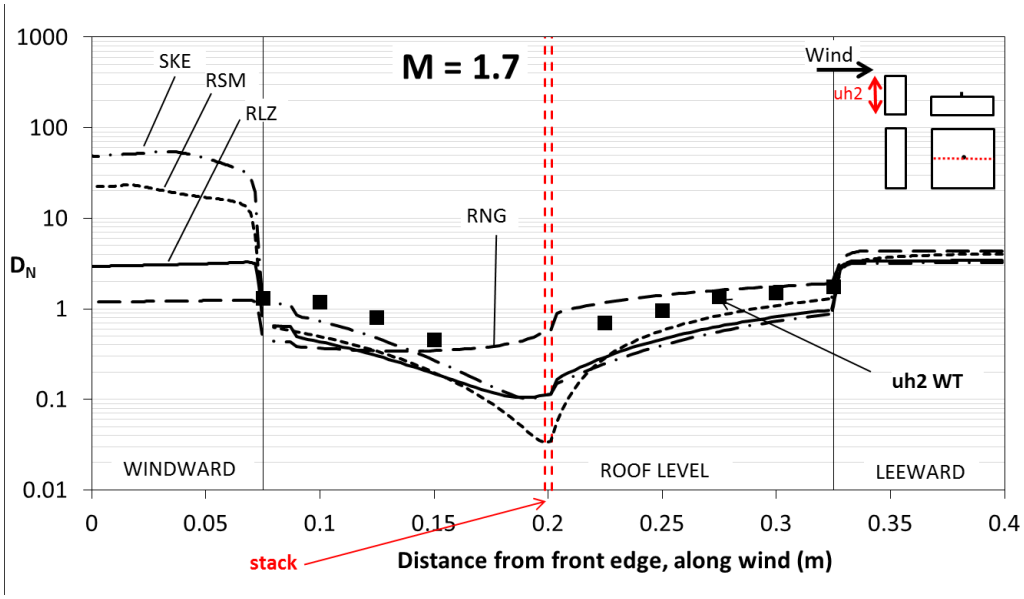

Figure 5-7. Turbulence model on a non-isolated building (uh2 upstream of b1). Using Sc_t=0.7

5.4.2 Turbulent Schmidt number

As discussed in Chapter 4, turbulent Schmidt number (Sc_t) has an important influence in dispersion simulation, and the value used for CFD simulation varies depending on flow characteristics. The following is a sensitivity analysis on Sc_t for same two configurations seen in previous section. All the cases are computed using RLZ turbulence model.

Figures 5-8 and 5-9 show streamlines, velocity contours and D_N prediction for the isolated building and two-building configuration. Three Sc_t values are used in each case. Observing both figures, it is seen that Sc_t has a major influence for the isolated case compared with the two-building case. The underestimation of D_N perceived when using the standard Sc_t = 0.7 can be compensated by reducing Sc_t value. Hence, for the isolated building case and the two-building configurations the optimum Sc_t would be 0.1 and 0.3 respectively. It should be mentioned that Sc_t modification influences only the diffusion mechanism and not the fluid dynamics. The reduction of Sc_t tends to assist the weakness of RANS in simulating fluctuations that activate turbulent diffusion in the wake. However, as discussed by Tominaga and Stathopoulos, (2009) this kind of

cancelation of error cannot be generalized, since there is a strong dependence on flow characteristics. This is clearly confirmed by observing the two figures shown below.

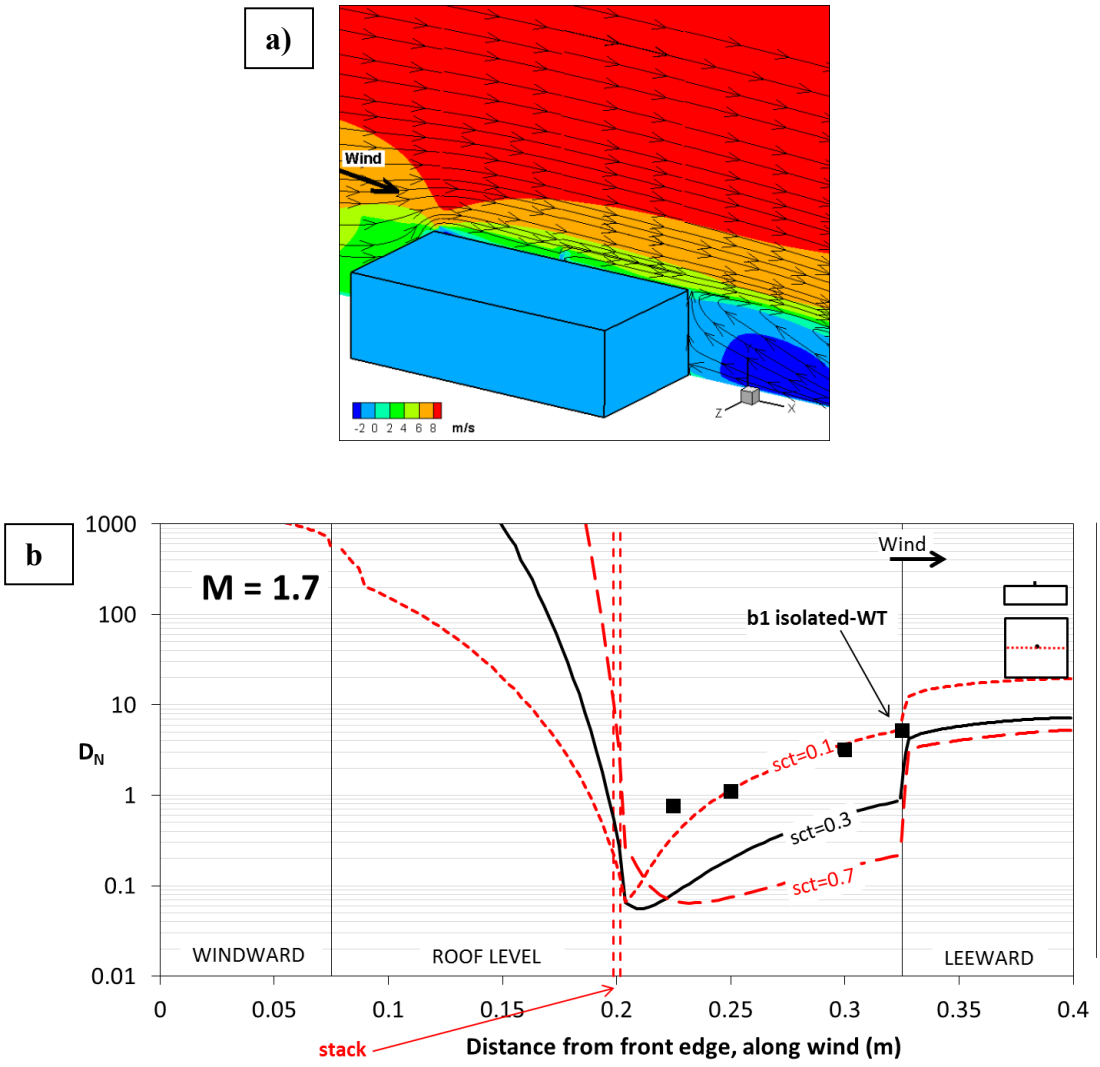

Figure 5-8. Effect of turbulent Schmidt number on an isolated emitting building (b1) using RLZ

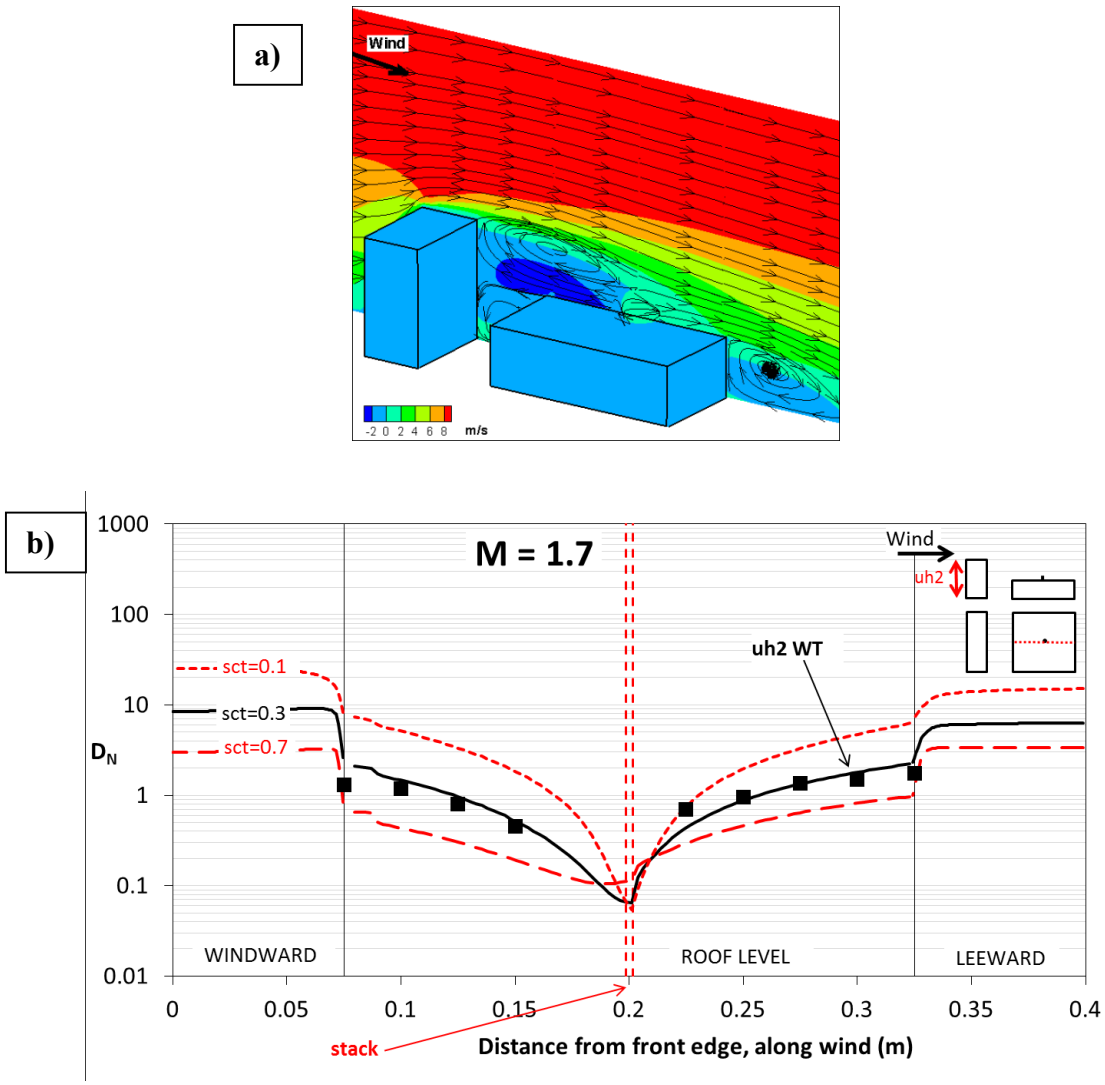

Figure 5-9. Effect of turbulent Schmidt number on a non-isolated building (uh2 upstream of b1) using RLZ

To better visualize the effect of Sc_t on D_N prediction, iso-contours in all surfaces plus iso-surface of $D_N = 1$ have been plotted in Figure 5-10. The iso-surface $D_N = 1$ permits to see the tridimensional behaviour of the plume for different building configuration. It is clearly observed that a lower Sc_t value (0.1) produces a predominant mass diffusivity leading to a plume spreading in all directions with a reduced diffusion along the flow. Then, as Sc_t increases the transport mechanism changes and the plume is progressively advected by the computed dominant flow against reduced mass diffusion. Sc_t influences the mass transport mechanism and not the fluid

dynamics (Di Sabatino et al. 2007). The computed flow, for both cases, plotted in terms of streamlines is included for each case. As shown in this comparison, Sc_t has a large influence on dispersion and the adequate value is highly case-dependence. In the following section, several experimental cases are compared with CFD, in order to detect the most appropriated Sc_t.

5.5 Results

5.5.1 Description of cases

This section compares several wind tunnel cases with CFD results, the objective is to validate the numerical methodology to be used in the current work.

Three different non-isolated building configurations have been considered: a building named ul2 ($2H_b$ x $2L_b$ x W_b) placed upstream of the emitting building (b1), a building named dh4 ($4H_b$ x L_b x W_b) placed downstream of b1 and a third case involving both ul2 placed upstream and dh4 downstream of b1. The three configurations are represented in Figure 5-11. The actual dimensions of the building can be found in Table 7-1 and 7-2.

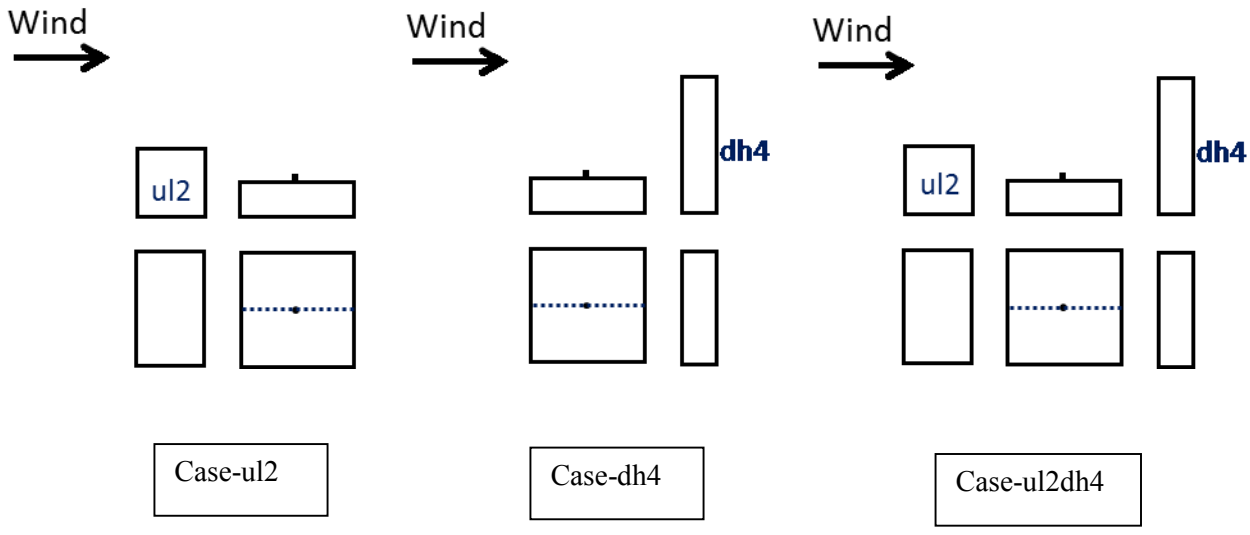

Figure 5-10. Non-isolated building cases used for comparison between CFD and wind tunnel data.

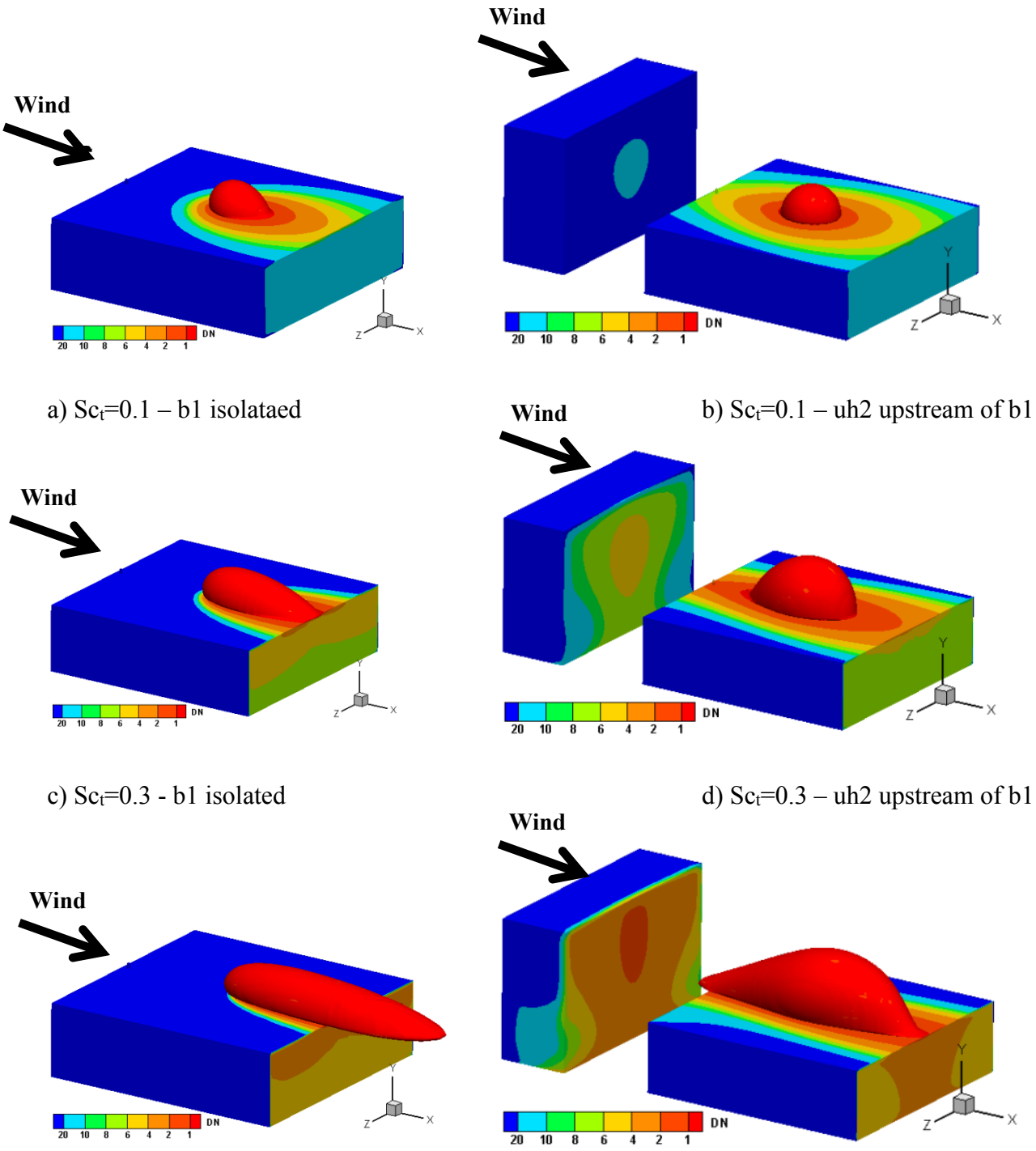

a) Sc_t=0.1 – b1 isolataed

b) Sc_t=0.1 – uh2 upstream of b1

c) Sc_t=0.3 - b1 isolated

d) Sc_t=0.3 – uh2 upstream of b1

e) Sc_t=0.7 - uh2 upstream of b1

f) Sc_t=0.7 – uh4 upstream of b1

Figure 5-11. D_N contours for isolated and a two-building configuration using Sc_t=0.1, 0.3 and 0.7 (RLZ)

For all cases a single wind direction perpendicular to the building face was considered. Dilution concentration measurements were carried out using 9 receptors located centrally on the rooftop of b1 (emitting building) and spaced 0.025m apart and 0.125m from the lateral edges, as shown in the experimental methodology. For Case ul2dh4, 8 receptors were also placed along the windward wall of dh4. These receptors were located centrally, 0.025 m apart starting at 0.075 m from the ground.

5.5.2 Pollutant dispersion in the presence of an upstream building (case-ul2)

Figure 5-12 presents normalized dilution comparisons between wind tunnel, CFD for different Sc_t and ASHRAE-2011 for Case-ul2 when using M =1 and M =3. Receptors were located on rooftop of b1 upwind and downwind the stack. In general, it is observed that a taller upstream building generates lower dilutions on the rooftop of the emitting building. Similar observations were made in the field study carried out by Stathopoulos et al. (2008) on a low-rise building with a taller upstream building. In that study very low dilutions were also registered at the rooftop of emitting building caused by the influence of the upstream building.

Observing both Figures 5-12 (a) and (b) and focusing on the experimental data, it is observed that pollutant were detected in both sides of the stack, but following different trends. For case (a) when M = 1, more pollutants were found in the portion upwind of the stack. This is revealed by low D_N values registered. This phenomenon makes sense since low exhaust momentum at the outlet of the stack do not give pollutants chance to escape from the recirculation zone created by the upstream building. Then, pollutants are likely trapped by the backflow which increases concentration (or decrease D_N) in the upwind portion of the roof. On the other hand, for M = 3 pollutants probably have more chance to get through the recirculation envelope and be transported away for the wind flow. This explain greater D_N compared with M = 1 especially upwind the stack. Moreover, for M = 3 pollutant distribution seems to have a uniform distribution over the entire roof which probably means that pollutants, within the recirculation zone, are well mixed due to turbulence.

Observing the same figures, but now focusing on CFD simulations in particularly for the standard Sc_t which is 0.7, it is noticed that CFD tends to systematically underestimate D_N

downwind of the stack. The underestimation is more pronounced for M = 3 in the downwind part of the roof. It is observed that, in general, D_N prediction is very sensitive to Sc_t used in particular for locations far away from the stack.

In Figure 5-12 (a), which corresponds to a 1 m stack at M = 1, it is noticed that D_N from wind tunnel and CFD compare well for Sc_t = 0.3 at receptors located downwind of the stack. However, upwind of the stack wind tunnel data and CFD compare well using the standard Sc_t = 0.7. In Figure 5-12 (b), which corresponds to a 1 m stack at M = 3, it is noticed that D_N from wind tunnel and CFD compare well for Sc_t = 0.1 at receptors located downwind of the stack. Upwind of the stack wind tunnel data and CFD compare well using the Sc_t = 0.3. However, it should mentioned that CFD results with Sc_t =0.3 and 0.7 upwind of the stack are very similar, then in this portion of the roof could be appropriated either 0.3 or 0.7.

ASHRAE-2011 predicts very low dilutions (too conservative) at all receptors making it necessary to re-visit its formulations. Although, ASHRAE 2011 is based on wind tunnel experimental data the terrain roughness and turbulence generated due to local topography and buildings to assess plume dilutions have not been considered. Additionally, the plume rise equation of Briggs (1984) predicts low plume rise resulting in less plume spread along the roof of the building. Therefore, the dilutions predicted by ASHRAE are overly conservative. Additional limitations include its inability to simulate rooftop structures and assessing dilutions on the wall of the adjacent building (see Hajra, 2012).

5.5.3 Pollutant dispersion in the presence of a tall downstream building (case-dh4)

Figure 5-13 presents normalized dilution comparisons between wind tunnel, CFD for different Sc_t and ASHRAE-2011 for case-dh4 when using M =1 (a) and M =3 (b). It should be mentioned that no concentrations were found upstream of the stack for both cases. This is why no experimental data were plotted in both figures for this portion of the roof.

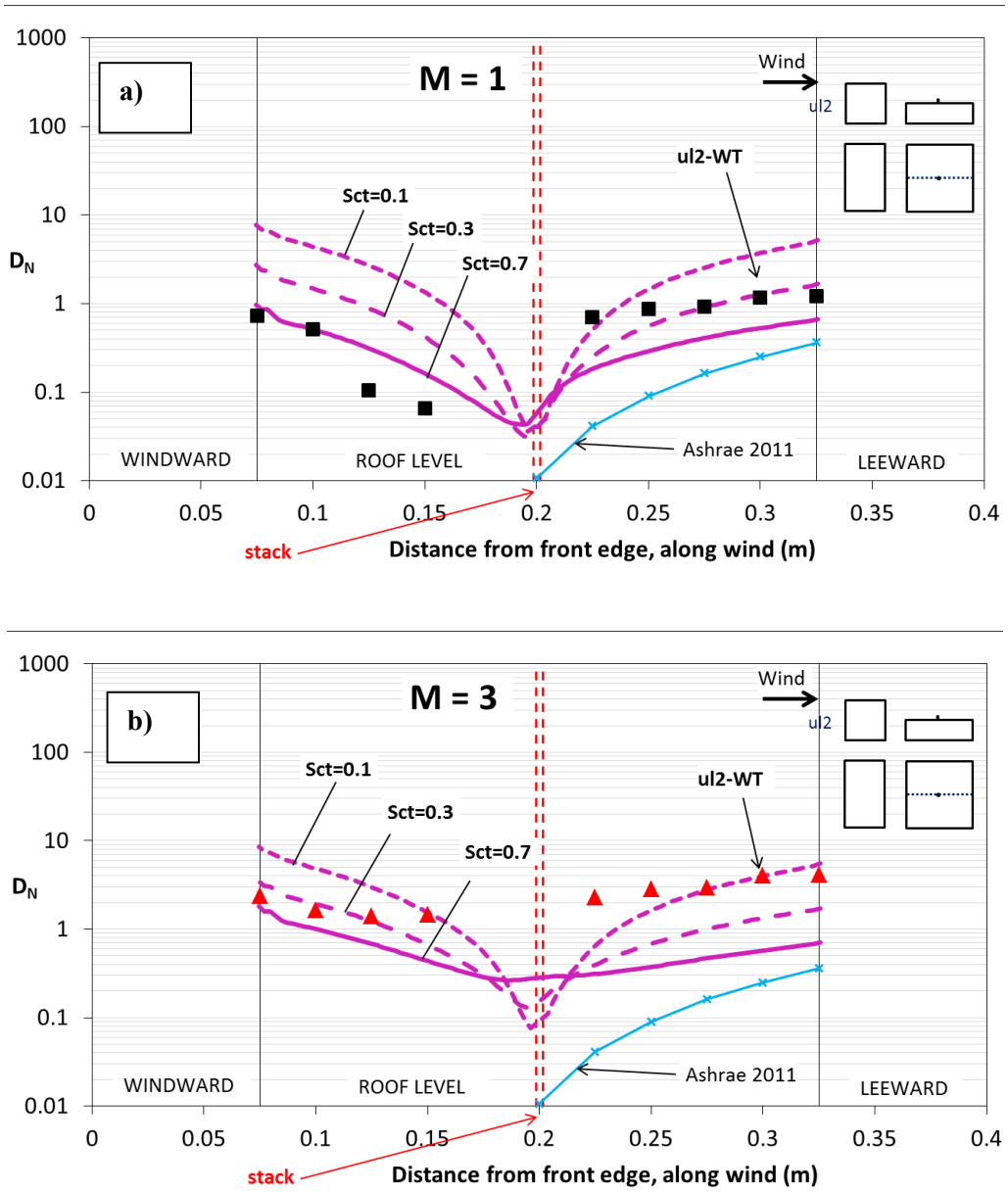

Figure 5-12. D_N prediction for a non-isolated building (ul2 upstream of b1) when stack is in the middle of the roof using RLZ. M = 1 (a) and M = 3 (b)

Focusing on the experimental data in Figure 5-13 (a) and (b), it is observed that both cases show similar trends of dispersion distribution, which is D_N increases almost linearly from the stack toward the back edge of b1. This reveals that pollutants are diluted by the wind as they are transported downwind from the stack. For M = 1, about 10 times more pollutants were detected

all along the roof level of b1 compared with M = 3. This difference makes sense since M = 1 reduces the spreading in the atmosphere due to low expulsion velocity, therefore greater concentrations are found at low surfaces (roof level).

The numerical results show that D_N is strongly sensitive to Sc_t. It can be mentioned that Sc_t behaves very similar to the isolated building case observed in Figure 5-6. The numerical simulations show that D_N is somewhat well predicted when the standard $Sc_t = 0.7$ is used for M = 1. However, as the exhaust momentum increases to M = 3, CFD modelling underestimate D_N values for $Sc_t = 0.7$. To approximate numerical results with experimental data Sc_t should be decreased somewhere between 0.1 and 0.3.

ASHRAE 2011 results shows an acceptable agreement with experimental data for M = 1; however for M = 3 it shoes an important underestimation, as seen previously.

5.5.4 Pollutant dispersion between two adjacent buildings (case-ul2dh4)

Figure 5-14 presents normalized dilution comparisons between wind tunnel, CFD for different Sc_t and ASHRAE-2011 for case-ul2dh4 when using M =1 (a) and M =3 (b).

Observing the experimental data, it is noted that the addition of a third building upstream of b1 generates much lower D_N upwind of the stack in comparison with the previous case (case dh4). In fact, the present three building configuration is the worst case (in terms of low dilution at roof level) among the configurations presented in the current section. As case-ul2, pollutants are dragged towards the leeward of the upstream building showing lower D_N values in all the upwind portion of the roof. Same pattern is registered for both M = 1 and M = 3.

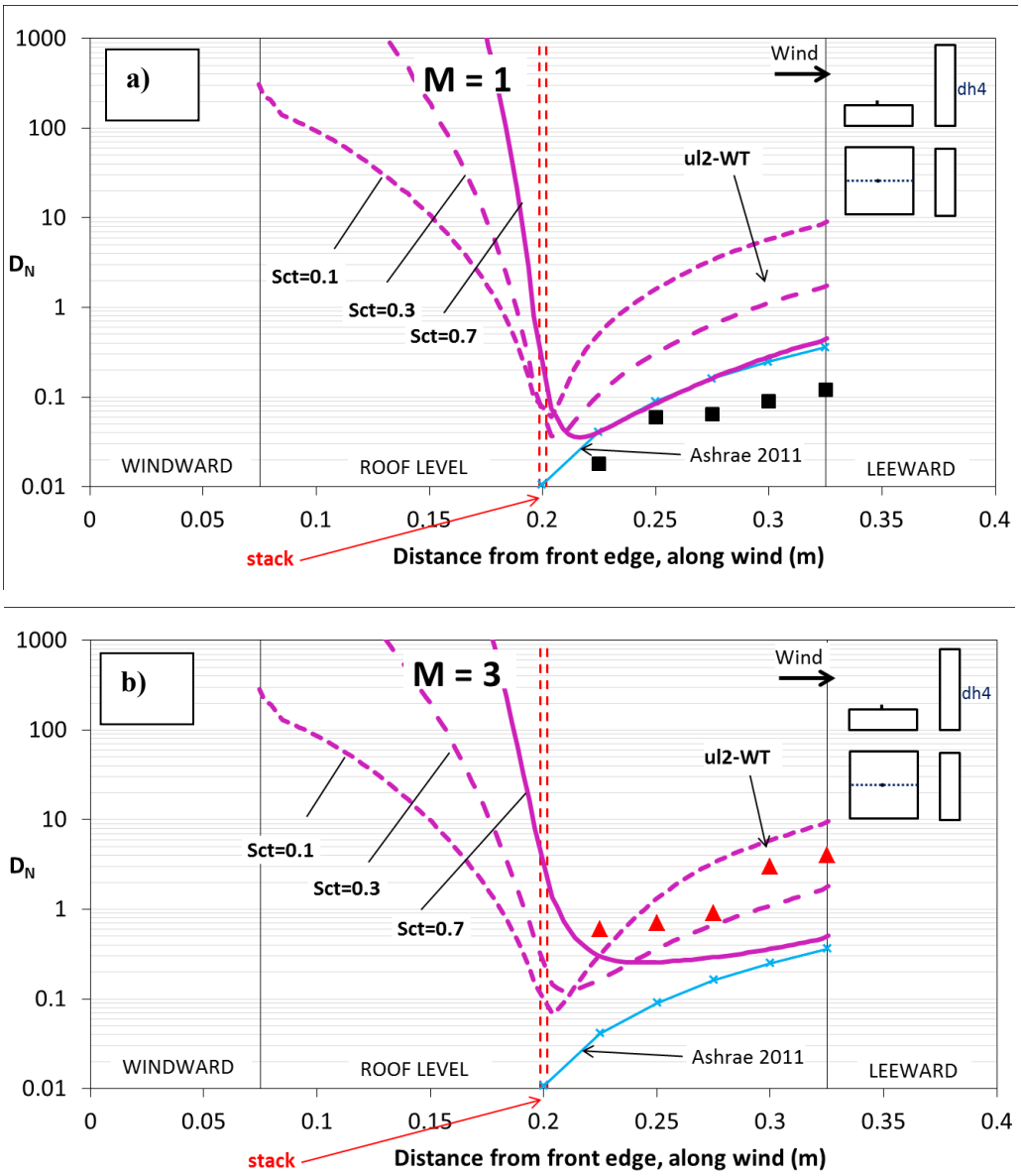

Figure 5-13. D_N prediction for a non-isolated building (dh4 downstream of b1) when stack is in the middle of the roof using RLZ. M = 1 (a) and M = 3 (b)

It is observed that the trend obtained by CFD using $Sc_t = 0.7$ agree well with experimental data for both cases M = 1 and M = 3. It is also noted that D_N is strongly sensitive to Sc_t upwind of the stack and very low sensitive downstream the stack.

D_N were also found on the windward wall of the downstream building (dh4). Wind tunnel data were found to be comparable with those from CFD, irrespective of the value of Sc_t, in the upper part of dh4 as shown in Figure 5-15. In the lower part of dh4 some overestimation is detected with $Sc_t = 0.7$; however the trend are comparable. This agreement indicates that CFD reproduces well dilutions in the downwind region of the stack between b1 and the downstream building.

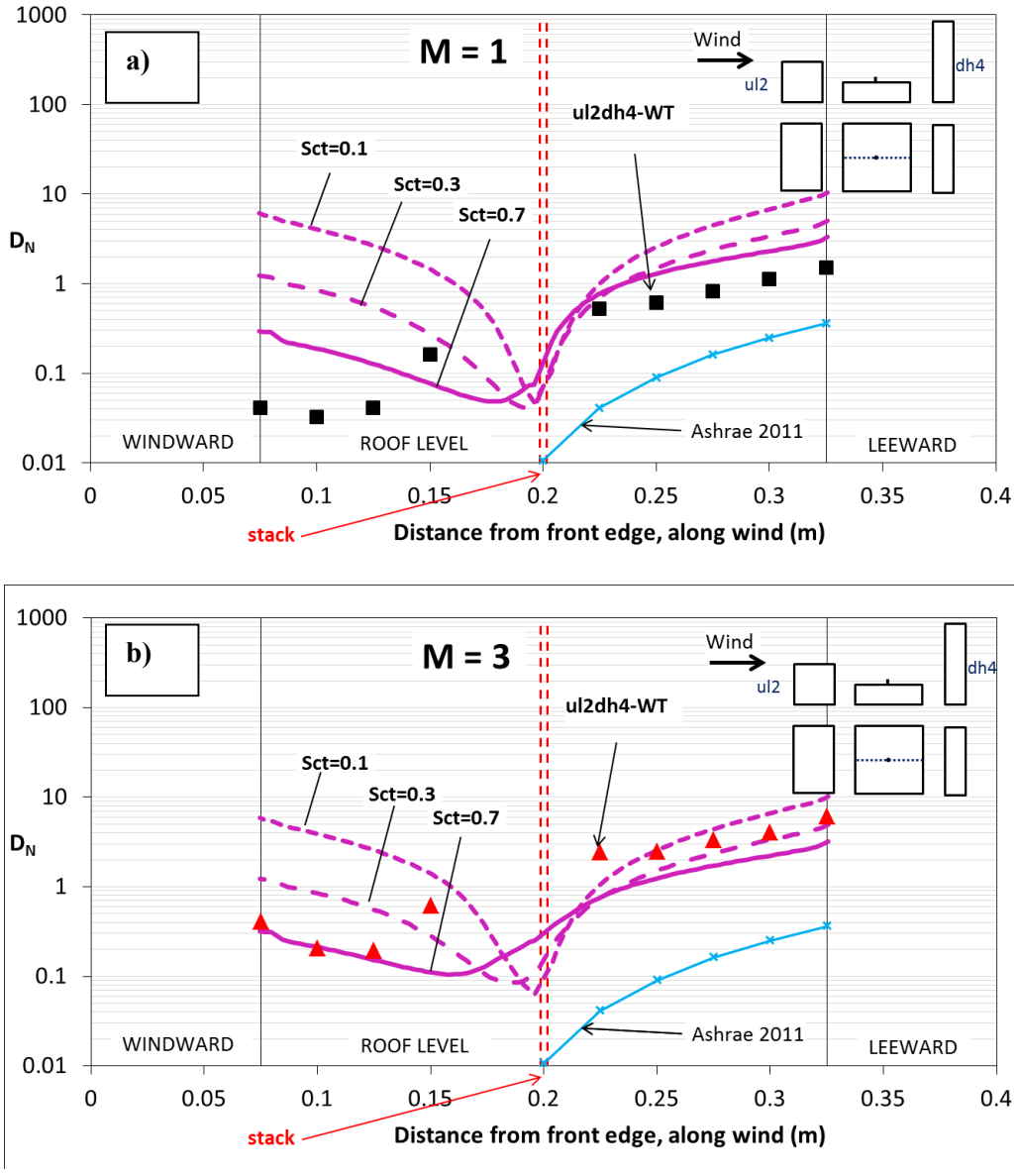

Figure 5-14. D_N prediction for a non-isolated building (b1 between ul2 and dh4) when stack is in the middle of the roof using RLZ. (a) M = 1 (a) and (b) M = 3

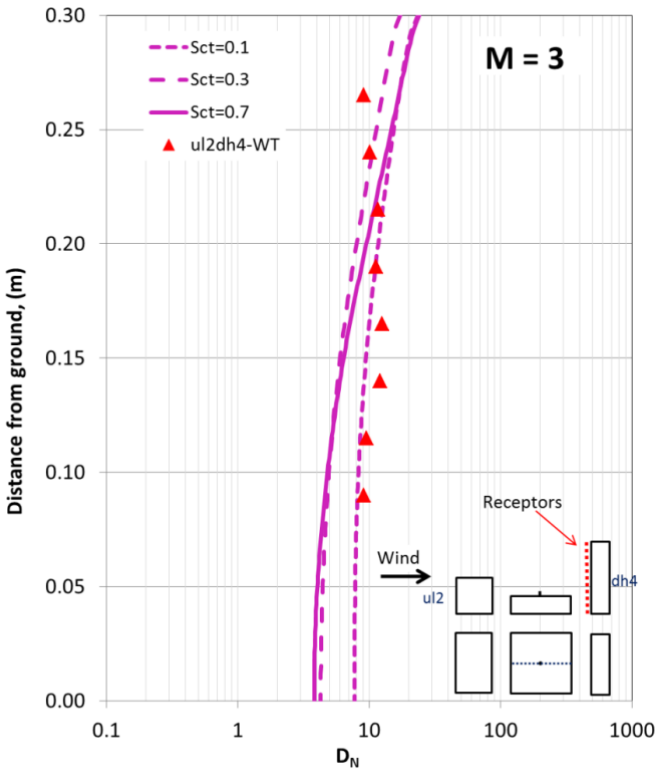

Figure 5-15. D_N prediction for a non-isolated building (b1 between ul2 and dh4) when stack is in the middle of the roof using RLZ. M = 3

5.6 Additional remarks about turbulent Schmidt number

The numerical results show generally acceptable D_N trend compared with experimental data for all the cases when low exhaust momentum (M = 1) and standard Sc_t (=0.7) is specified. Therefore, for those cases, it can be said that CFD reproduces well the physics of the problem. However, as observed along the three previous cases, numerical results show a systematic underestimation of D_N values when high exhaust momentum (e.g. M =3) is specified. This is especially true for simple building configurations as isolated emitting building or two-building configurations. In these cases a reduction of Sc_t number, which artificially increases turbulent diffusion, can help to match with experimental data. For complex building configuration, as a three-building case, it seems that standard Sc_t (0.7) performs well independently of M used, thus no changes on Sc_t are needed.

It is impossible to generalise a particular Sct in CFD due to the complex flow structure of pollutant transport which are unique to each case. However, based in the current study some suggestion can be made. These suggestions are summarized in Table 5-1.

Table 5-1. Suggestions of Sct for different building configurations

	Low M (e.g. M = 1)	High M (e.g. M = 3)
Isolated b1	Sc_t = 0.7	Sc_t = 0.1 - 0.3
A building located downstream of b1	Sc_t = 0.7	Sc_t = 0.1 - 0.3
A building located upstream of b1	Sc_t = 0.7	Sc_t = 0.3 - 0.5
b1 between two or more buildings	Sc_t = 0.7	Sc_t = 0.7

5.7 Summary

This Chapter presented steady CFD simulations and compared results with wind tunnel data for validation purposes. Turbulence model and turbulent Schmidt number (Sc_t) were analysed in order to determine the appropriated approach to be used in the rest of the current work. Realizable turbulent model was chosen and particular Sc_t coefficients, depending on the building configuration, were suggested. ASHRAE prediction model was tested and compared with wind tunnel and CFD. It was concluded that ASHRAE is overly conservative for D_N prediction. Based on these results, suggestions of Sc_t for different building configurations were presented.

6. COMPARISON BETWEEN UNSTEADY CFD, WIND TUNNEL AND ASHRAE MODEL

6.1 General

This chapter addresses pollutant dispersion for a two-building configuration focusing on transient CFD simulation approaches. Three unsteady modelling techniques are compared: unsteady Reynolds-Averaged Navier-Stokes (URANS), Large Eddy Simulation (LES) and Detached Eddy Simulation (DES). Wind tunnel data for the same configuration is used as reference results. The influence of three numerical parameters: mesh size, time step and inlet boundary conditions are evaluated in terms of normalized dilution, D_N, at the roof level of the emitting building b1.

6.2 Introduction

Flows within urban areas are highly turbulent and this causes pollutant mixing and rapid dilution in the near field from the source. The existence of complex vortical structures around buildings is the main difficulty to predict accurately pollutant concentrations. The most frequently used approach for turbulent flow simulation is the set of Reynolds-Averaged Navier-Stokes (RANS) equations. However, numerous publications confirm that inaccuracies for dispersion prediction, especially in the near-field of an emitting building, are detected due to the RANS inherent incapability of reproducing flow unsteadiness in detached regions (Chavez et al. 2012).

To address this issue – while keeping low computational cost – some effort was made to use the unsteady RANS approach (URANS) with unsatisfactory results. Indeed URANS performance problems can be found in the literature, which suggests that further investigation is needed for complex flow conditions (Iaccarino et al. 2003). For this reason, RANS is being replaced by the unsteady approach LES. The attractiveness of LES lies on the fact that only small scales of turbulence are modeled, while large turbulent structures are directly solved. This is beneficial for dispersion modeling since the transport of pollutants is mainly driven by large scales of turbulence (Gousseau et al. 2011). The computational cost of LES, however, is extremely high. To solve the computing effort issue, a hybrid URANS/LES technique called Detached Eddy

Simulation (DES), known as the most widely used hybrid modeling strategy (Franke et al. 2009), is being increasingly used for modeling flow around complex geometries. A hybrid method incorporates a turbulence model near the wall and solves directly the flow in regions of free and separated flow. In other words, hybrid approaches combine the strengths of URANS and LES. In the present chapter, the DES technique has been used and compared with URANS and LES models.

6.3 Methodology

As already mentioned, the present chapter investigates the dispersion of pollutants using three unsteady approaches: URANS, LES and DES. The physical model used is a two-building configuration corresponding to case-uh2 already presented in Figure 4-1 in Chapter 4. The meshing is constructed principally using hexahedral grids with structured mesh refinement near the walls of both buildings. Two meshes with a refinement factor of 1.5 are tested for each numerical approach. The meshes used are: coarse mesh (624,893 cells) and fine mesh (1,460,520 cells). The pollutant exhaust momentum, which is the ratio between the exhaust velocity and the mean wind speed at the building height: $M=Ve/U_H$ (where Ve is the exhaust velocity = 6.2 m/s) is the same in all numerical simulations as M = 1.7. It should be mentioned that M = 1.7 correspond to a Re at the stack of 2016, which is the minimum Re to assure turbulent flow in a pipe, as suggested by Snyder (1981), and discussed in Chapter 3.

Since the experimental data used were obtained for M =1 and M = 3, a linear interpolation of those data is made in order to have a comparable set of numerical and experimental results. The Sc_t is specified equal to 0.3 for dispersion modelling which, as seen in previous chapter, it represents a good comprise for acceptable agreement between CFD and wind tunnel data for non-isolated configurations. When performing unsteady simulation, time step size is an important parameter to observe. In this chapter, different time steps are tested in order to determine its influence on D_N predictions. Hence, URANS simulations were performed using 0.1s, 0.01s and 0.001s. Similarly, DES and LES were performed using 0.1s, 0.01s, and 0.005s.

The inlet boundary conditions for URANS followed the suggestions proposed in Chapter 4. For DES and LES random perturbations at the inlet velocity profile are tested following the Vortex Model (VM) proposed by Sergent (2002) and implemented in Fluent (Fluent, 2009). In essence, the VM generates two-dimensional transverse fluctuations which are added to the mean velocity profile.

For the URANS and DES simulations all the transport equations are discretized using a second-order upwind scheme and the SIMPLE algorithm is used for pressure-velocity coupling. For LES the filtered momentum equation is discretized with a bounded central-differencing scheme. For the energy and concentration equations a second-order upwind scheme is used. Pressure interpolation is defined second order. For LES approach, the smallest scales of flow are modeled with a standard Smagorinsky model.

It should be said that LES simulations are performed without applying any particular meshing strategy more than the two meshes mentioned before. This is a relevant issue considering that LES is highly sensitive to mesh quality in particular near to walls. The aim is to compare unsteady approaches under similar conditions, including meshing characteristics. In this sense the LES simulations performed in the current work should be considered as yielding preliminary results.

All cases are started from a converged steady RANS (using Realizable turbulence model) solution and stabilized during 5s, which was the time duration to observe a statistically stable unsteady solution. The average mean values for velocities and D_N values in the unsteady solution are calculated considering 5s simulation. This simulation period represents approximately 5 times the mean flow residence time (L_{domain}/U_H) where L_{domain} is the length of the computational domain (Fluent, 2009).

6.4 Validation and sensitivity analysis

In this section, three numerical parameters (mesh size, time step and inlet boundary conditions) are evaluated for each unsteady approach. The objective is to determine the range of influence of such parameters for D_N prediction in a non-isolated building configuration. Inspired

by Meroney et al. (1999), it must be mentioned that no further effort, apart from the investigation of mentioned parameters, is given to find the best numerical model in order to maximize the agreement with experimental data. In fact, standard coefficients and common numerical configurations are used to compare URANS, DES and LES for simulating a practical engineering problem such the representative urban pollutant situation shown in Figure 4-1.

6.4.1 URANS

6.4.1.1 Effect of meshing

This subsection examines the influence of meshing for D_N prediction at walls and roof of b1 for URANS approach. It should be mentioned that steady RANS simulation is included in the analysis for comparison purposes. All the cases are computed using RLZ turbulence model.

Figure 6-1 shows a comparison of RANS with fine and coarse mesh and URANS with fine mesh only. The unsteady calculation is performed using a fixed time step of 0.01s. Simulations with three Sc_t are also presented for RANS, but only Sc_t = 0.3 for URANS. It is verified, as mentioned in previous chapters, that for a two-building configuration the choice of Sc_t = 0.3 is justified due to better agreement with experimental data. The results for coarse and fine meshes show very small difference on D_N prediction at roof level of b1. A small effect is only perceived on the windward wall of b1 when using a standard Sct = 0.7. It should be mentioned that during the calculation of URANS any turbulent structure was found in the wake of b1, in consequence, the results converged to same values obtained by RANS.

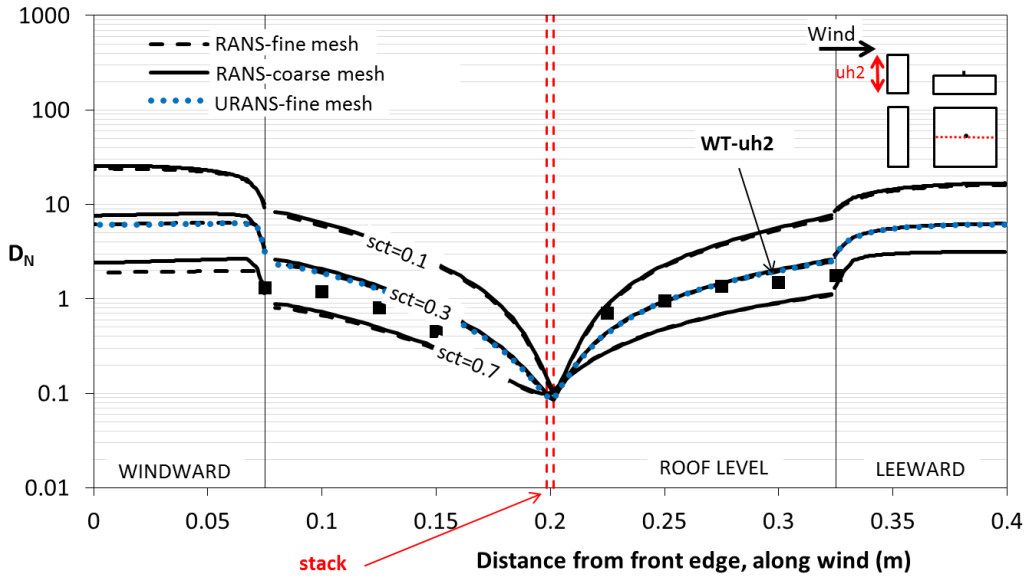

Figure 6-1. D_N prediction obtained by RANS (fine and coarse mesh) and URANS with fine mesh and time step = 0.01s using RLZ

6.4.1.2 Effect of time step

The URANS equations are the usual RANS equations, but with the transient term retained. The interest of running URANS calculation is to detect unsteadiness in the flow by using less computational effort compared with more expensive approaches (e.g. LES) (Davidson, 2003). The basic assumption is that turbulent time scale is much less that mean flow time scale; then, if the averaging time (time step) is larger than turbulent time scale but smaller than the mean flow time scale it would be possible to capture large-scale unsteadiness (Frohlich and Terzi, 2008). Such unsteadiness is governed by large separations and pronounced turbulent structures such as those found in wake flow. The following is a sensibility analysis of time step reduction for URANS. Figure 6-2 shows the results of three time step; 0.1, 0.01, 0.001s. The observation of results reveals that no changes in D_N prediction are registered and solutions are identical. As previously mentioned, no fluctuations were captured during the simulations. The reason is likely because the turbulence model used for URANS (Realizable k-ε) is still too dissipative, which damps out unsteadiness cancelling the possible oscillations.

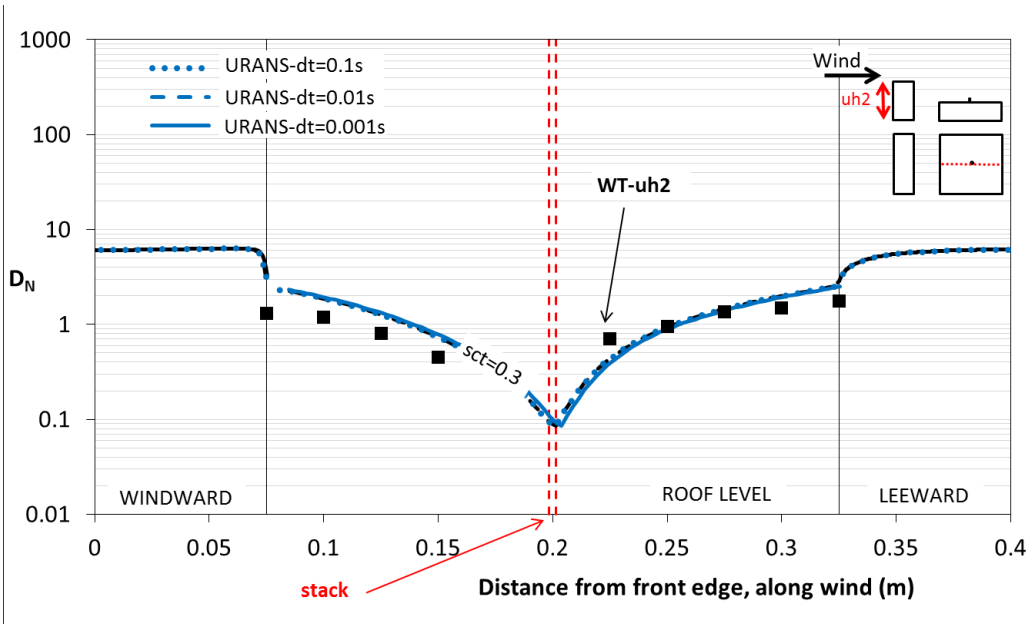

Figure 6-2. D_N prediction obtained by URANS, for different time steps using fine meshing

6.4.2 DES

6.4.2.1 Effect of meshing

This subsection examines the influence of meshing for dilution prediction at walls and roof of b1 for DES approach. As described in Chapter 4, DES is a hybrid model that combines URANS and LES strategy based on the grid resolution. In the near wall region or in regions were the grid resolution is not sufficiently fine URANS equations are applied. In the rest of domain LES is used where its performance is superior to URANS. The switching from URANS to LES is made by a comparison of turbulent length scale with the grid spacing. Then, as the grid is refined below the turbulence length a "DES-limiter" is activated and switches from URANS to LES mode (Fluent, 2009).

Figure 6-3 shows DES solutions using fine and coarse mesh and compared with wind tunnel data. The time step used was 0.01s. In general, it is perceived that an important disagreement with experimental results is obtained with both meshes, and this, at both sides of the stack. Upwind the stack D_N is underestimated and downwind the stack D_N is overestimated. It is interesting to

mention that DES prediction seems to be favorably affected by mesh refinement downwind of the stack only. This is probably related to the location of the reattachment point of the recirculation region behind the upstream building which is a complex flow structure. The difference in D_N observed suggest that more mesh is needed.

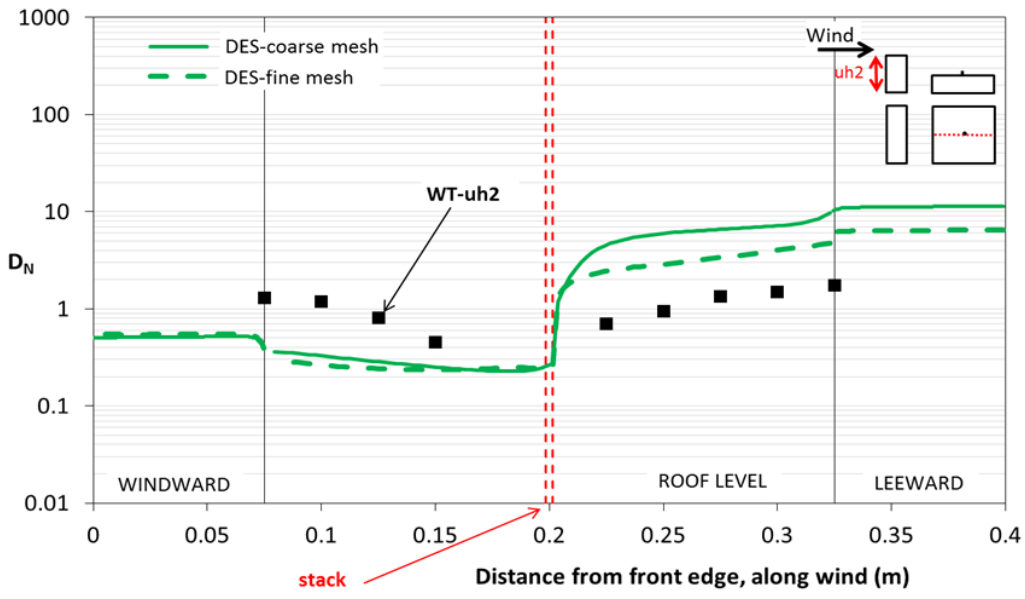

Figure 6-3. D_N prediction obtained by DES (fine and coarse mesh) and time step = 0.01s

6.4.2.2 Effect of time step

Figure 6-4 describes the effect of reducing time step size for DES. Considering a fine mesh D_N prediction is plotted for three time step: 0.1s, 0.01s, and 0.005s. The observation of results, regardless the disagreement with experimental data, reveals a monotonic convergence as the time step decreases. Additionally, as observed with meshing effect, time step reduction only affect the downwind part of the roof.

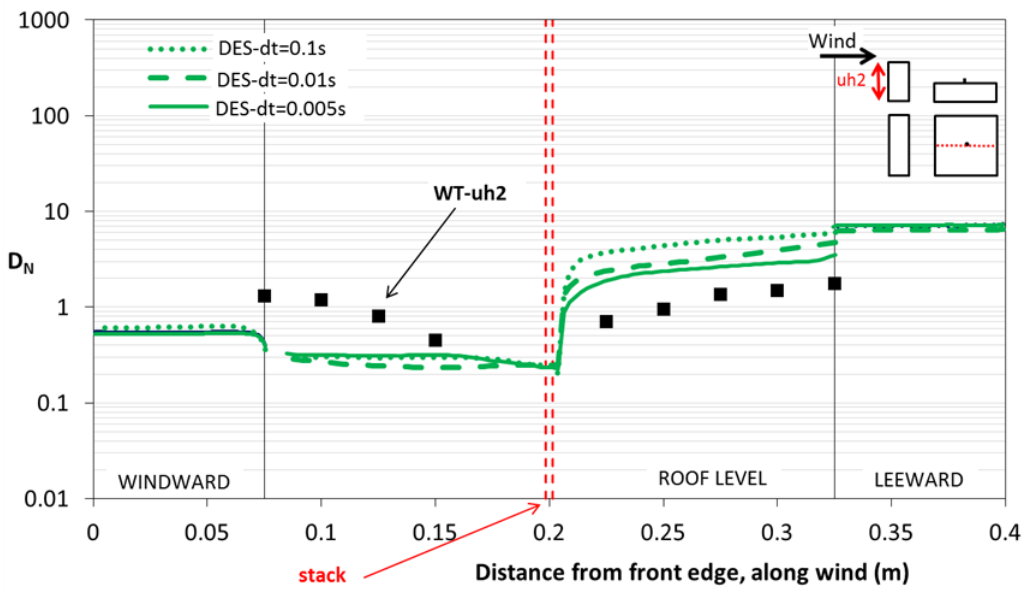

Figure 6-4. D_N prediction obtained by DES, for different time steps using fine meshing

6.4.2.3 Effect of vortex generator

Figure 6-5 shows the effect of including a time-dependent inlet condition in DES. Two cases were evaluated, with and without inlet perturbations. Not considering perturbations means that fluctuations in the approaching flow are neglected, so the instantaneous velocities at the inlet are identical to the mean velocities. This option is suitable when the level of turbulence at the inlet boundaries do not affect the accuracy of results (Fluent, 2009). Considering perturbation means to generate a time-dependent inlet condition by including 2D random fluctuations in the plan normal to the streamwise direction (Sergent, 2002). The fluctuations are introduced in the calculation by specifying a number of vortices, in this case 200, at the inlet boundary condition. The vortex model (VM) algorithm is already implemented in Fluent (Fluent, 2009).

The solution presented in Figure 6-5 reveals that inlet VM has an important effect of D_N prediction. In fact, when considering VM in the numerical model the solution reaches a good agreement with experimental data in practically all the points. It is noted that including VM makes D_N prediction decrease downwind of the stack and increase upwind of the stack. It seems that additional fluctuations in the approaching flow change the length of the recirculation region in the

along wind direction. In fact the "no VM" case shows lower dilution in the upwind part of the roof and higher dilution in the downwind part of the roof. This means that the plume was completely trapped by the recirculation region and practically all the pollutants were dragged upwind (this also explain the abrupt change of D_N at the stack location). In this case the recirculation length is some were downwind the stack. On the other hand, when VM is included, D_N increases upwind of the stack and decreases downwind of the stack. In this case, the plume seems to be partially trapped by the recirculation region, and pollutants are spread in both sides of the roof. This change in D_N prediction might be because of the intermittent summary of high and low concentrations produced by the flow fluctuation of VM at the inlet.

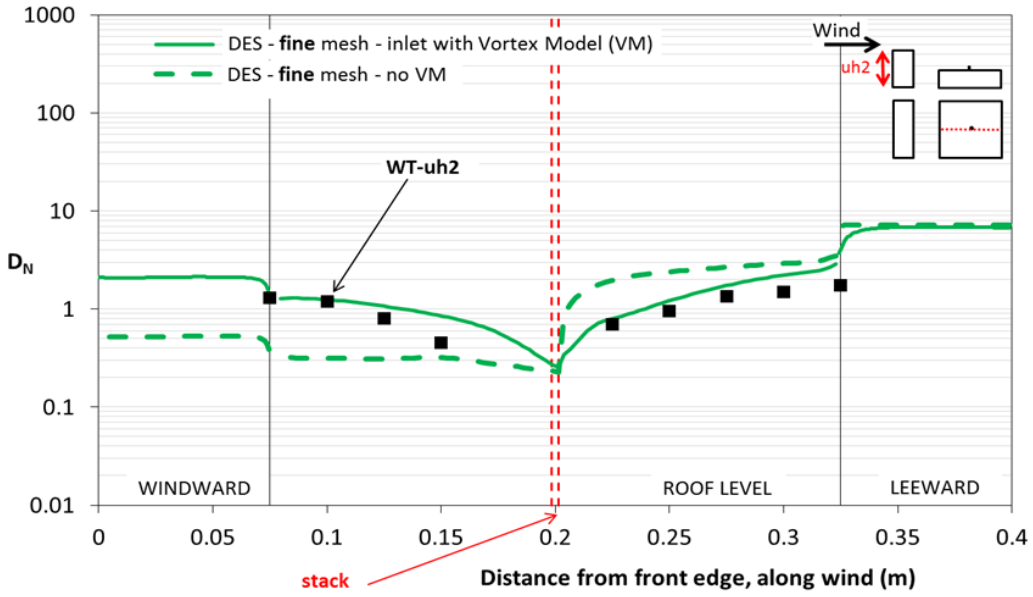

Figure 6-5. D_N prediction obtained by DES, for fine mesh, time step = 0.005s and two different inlet conditions

6.4.3 LES

6.4.3.1 Effect of mesh

As for previous cases, fine and coarse mesh are tested with LES model, the results are shown in Figure 6-6. The simulations are performed using a time step = 0.01s and transient perturbations at the inlet are not considered.

The results show very little changes on D_N prediction upstream of the stack. This is probably because mesh refinement was not sufficient to capture additional turbulent structures near the roof and walls. As mentioned before, the current work used LES for exploratory purposes. For more suitable results, additional tests are needed.

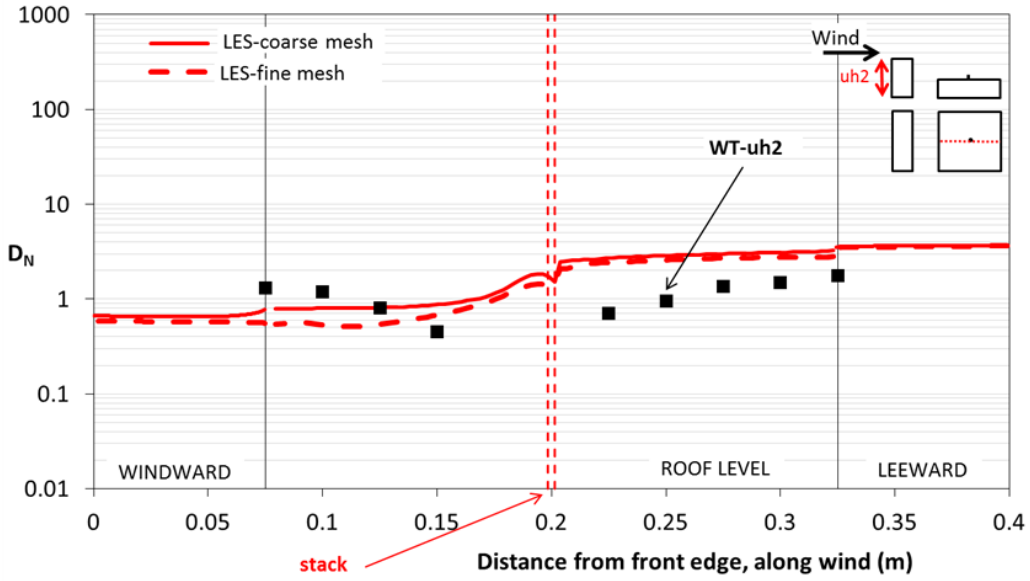

Figure 6-6. D_N prediction obtained by LES (fine and coarse mesh) and time step = 0.01s

6.4.3.2 Effect of time step

The influence of time step when using a fine meshing is shown in Figure 6-7. The curve for time step 0.1s seems to oscillate about one another. However, as the time step decreases a stable D_N prediction is observed.

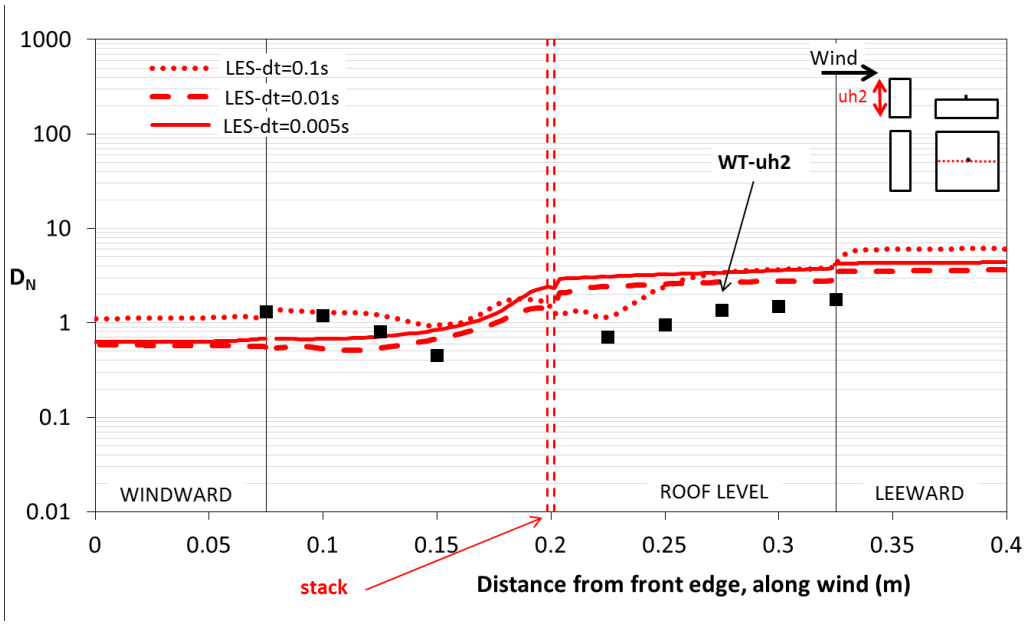

Figure 6-7. Comparison of D_N for different time steps using fine meshing

6.4.3.3 Effect of vortex generator

The same vortex model used for DES is applied for LES. Figure 6-8 shows the comparison with and without VM for D_N prediction when using fine mesh and time step of 0.005s. The results reveal that VM has an important effect on D_N prediction. In fact, when considering VM in the numerical model the solution reaches a good agreement with experimental data in points located away from the stack. It can be said that the global behaviour of including VM is similar to what was already discussed for the DES model. The difference, in this case, is that close to the stack some discrepancies are noted and LES seems to overestimate dilution in this region. It can be said that inlet condition has a major effect on D_N prediction.

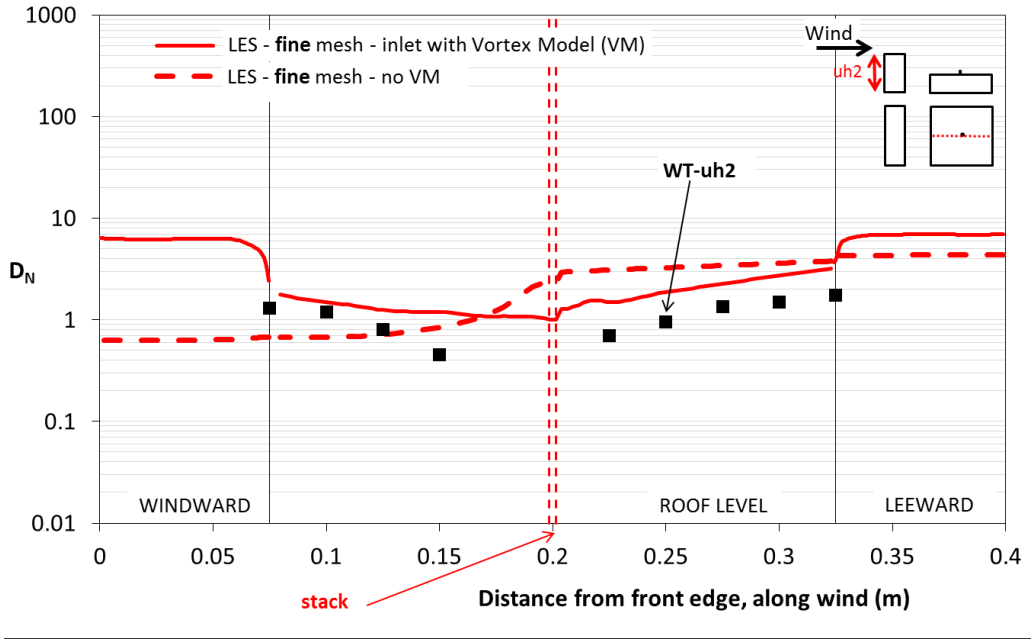

Figure 6-8. D_N **prediction obtained by** LES, **for fine mesh, time step = 0.005s and two different inlet conditions**

6.5 Results

6.5.1 Iso contours of mean D_N and streamlines

Figure 6-9 shows in detail the mean streamlines and dilution contour lines for all the unsteady approaches. All cases consider fine mesh and time step of 0.005s, and inlet VM is used for DES and LES only. The plotted area correspond to the middle vertical plan and the horizontal half plan at the height y = 0.008 m, which is the location in the vertical axis of the stack outlet.

Observing the streamline of the three cases, LES is the only one that successfully detects flow detachments and vortices at the front edge and side corners. Those detachments promote higher and wider recirculation region compared with URANS and DES. In the horizontal plan, all models capture vortex structures developed in both sides of the wake; however the vortex from URANS seems to be larger. In the vertical plan, vortices between both buildings are similarly reproduced in term of size, and the recirculation lengths are similar for DES and URANS except for LES which seems to be shorter.

Looking at the spatial distribution of D_N in the vertical and horizontal plan for the three cases, it appears that the mixing effects of DES and LES are stronger than URANS. It must be mentioned that contour lines represent a locus of constant dilution, and hence regions where contour lines cluster together are regions of large dilution gradient. In the vertical plan, the higher gradient is obtained by URANS and the lower by LES. This is in correspondence with flow characteristics in the vertical plan. LES shows a clear taller recirculation region which is characterized by high turbulence activity and high mixing which promotes spreading in the y axis direction. The same vertical plane shows that DES predicts lower D_N (high concentration) in the space between both buildings. This is produced by turbulent activity but also because the plume is complete within the recirculation region, which is not the case for LES.

The observation of D_N distribution in the horizontal plan shows again URANS as having the highest gradient. A global comparison reveals that DES detects a large zone of pollutants within the recirculation region compared with the other models. The reason is because in DES the plume is completely inside the recirculation region, so pollutants are mainly transported upwind of the stack by backflow streamlines. In LES the plume is located in the frontier of the recirculation region, so pollutants are spread upwind and downwind of the stack. In URANS, even if the plume is within the recirculation region, the plume successfully escapes from the recirculation region due to high vertical velocities. This can be better appreciated in Figure 6-10 a).

Globally, it should be mentioned that D_N distribution in the along wind direction near the stack is similar for all the approaches. This is because the transport of pollutant in this direction is mainly produced by advection affect. In the horizontal plan; regardless of the issue of different recirculation length, DES and LES have a similar lateral spreading. This is because both reproduce the lateral fluctuations caused by vortex shedding. URANS successfully advects pollutants along wind direction since transport caused by mean velocities is predominant in this direction; however it has difficulties in the lateral direction. This is because the inherent limitation of reproducing lateral unsteadiness -and the associated turbulent mass fluxes-, which is the predominant pollutant transport mechanism in this direction (see also, Gousseau et al. 2011).

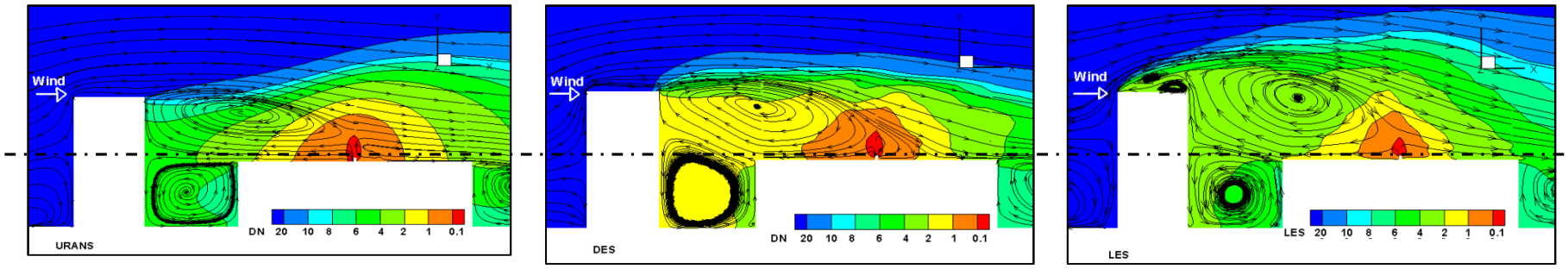

a) Elevation,URANS b) Elevation, DES c) Elevation, LES

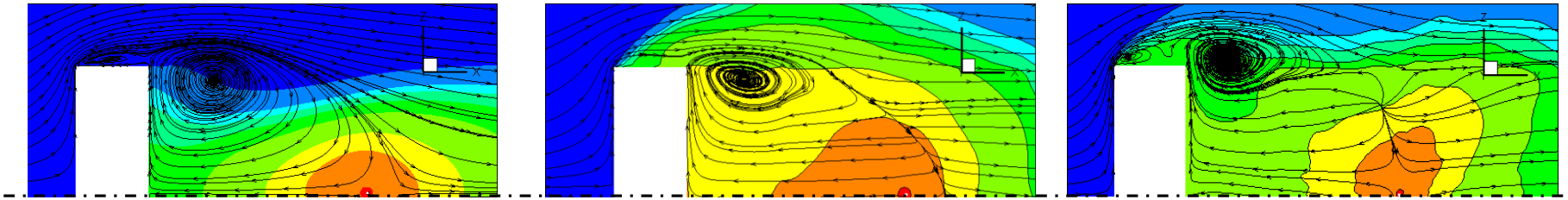

Half-horizontal plan view Half-horizontal plan view Hlaf-horizontal plan view

Figure 6-9. Elevation (middle plan) and half-horizontal plan view (at stack outlet height, y = 0.008m) of mean streamlines and D_N iso-contours of URANS, DES, LES after 5s simulation (time step 0.005s) and fine mesh

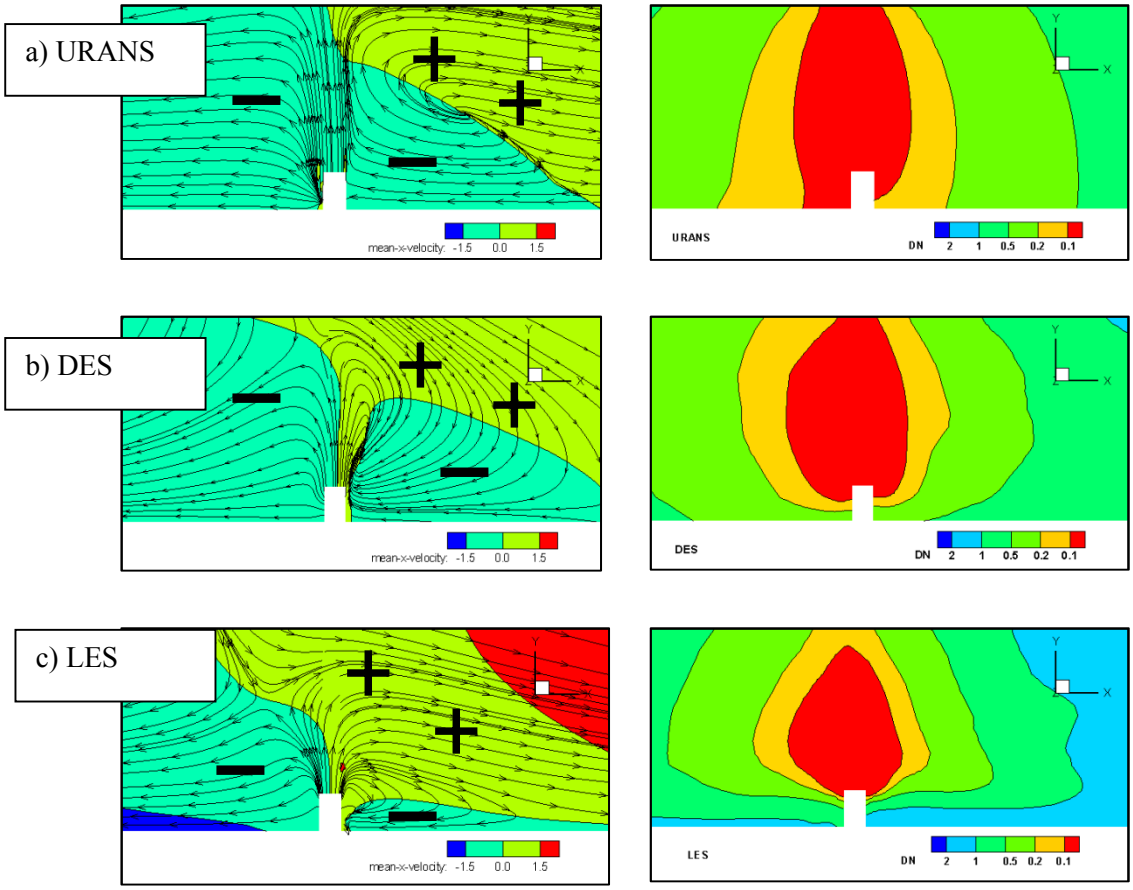

Figure 6-10. Mean streamlines, Ux and Normalized dilution contours close to the stack. URANS, DES and LES

6.5.2 Mean velocity profile along wind direction

Mean velocity along wind (Ux) was evaluated for all cases along three vertical lines, as presented in Figure 6-11. The results show the progression of Ux profile along wind direction. The observation of Ux profiles reveals that URANS and DES have very similar recirculation size in the vertical direction and both are lower than LES. However, LES has a shorter recirculation size along wind direction. This is deducted by identifying the position where "velocity zero" crosses the plotted vertical line in Figure 6-11 (a), (b) and (c).

The comparison of Ux profile shows differences within the wake of the upstream building. However, as the flow blows away along wind, all profiles tend to converge. URANS and DES have very similar trends at the three locations except between the two buildings where DES shows reduced Ux velocities. This is because the backflow for DES in this area is oblique with an important vertical component rather than mainly horizontal velocities as for URANS.

It may be noted that for LES, the downward flow at the right border of the recirculation region, passes exactly where the stack is located. For DES and URANS the recirculation border is somewhere in the roof of b1, but downwind the stack. This is relevant because the structure of airflow near the stack for LES is composed by a mixing of positive and negative velocities. In contrast, for DES and URANS the stack is completely immersed in negative velocities. This is also appreciated in Figure 6-10. This flow pattern difference has an important effect on the characteristics of pollutant dispersion within the wake as it will be discussed further.

6.5.3 Normalized dilution prediction

Figure 6-12 shows a comparison of all the unsteady approaches together. All cases correspond to fine mesh, time step of 0.005s and VM at the inlet for DES and LES only. In general, it is noted that the three approaches converge to similar results away from the stack. A good agreement with experimental data is observed specially for DES in these zones. Close to the stack, low D_N peaks are registered by URANS and DES. It must be noted that there is no data to verify the trend of dilution in this location; however these peaks could be associated to the proximity with the pollutant source combined with the gradient diffusion hypothesis used to estimate the turbulent mass flux in URANS formulation combined with the underestimation of fluctuations (mixing) close to the stack. LES predicts a homogenous relative high D_N closed to the stack. This is due to high mixing effect produced by the recirculation frontier issue already mentioned.

To quantify the proximity of numerical solution to the experimental data, the variance for each approach was calculated. The results were: URANS = 0.8, DES = 0.26 and LES = 1.43. In consequence, and considering the current numerical setup, DES results are indicated as the most close to the experimental data for this case.

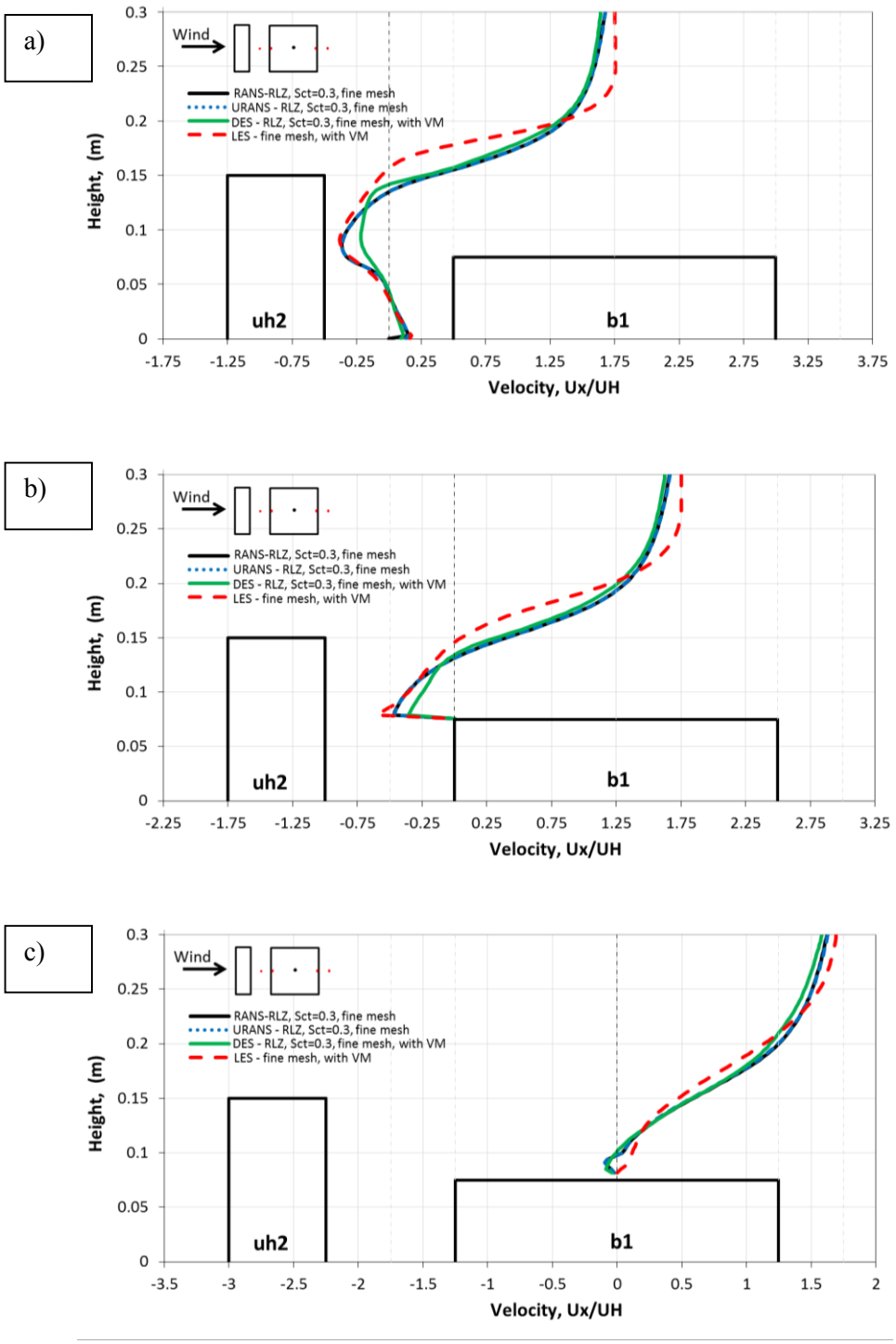

Figure 6-11. Velocity profile progression along wind for RANS, URANS, LES and DES – coarse and fine mesh

It should be mentioned that ASHRAE 2011 prediction model was included for comparisons purposes. It is clearly observed that ASHRAE 2011 underestimate dilution by more than one order of magnitude. This underestimation is expected since ASHRAE formulations do not include the extra mixing produced by upwind adjacent buildings.

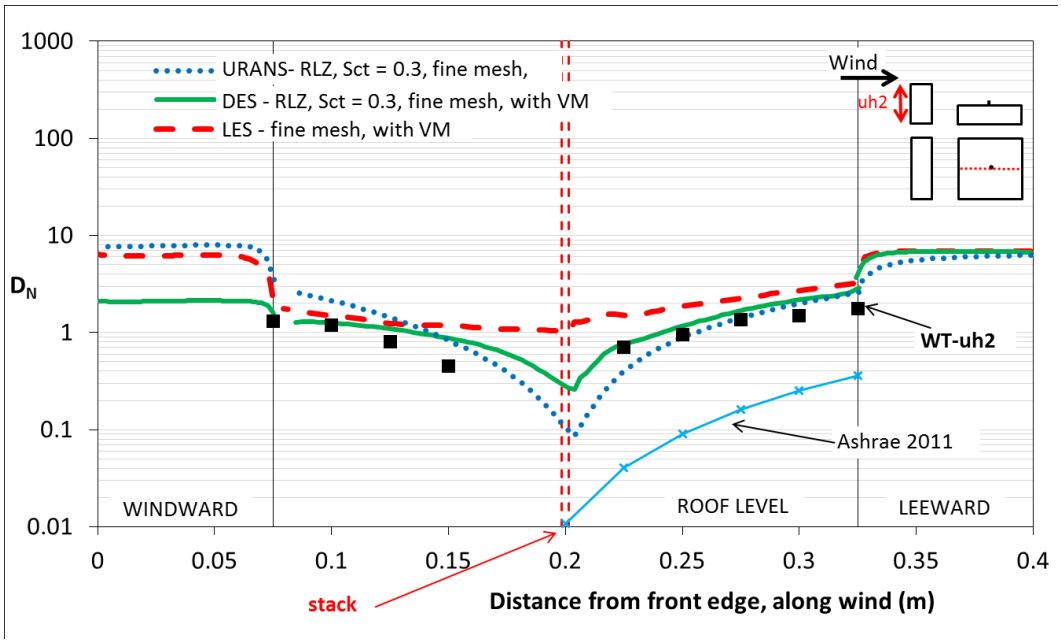

Figure 6-12. Comparison of three unsteady approaches: URANS, DES, LES using fine mesh, time step = 0.005s and VM at the inlet for DES and LES. URANS uses RLZ turbulence model.

6.6 Summary

In this chapter, the performance of three unsteady approaches (URANS, DES and LES) was evaluated against wind tunnel data for a two-building configuration. A sensitivity analysis was carried out to determine the effect of some numerical parameters on D_N prediction. The parameters analysed were; mesh size, time step and inlet boundary conditions (DES and LES only).

It should be recalled that the current LES simulations were performed without adopting any additional meshing strategy than the two meshes presented in section 6.3. This is a relevant

issue since it is known that LES results are very sensitive to mesh refinements in particular close to the walls. The purpose was to compare three unsteady approaches under same conditions, including meshing characteristics, and this, being aware that some turbulent structures would not be captured by LES due to lacking of very fine mesh close to the walls. In this sense, the current LES simulations should be taken as preliminary results. URANS and DES have not mayor problems with simulations close to walls since they have the advantage of using wall functions.

The most relevant conclusions of this chapter are:

- In URANS, no effect of reducing time step was found and the results converged to RANS solution. This is probably due to turbulence model which is too dissipative. High dissipation calms down unsteadiness, and no oscillations are captured. Significant underestimations of D_N in the lateral directions occur given that these are actually RANS model.

- In DES, meshing and time step were critical downstream the stack. It was found that including inlet fluctuations is necessary for better agreement with experimental data. Under the conditions presented, DES shows results closer to the experimental data than all other approaches considered.

- In LES, meshing changes did not show notorious improvements on D_N predictions. This shows that the mesh used was not sufficiently refined near the walls and thus failed capturing relevant turbulent structures in the boundary layer. In consequence, major efforts at least in terms of meshing strategy, should be considered in order to run an appropriate LES simulation. The time step is of course critical. As in DES, better agreement was found when using vortex generator model at the inlet.

7. PARAMETRIC STUDY OF ADJACENT BUILDINGS GEOMETRY

7.1 General

This chapter presents a parametric study of geometric characteristics of an adjacent building and its effect on D_N prediction at roof level of the emitting building, b1. The analysis has taken the form of parametric study in which a single parameter, height, width or length of an adjacent building is systematically changed, keeping all other variables constant.

7.2 Introduction

Complexities in airflow and pollutant transport due to terrain conditions, local topography and buildings make it very difficult to assess plume concentrations (Saathoff et al., 2009). This Chapter is an effort to improve the understanding of dispersion for non-isolated building configurations. The motivation behind this study is to give valuable insights concerning dispersion of pollutants for a small-scale urban layout, which is a step forward from the classic isolated building case. The objective is to detect the parameters that govern dispersion in a non-isolated building configuration. The parametric analysis is performed on three non-isolated building configurations as is described in the following sections.

7.3 Methodology

The following is a purely CFD study to predict flow and dispersion for various building configurations. The approach used was the steady RANS since it has been proved in the previous chapters it provides acceptable agreement with a reasonable computational cost. All the numerical details were applied following the suggestions from Chapter 5. The turbulent Schmidt number was fixed as 0.3 for all the cases. The study considers a standard single-story building with a stack in the middle of the roof. The objective is to evaluate D_N variation along the middle central line at roof level and walls when different adjacent buildings are incorporated in the layout.

7.4 Description of cases

Three different building configurations were used for the parametric study; (a) a building located upstream of b1, (b) a building located downstream of b1 and (c) b1 between two tall buildings. A schematic representation is presented in Figure 7-1, and the actual dimensions are detailed in Table 7-1, 7-2 and 7-3. It should be noted that cases uh2, ul1and uw2 are identical, similarly for cases dh2, dl1 and dw2.

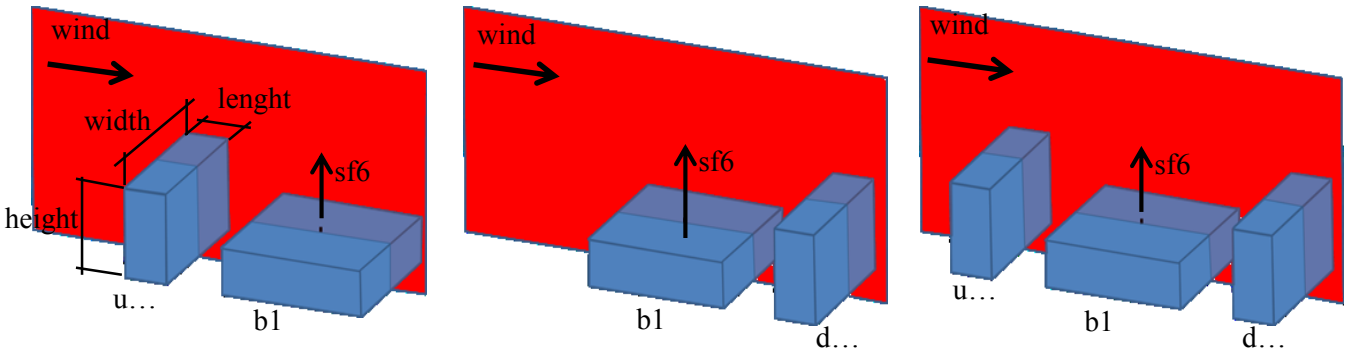

a) b1 with an upstream (u…) building

b) b1 with a downstream (d...) building

c) b1 with both, upstream (u…) and downstream (d…) buildings

Figure 7-1. Emitting building and three configurations of adjacent buildings.

In total, 29 configurations were tested using a constant exhaust momentum M = 1.7 and stack located in the middle of the roof of the emitting building, b1. The gas properties used at the stack were the same as previous chapters, which means 10 ppm of SF_6. Additional cases, in particular when the stack is located in the front edge of b1, are presented in Appendix A. For all cases, geometric characteristics of b1 were unvarying and a single wind direction perpendicular to the building face was considered. The meshing procedure for all the numerical models followed the strategy presented in Chapter 4.

Table 7-1. Dimension of buildings placed upstream of b1

case	Height (m)	Length (m)	Width (m)
uh1	0.075	0.075	0.25
uh2	**0.15**	**0.075**	**0.25**
uh3	0.225	0.075	0.25
uh4	0.3	0.075	0.25
ul1	**0.15**	**0.075**	**0.25**
ul2	0.15	0.15	0.25
ul3	0.15	0.225	0.25
uw1	0.15	0.075	0.125
uw2	**0.15**	**0.075**	**0.25**
uw3	0.15	0.075	0.375
uw4	0.15	0.075	0.5

Table 7-2. Dimensions of buildings placed downstream of b1

case	Height (m)	Length (m)	Width (m)
dh1	0.075	0.075	0.25
dh2	**0.15**	**0.075**	**0.25**
dh3	0.225	0.075	0.25
dh4	0.3	0.075	0.25
dl1	**0.15**	**0.075**	**0.25**
dl2	0.15	0.15	0.25
dl3	0.15	0.225	0.25
dw1	0.15	0.075	0.125
dw2	**0.15**	**0.075**	**0.25**
dw3	0.15	0.075	0.375
dw4	0.15	0.075	0.5

Table 7-3. Dimensions of buildings located upstream and downstream of b1

case	Height (m) of the upstream building	Height (m) of the downstream building	Length (m)	Width (m)
uh1dh4	uh1=0.075	dh4 = 0.3	0.075	0.25
uh2dh4	uh2=0.15	dh4 = 0.3	0.075	0.25
uh3dh4	uh3=0.225	dh4 = 0.3	0.075	0.25
uh4dh4	uh4=0.3	dh4 = 0.3	0.075	0.25
uh4dh1	uh4=0.3	dh4 = 0.075	0.075	0.25
uh4dh2	uh4=0.3	dh4 = 0.15	0.075	0.25
uh4dh3	uh4=0.3	dh4 = 0.225	0.075	0.25

7.5 Results

7.5.1 General comparison of three non-isolated building configurations

One of the advantages of CFD simulations is the possibility to obtain a solution in the complete domain. This feature is exploited in Figure 7-2 where the iso-contour of D_N in the middle vertical plane for three representative configurations (case uh4, dh4 and uh2dh4) are presented. It is important to mention that the D_N plotting range was arbitrarily limited from 0.1 to 30 to better visualize D_N variations.

General views of the computational results of case uh4, presented in Figure 7-2 (a), show a good qualitative agreement with wind tunnel visualization test shown previously in Figure 3-2 (b). It is clearly observed that a tall building located upstream of a low emitting building causes the plume to be dragged towards the leeward of the upstream building. Such dispersion behaviour affects the complete leeward wall of the upstream building as well as the upstream part of the roof and windward wall of the emitting building. This observation was also verified experimentally by Hajra et al. (2011).

Figure 7-2 (b) shows the D_N contours of a tall building located downstream of b1, corresponding to case dh4. It is noted that the stack plume is dragged downstream by the wind reducing its concentration by mixing with the atmospheric clean air. The zones affected are mainly the lower part of the downstream building as well as the downstream part of the roof and leeward wall of the emitting building.

Finally, Figure 7-2 (c) shows the effect of placing an emitting building between two buildings, case uh2dh4, frequently encountered in urban areas. In this case, it is noted that pollutants reach the leeward and windward walls of both adjacent buildings.

In general, qualitative comparison demonstrates that significant differences can be obtained on the D_N field when the building layout increases its complexity from isolated to multiple-building configuration. More details about the D_N fields, in particular along the central line at the roof level of b1, which is affected by the adjacent building geometry, are discussed in the following sections.

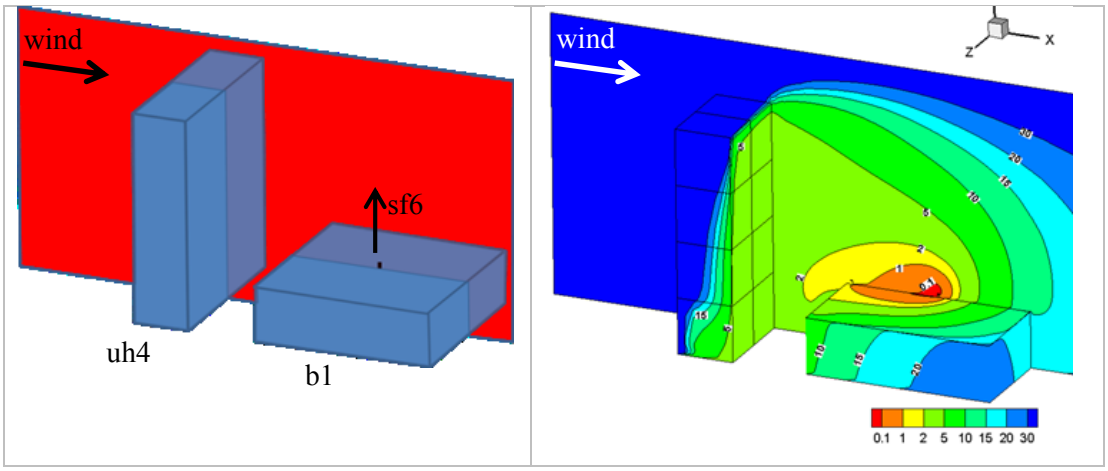

a) A tall building located upstream of an emitting building (case uh4)

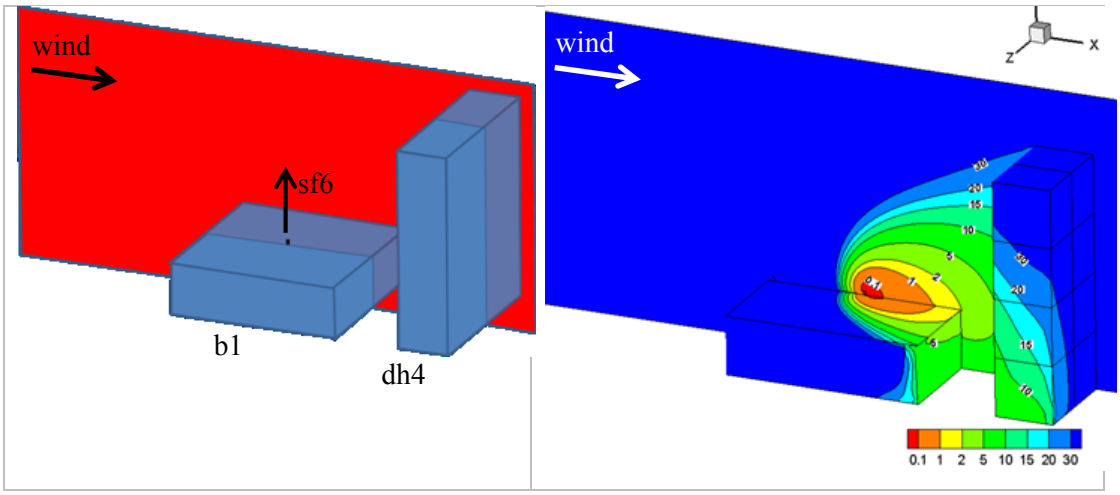

b) A tall building located downstream of an emitting building (case dh4)

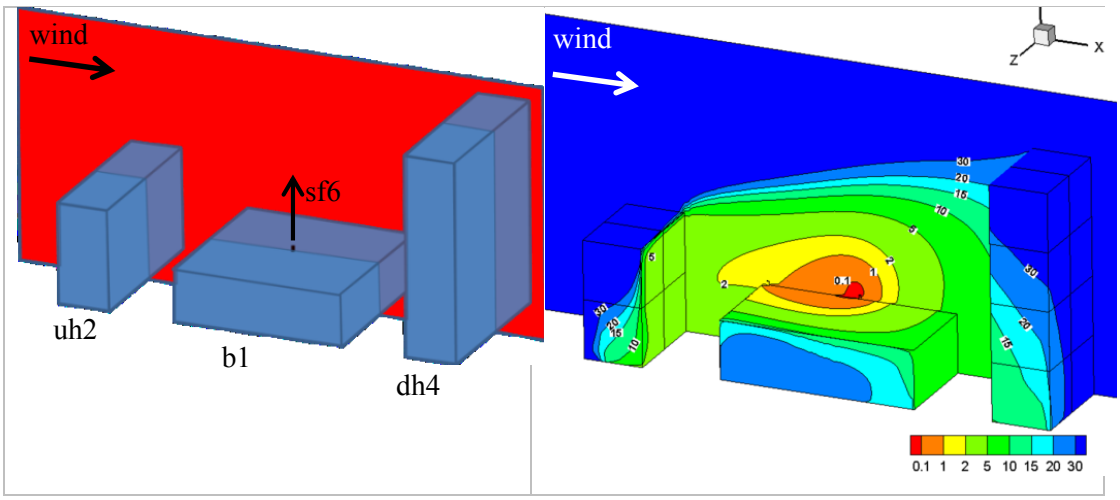

c) An emitting building located between two buildings (case uh2dh4)

Figure 7-2. D_N in the middle plane for different building configurations.

7.5.2 Effect of a building located upstream of an emitting building

This subsection discusses the effect of the upstream building geometry on D_N prediction at the roof level of b1. The discussion is divided in three parts: (a) the effect of upstream building height, (b) the effect of upstream building length and (c) the effect of upstream building width.

Effect of upstream building height

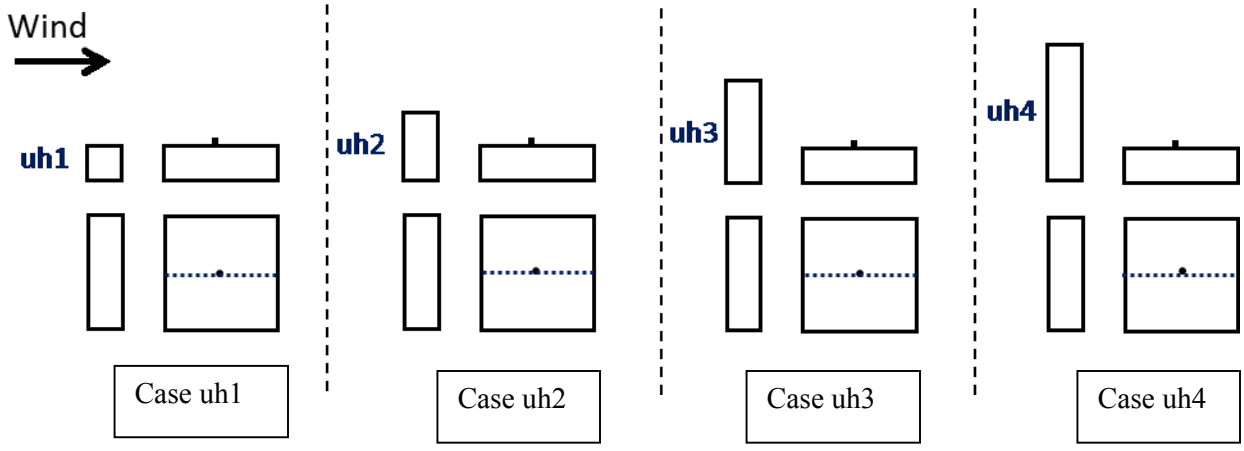

Figure 7-3. Cases used to analyse the effect of the upstream building height

Figure 7-3 shows four configurations to analyse the effect upstream building height. It may be noted that uh = 1, 2, 3, 4 are the corresponding upstream building heights when it is equal, two, three and four times the height of the emitting building. Figure 7-4 shows the comparison of horizontal components (Ux) in the vertical line above the stack when the height of the upstream building is varied. It is observed that as the upstream building height gradually increases; the along wind component velocity (Ux) gradually passes from positive to negative in the vertical profile at the stack location. Accordingly, the height of the recirculation region in the wake of the upstream building increases as well.

Case-uh4 seems to be the extreme case where velocities near and above the stack are mainly directed upwind. On the other hand, it is observed that for the same vertical plotting line, the entire profile of Ux is directed downstream for the isolated building case. It may be noted that for case uh1, very limited influence of uh1 is perceived on the velocity field, thus Ux profile remains very similar as the isolated building case. The ranges of maximum normalized velocities (Ux/U_H) are near to 0.5 upwind for case-uh4 and 1.5 downstream for case uh1. For configurations in between these two, the wind profile has a combination of components upwind and downwind.

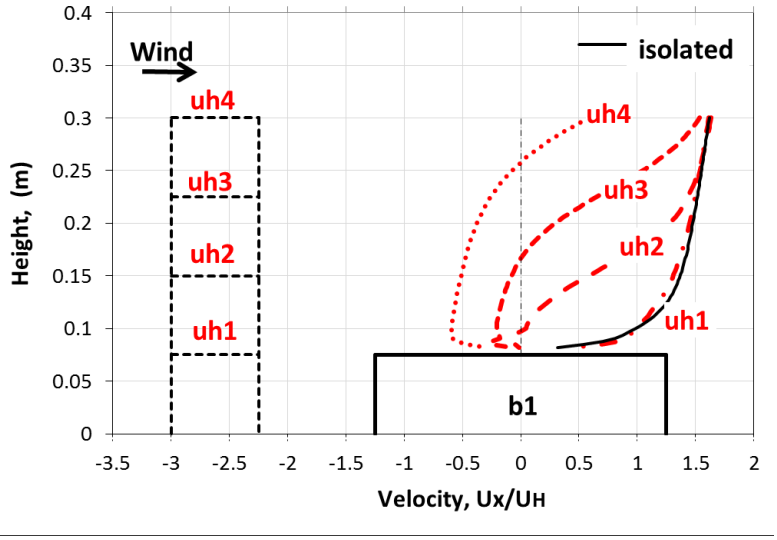

Figure 7-4. Velocity profile at stack location. Effect of the upstream building height

As noted in Figure 7-5 the dilution field is affected by these different local velocities in the wake, especially downstream of the stack. In this zone dilution increases as the upstream building height increases following an asymptotic behaviour. This observation suggests that a change of the upstream building height does not affect significantly the dilution downwind the stack after four times the height of the emitting building. On the other hand, dilution distribution upwind of the stack seems to be independent of the upstream building height when a "critical height", close to uh = 2 is reached. For heights above this "critical value" dilution distribution seems to be constant upstream the stack. For heights below this "critical height" dilution distribution is extremely dependant on the upstream building height upwind the stack. Moreover, for any height below the "critical value", high dilution (low concentrations) upwind the stack is expected. This

phenomenon is explained by the size of the recirculation zone created by the upstream building and the relative location of the stack (for unvarying exhaust momentum, M, and stack height). A low upstream building creates a small recirculation zone, which may not affect the plume. Then, the plume is mainly dragged downstream by wind flow. This is exactly reflected in case uh1 (uh1 upstream of b1), the observed high dilution upstream and low dilution downstream the stack is because the plume is practically completely dragged downstream the stack.

On the other side, case-uh4 (uh4 upstream of b1) the observed low dilution upstream and high dilution downstream the stack is because the plume is mostly trapped by the recirculation zone and then transported towards the leeward of the upstream building. It can thus be concluded that dilution is very sensitive to the height of upstream buildings in areas downstream the stack. Upstream the stack dilution seems to be sensitive only for low upstream buildings heights; then as the height increases and the plume gets trapped in the recirculation zone, a rapid drop in dilution is detected.

As gradually the plume is covered by the recirculation, dilution upstream the stack seems to be independent of the upstream building height. It is interesting to note that the isolated case shows lower dilution than case-uh1 upstream the stack. This is likely because the reattachment length of the isolated building is shorter compared with case uh1 which is composed by two buildings, then isolated building case transports somehow more pollutants against the roof than case uh1. To visualize the effect of the upstream building height in the complete vertical middle and horizontal plane, dilution contours and streamlines can be viewed in Appendices I and J, respectively.

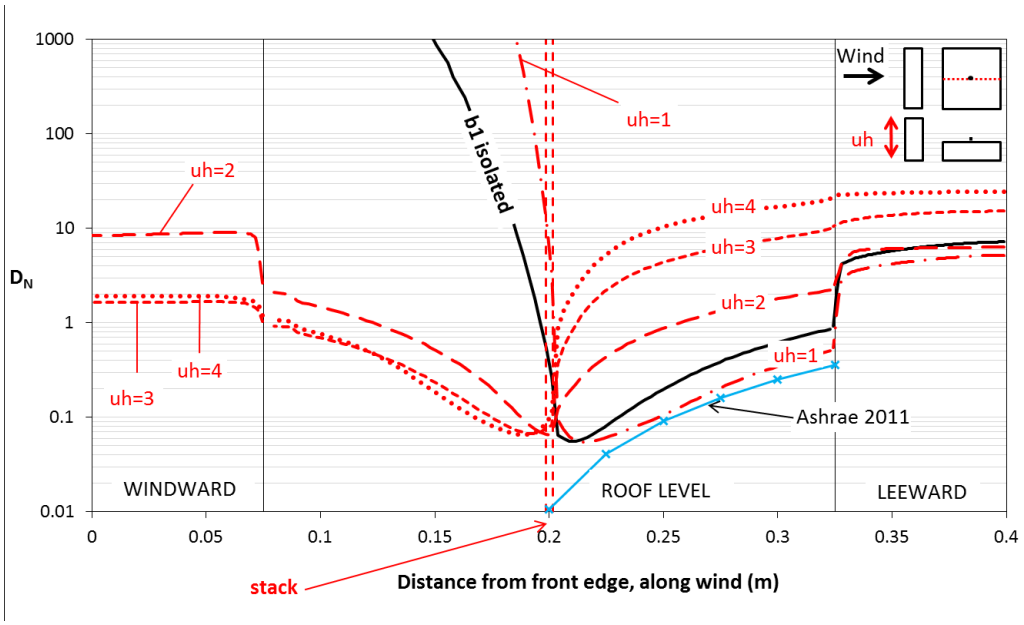

Figure 7-5. Effect of the upstream building height

Effect of upstream building length

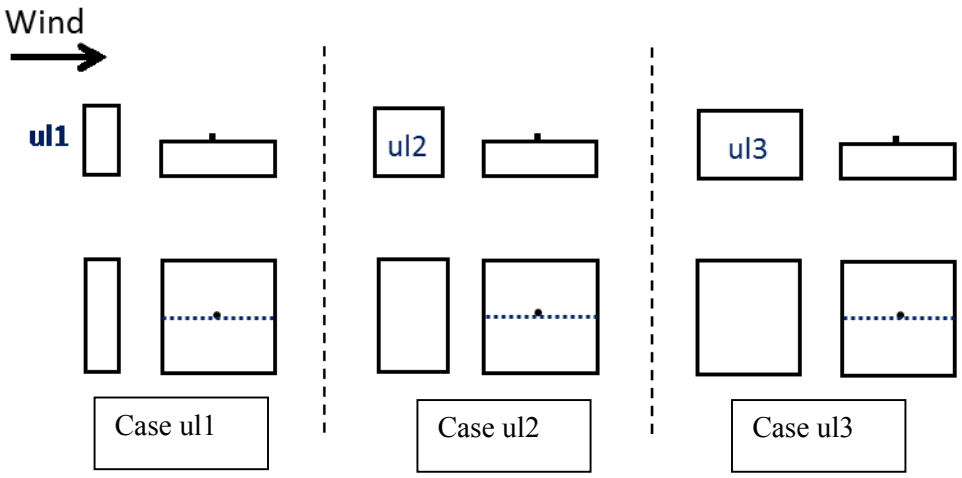

Figure 7-6. Cases used to analyse the effect of the upstream building length

Figure 7-6 shows three configurations used to analyse the effect upstream building length, which is the dimension along wind. It may be noted that ul = 1, 2, and 3 are equivalent to $1xH_b$, $2xH_b$ and $3H_b$ respectively, where H_b is the height of the emitting building (0.075 m).

Figure 7-7 shows comparison of horizontal components (Ux) in the vertical line above the stack when the length of the upstream building is varied. It is noted that, even though Ux is slightly affected and the profile remains very similar to each other, some increment on Ux downwind is perceived as the upstream building length increases. Case ul3 shows somewhat the higher positive velocities downstream the stack, and this, all along the vertical line. Case ul1 shows some negative velocities near the roof, revealing the existence of a small backflow for this case. The figure also shows significantly lower velocities compared with the isolated building case; revealing that the emitting building is partially enveloped by the recirculation zone created by the upstream building. It is observed that all velocity profiles converge to same values at a height equivalent to twice the upstream building height (in this case near to 0.3 m).

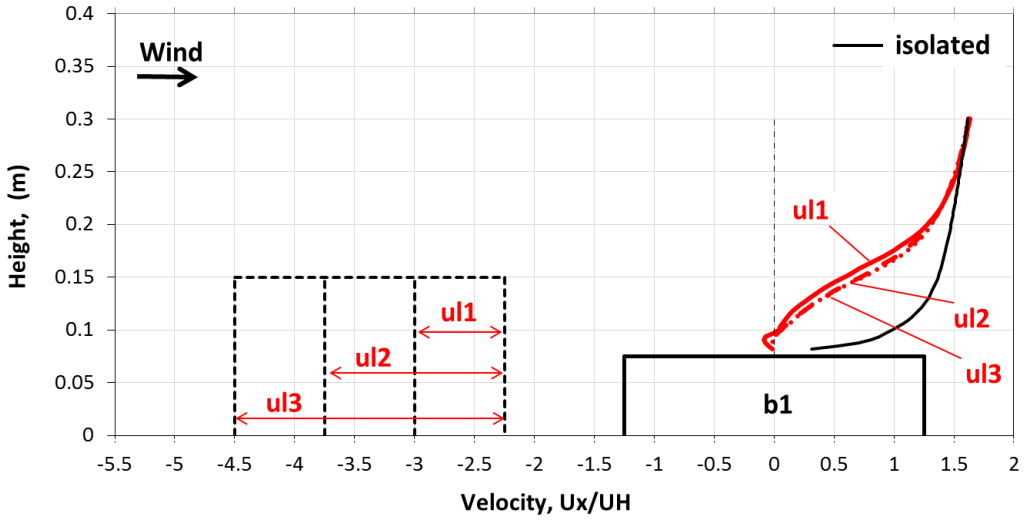

Figure 7-7. Velocity profile at stack location. Effect of the upstream building length

Figure 7-8 shows the comparison of D_N predictions for different upstream building length. It is observed that almost equal spreading of pollutants is produced in both side of the stack at the

roof level of b1. However, significant differences are note in the windward of the emitting building, where high dilution values are perceived as the length of the upstream building increases. This is likely because the re-attachment length at the lateral wall of the upstream building is produced somewhere along the wall before the back edge. This produces somehow high velocities when the flow re-detaches from the block creating strong vortical structures between both buildings. These vortical structures increase the mixing and then dilution increases in consequence. When the length of the upstream buildings is short, wind flow does not re-attach in the lateral wall, and then the vortical structures between both buildings are less pronounced. This phenomenon is better visualized by the streamlines in the horizontal plane for case ul1 (or case uh2) and case ul3 (Appendix J). As previous case, all velocity profiles converge to same values at a height equivalent to twice the upstream building height (in this case near to 0.3 m).

The dilution upwind the stack seems to be independent of the upstream building length. However, observing dilution at roof level close to the windward edge of b1, D_N values tend to increase as the length of the upstream building increases. This is related with the phenomenon explained before. Dilution downstream the stack seems to decrease (higher concentration) as the upstream building length increases, this is because the higher positive velocity at the stack location observed previously in Figure 7-7, increments pollutant transport in this direction.

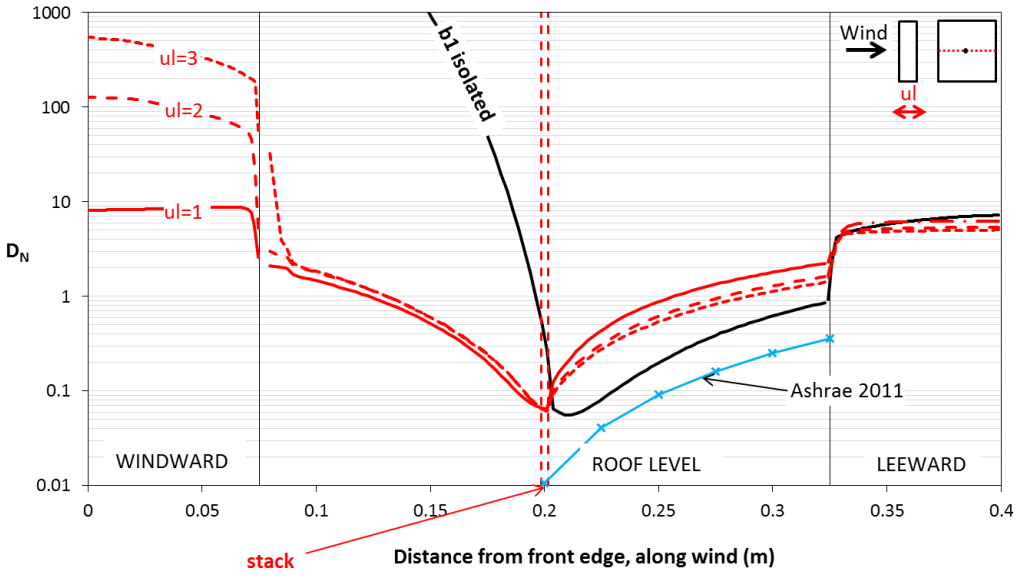

Figure 7-8. Effect of the upstream building length

Effect of upstream building width

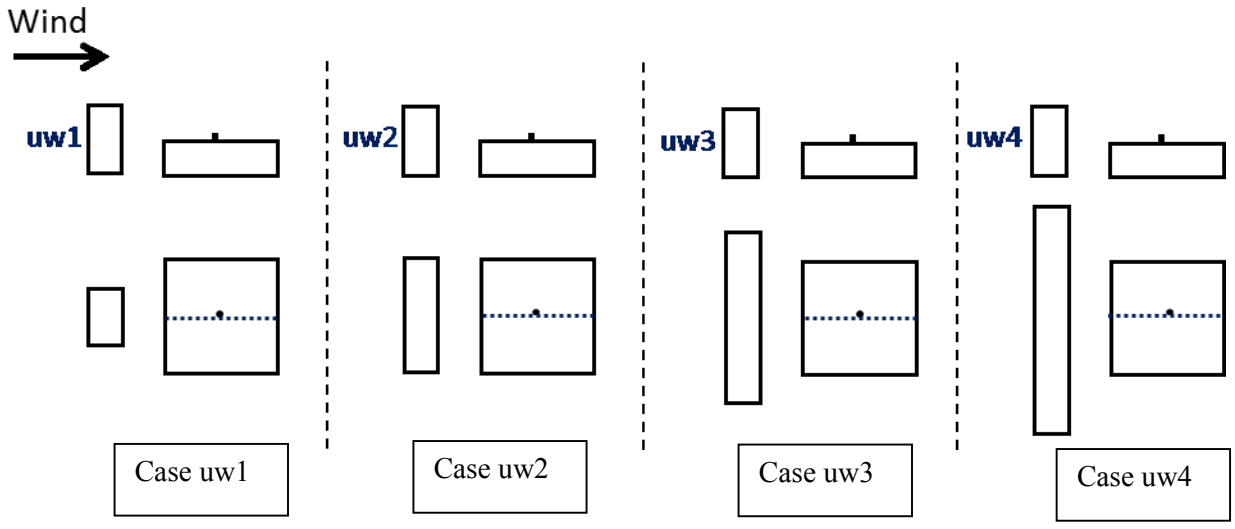

Figure 7-9. Cases used to analyse the effect of the upstream building width

Figure 7-9 shows three configurations used to analyse the effect upstream building width, which is the dimension perpendicular to wind. It may be noted that uw = 1, 2, 3 and 4 are equivalent to 1x(L_b/2), 2x(L_b/2), 3x(L_b/2), and 4x(L_b/2), respectively, where L_b is the width of the emitting building (0.25 m). It may be noted that uw2 has same length as the emitting building.

Figure 7-10 shows comparison of horizontal components (Ux) in the vertical line above the stack when the width of the upstream building is varied. It is observed that velocity profile is highly affected when the width of the upstream building is shorter that the emitting building width. In fact, observing the velocity profile close to the roof of b1, Ux is mainly positive and greater than all the other cases. It can be deducted that shorter upstream buildings brings higher positive velocities over the roof of the emitting building. As the width increases, Ux decrease revealing that b1 is being enveloped by the recirculation region created by the upstream building. It is also observed that as the width increases, velocities near the roof of b1 increases in the negative direction, which means a larger backflow develops. From case-uw2 to uw4, vertical velocity

profile at the stack location shows a combination of upwind and downwind flow. However, it can be assumed that an upstream building wider than uw4 probably will not further affect dilution distribution due to the asymptotic behaviour perceived on velocity profiles.

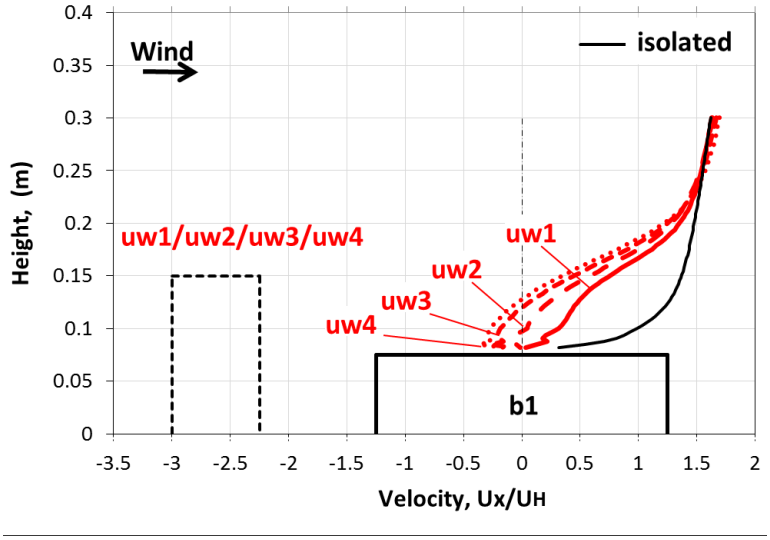

Figure 7-10. Velocity profile at stack location. Effect of the upstream building width

Figure 7-11 shows the effect of upstream building width in the along wind direction D_N distribution. D_N upwind the stack is very sensitive for widths shorter than emitting building width. This is in concordance with the wind velocity profile issue highlighted previously. In consequence for shorter width, D_N is expected to be very high upwind the stack due to high wind speed close to the roof which tends to rapidly drag the plume downstream the stack. As the upstream building width becomes equal the b1 width, the flow change completely and the created recirculation start dragging pollutants upwind the stack. As a consequence, dilution downstream the stack increases and upwind the stack decreases monotonically. An asymptotic behaviour is observed, which means after uw4 very small changes on dilution distribution at the roof level of b1 can be expected.

Observing the streamlines in the horizontal plane for the case uw4 (Appendix J) larger recirculation vortex on side of b1 carrying extra fresh air explain the increasing dilution downstream the stack. These strong lateral vortices can be identified as a second mechanism to increase dilution –after high backflow produced by the upstream building height– downstream the

stack. It can be concluded that low but wide upstream buildings affect D_N distribution in a similar way as tall and thin upstream building.

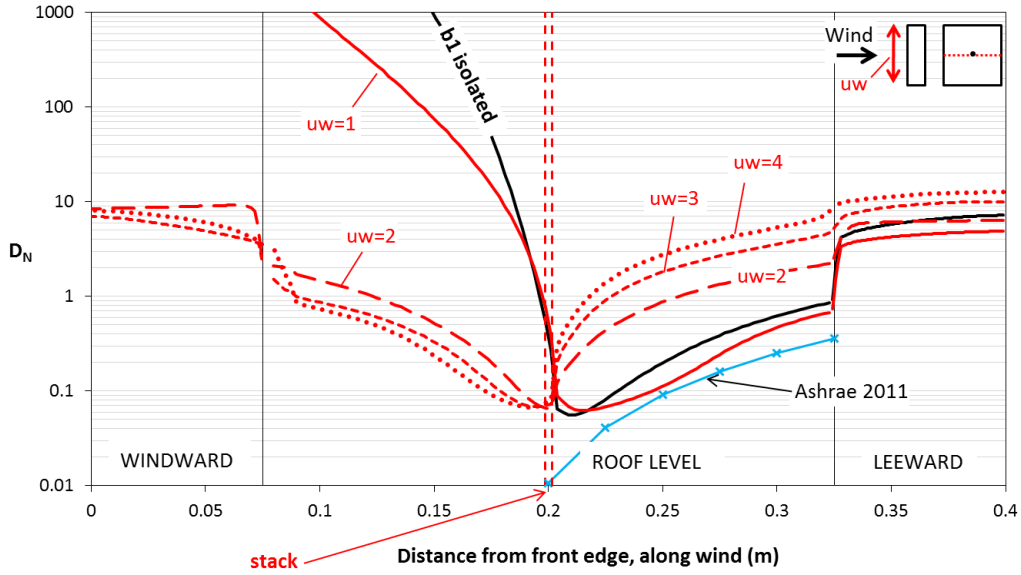

Figure 7-11. Effect of the upstream building width

Effect of spacing between the upstream building and the emitting

Figure 7-12 shows the effect of spacing between an upstream building and the emitting building, b1. Three spacings are tested; s1, s2 and s3 for two configurations: building uh2 upstream of b1 and building uh4 upstream of b1. The corresponding distance in wind tunnel scale are: s1 = 0.1m, s2 = 0.175m and s3 = 0.25m, which at full scale correspond to 20 m, 35 m and 50 m respectively.

Figure 7-12 (a) shows that D_N rapidly increases upwind the stack as the spacing between buildings increases. Downwind from the stack, D_N slowly decreases converging to the value obtained by the isolated building case. As the spacing increases the plume get out from the recirculation region, and then pollutant are mainly transported downwind the stack. For a taller upstream building, (Figure 7-12 (b)), the effect of spacing is similar as before; but the effect of high dilution upwind the stack is less notorious. This is because the recirculation region for uh4 is bigger than uh2, then at spacing s3 the plume is trapped by the recirculation region of uh4.

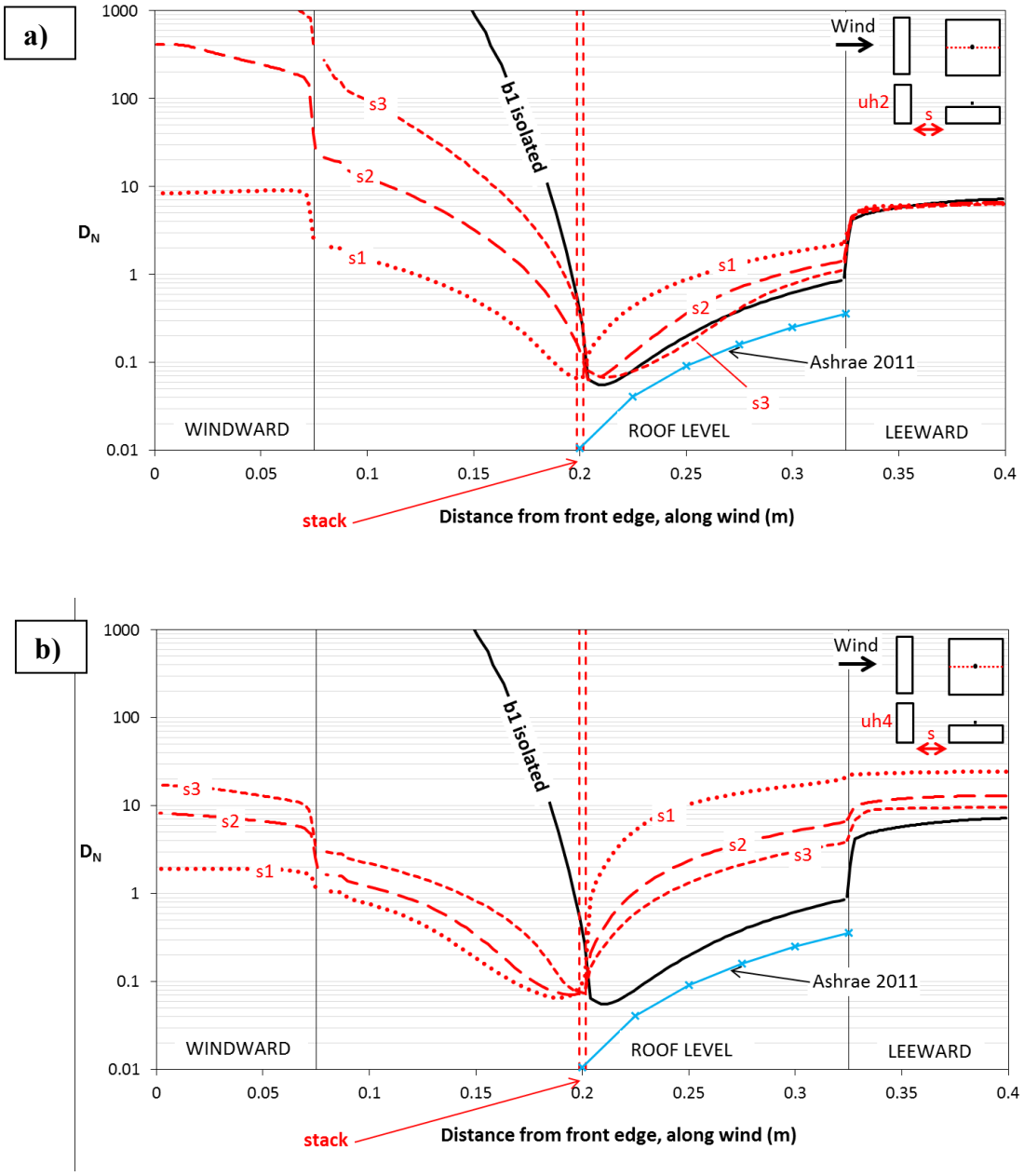

Figure 7-12. Effect of spacing between the emitting building, b1, and an upstream building uh2 (a) and uh4 (b)

7.5.3 Effect of a building located downstream of an emitting building

This subsection discusses the effect of downstream building geometry on D_N prediction at the roof level of b1. Following the methodology used in the previous section, the discussion is divided in three parts: (a) the effect of downstream building height, (b) the effect of downstream building length and (c) the effect of downstream building width

Effect of downstream building height

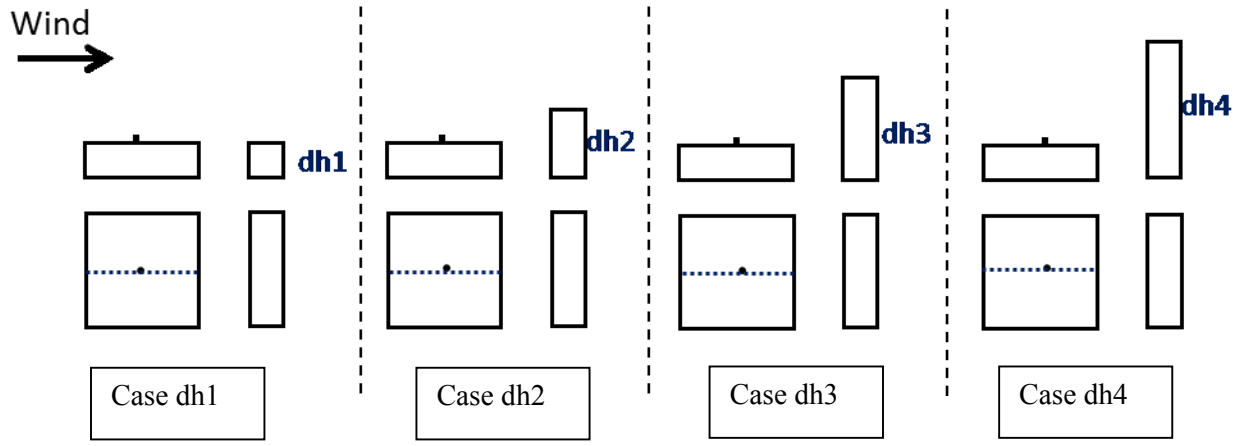

Figure 7-13. Cases used to analyse the effect of the downstream building height

Figure 7-12 shows four configurations to analyse the effect downstream building height. It may be noted that dh = 1, 2, 3, 4 are the corresponding downstream building heights when it has equal, two, three and four times the height of the emitting building. Figure 7-13 shows comparison of horizontal components (Ux) in the vertical line above the stack when the height of the downstream building is varied. It is observed that as the downstream building height gradually increases; the along wind component velocity (Ux) gradually reduces its magnitude. On the other hand, and because the conservation law should be respected, it is highly probable that lateral velocity components (Uz) of wind flow are somewhat increased consequently.

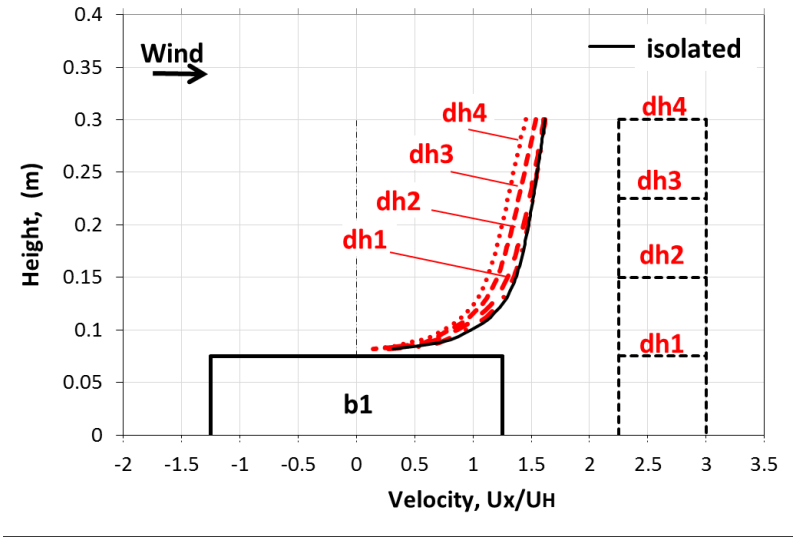

Figure 7-14. Velocity profile at stack location. Effect of the downstream building height

The corresponding D_N distribution at roof level of b1 is presented in Figure 7-14. It is observed that as height of the downstream building increases D_N decreases upwind the stack and increases downwind the stack. This is because the downstream building promotes dispersion of pollutants in the lateral direction reducing somehow dispersion along wind. This related with the velocity issue mentioned before.

It is interesting to note that case-h1 shows higher dilution values than case-h2 (downstream building is twice as tall as the emitting building), which seems to be the critical case at the emitting building leeward. It seems that when the downstream building has same height as the emitting building, the infiltration of pollutants between both is very limited. In consequence, high dilutions in the region between both buildings are detected. However, as soon as the height of the downstream building over passes the height of the emitting building, the infiltration occurs.

The lower D_N in the leeward of b1 was observed for case-dh2, as mentioned. D_N gradually increases along the central line as the downstream building height increases. This can be explained by the lateral velocity increment described before. The present of a downstream building promote dispersion in the lateral direction, then high dilution are detected along the central line. This dispersion behaviour can be clearly observed in the dilution contours and streamlines presented in Appendix J.

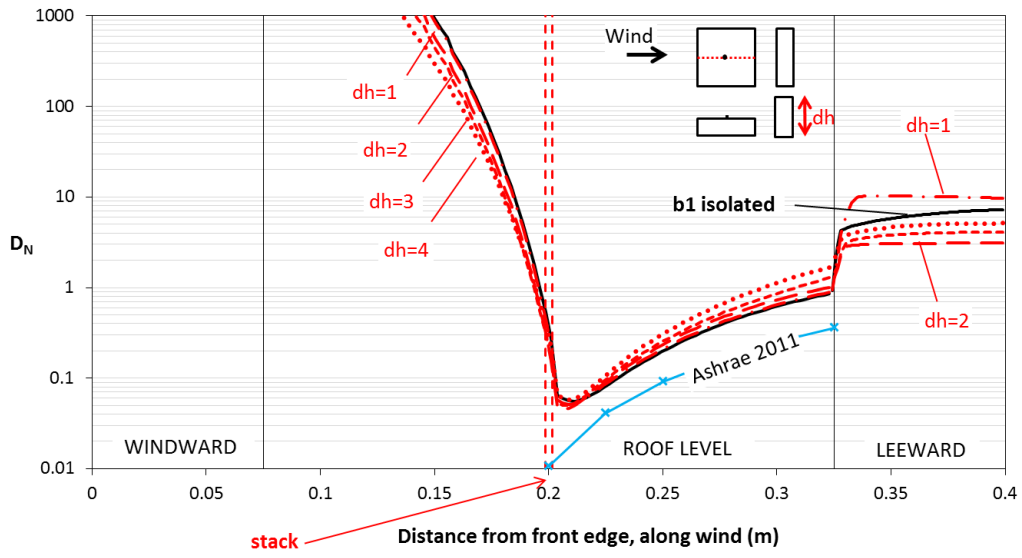

Figure 7-15. Effect of the downstream building height

Effect of downstream building length and width

Figure 7-15 and 7-16 show the effect of downstream length and width. It is clearly observed that none of those parameters have an influence on D_N along the central line at the roof of b1. The velocity profile of U_X is not presented because no changes when comparing with the isolated building case were perceived. The dilution distribution predicted for all the cases are almost identical to the case-dh2 presented previously. The lower dilution values observed at the leeward wall of the emitting building (compared with the isolated case), correspond to the infiltration of pollutants between both buildings that building dh2 produces. This issue was already analysed in the previous subsection.

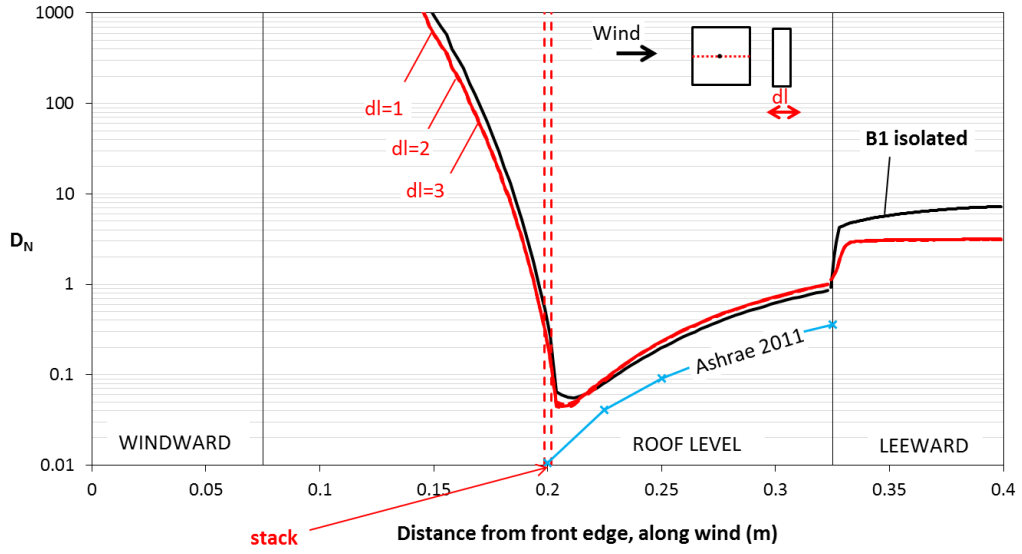

Figure 7-16. Effect of the downstream building length

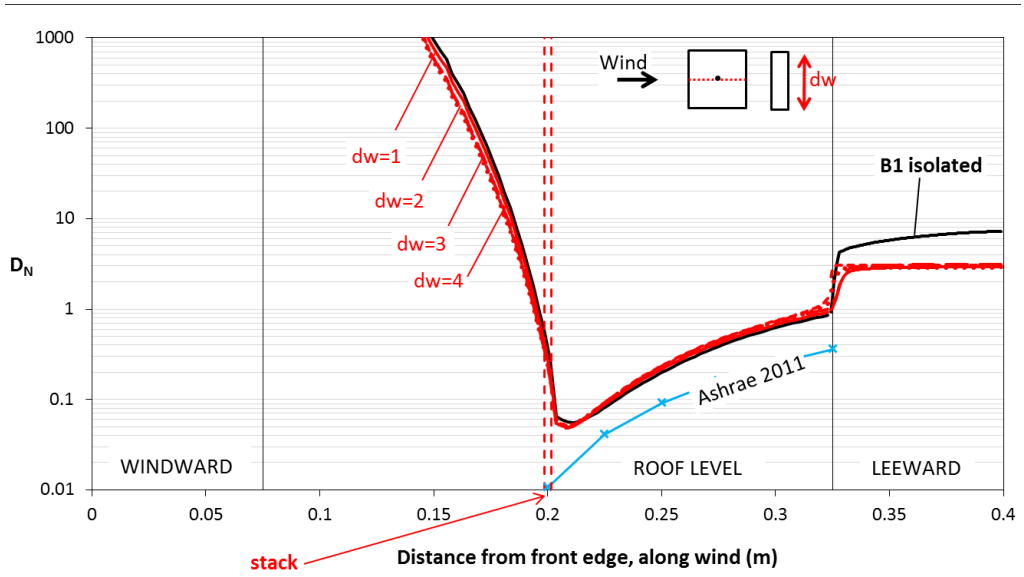

Figure 7-17. Effect of the downstream building width

7.5.4 Effect of an emitting building between two buildings

Figure 7-17 compares D_N predictions for a three-building configuration. In this case, the emitting building stands between a building which is four times taller located downstream and a

building having variable height located upstream, Figure 7-17 (a). The opposite case corresponds to Figure 7-17 b).

For the first case, D_N distribution is very similar to Figure 7-5 (effect of upstream building height). The D_N distribution at roof level of the emitting building is significantly affected by the geometry of the upstream building. When the height of the upstream building increases, the recirculation region increases and more pollutants are carried toward the leeward wall of the upstream building; consequently, fewer pollutants are spread downwind (high D_N are expected). Dilution upwind the stack seems not to be affected by the upstream height, however it is highly probable that instead to continue reducing D_N along the central line, pollutants are spread in the lateral direction. D_N does not change for height above uh3 (three times the emitting building height).

For the last case, Figure 7-17 b) reduced influence is observed when adding a downstream building. D_N distribution increases lightly when a taller downstream is considered. (dh4).

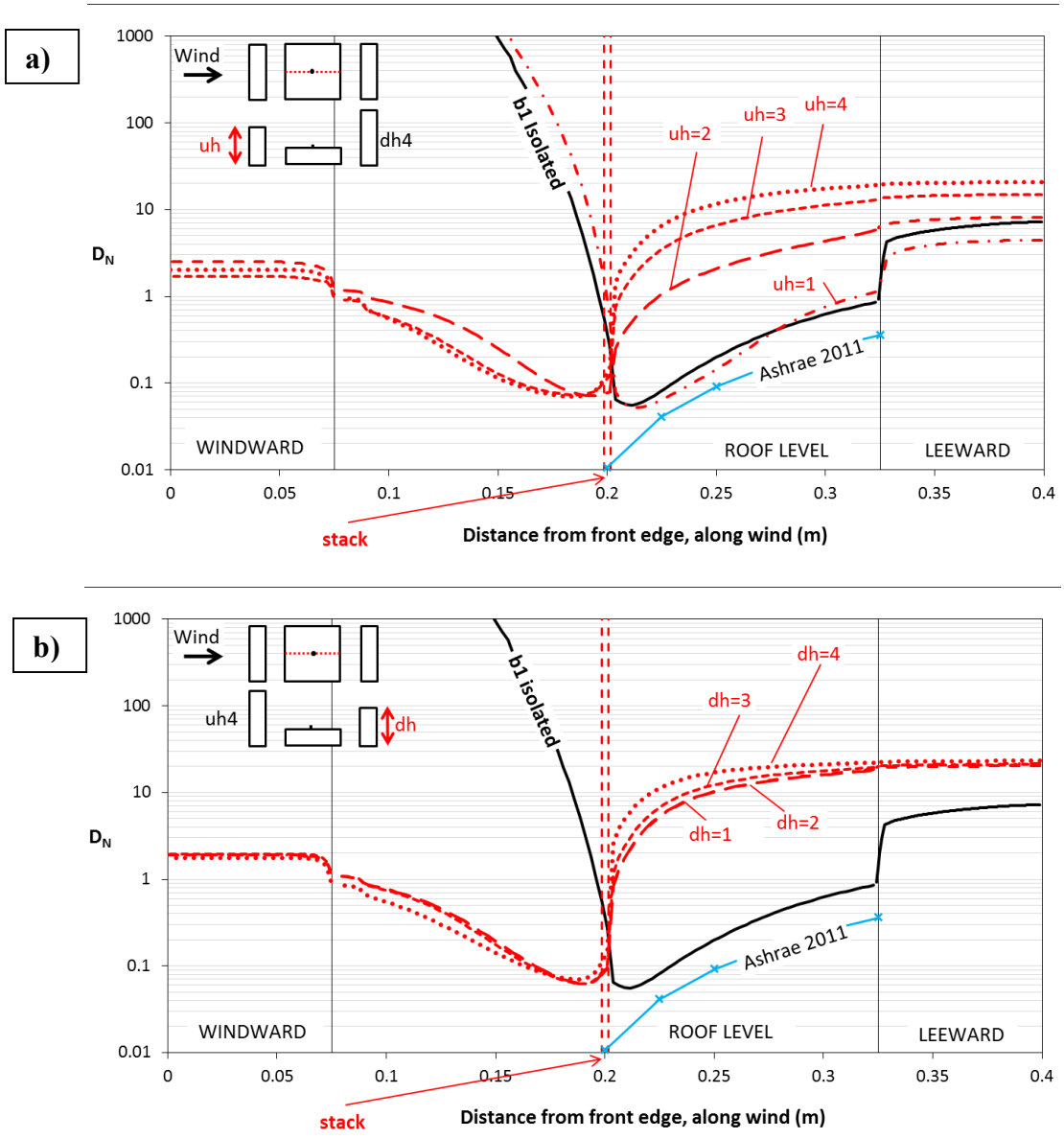

Figure 7-18. An emitting building between two buildings.

7.6 Guideline for safe placement of intakes on buildings

The current section presents a guideline for safe placement of intakes on buildings facades for all configurations seen in this study. Basically, the current guideline contains recommendations to avoid re-ingestion of pollutants for non-isolated building configurations. These practical

recommendations are a concrete contribution that can be used for engineers or practitioners involved in urban development projects.

The starting point of producing a guideline is the definition of dilution criterion for judging acceptability. In absolute terms, the dilution starts from unity and increases with the distance from the source. A dilution criterion tells how much dilution is needed to judge a particular region free of re-ingestion or at least having the required condition for placing an intake. This criterion is specified as the ratio between the concentration at the source over an allowable concentration. In this guideline the dilution criterion at intakes of 3000:1 is used. This value is based on Wong and Ratcliff (2003) suggestions to avoid odors and occupational health effects for a large group of chemicals. It should be note that this criterion is less restrictive than 5000:1 proposed in ASHRAE (2007). The conversion of 3000:1 to normalized dilution, D_N, used in this study (see eq. 3-1) gives $D_N = 6$.

Computational simulation results are plotted for all cases with an iso-surface corresponding to $D_N = 6$ permitting one to visualize regions where the dilution criterion is not satisfied. Therefore, regions wrapped by the iso-surface $D_N = 6$ identifies those regions should be avoided for installing intakes due to re-ingestion risk. As example, Figure 7-19, 20 and 21 show the evolution of the re-ingestion zone for different building configurations. Observing Figure 7-19 it is noted that the presence of a taller upstream building modifies the flow over the stack and pollutants are transported towards the upstream building. In this case, installing intakes in the complete leeward wall of the upstream building is clearly not recommended. Figure 7-20 shows that the presence of a taller building downstream produces a strong downwash and the space between both buildings becomes completely contaminated; however installing intakes in the upper part of the downstream building can be suggested. Figure 7-21 shows the effect of a three-building configuration, it is observed that the upstream building is the most affected by the re-ingestion region regardless the height the height of the upstream building. On the other side, the downstream building is practically free of re-ingestion, and then no restriction for intakes location can be proposed. The same kind of figures, for all the cases seen in the study, can be found in the Appendix K. The guideline, presented in Tables 7-4, 7-5 and 7-6, summarizes the most relevant issues involving adjacent buildings and their effects on pollution dispersion. It should be mentioned that the

suggestions presented in this guideline are consistent with previous results presented by Hajra (2012).

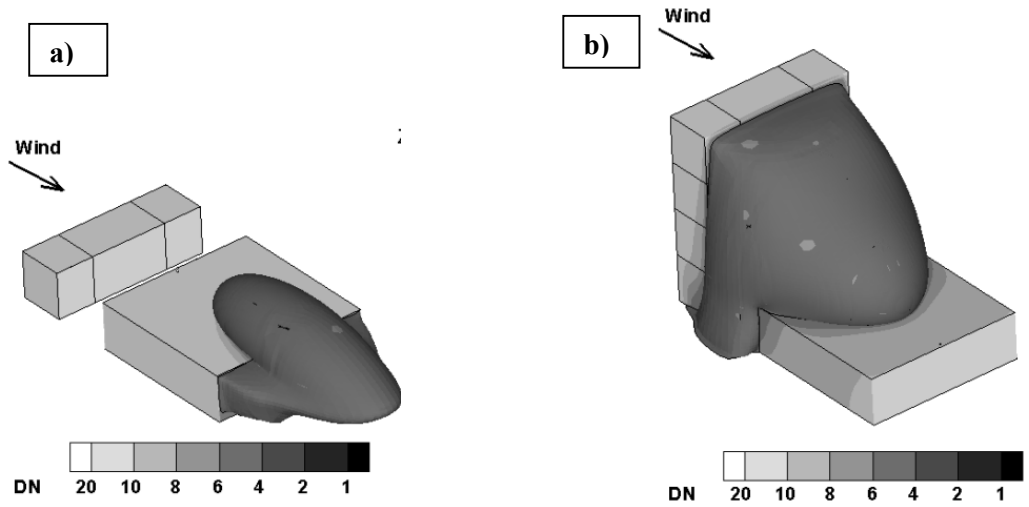

case-uh1, spacing = 0.1m (20m) case-uh4, spacing = 0.1m (20m)

Figure 7-19. Iso-surface $D_N = 6$ for case-uh1 (a) and case-uh4 (b)

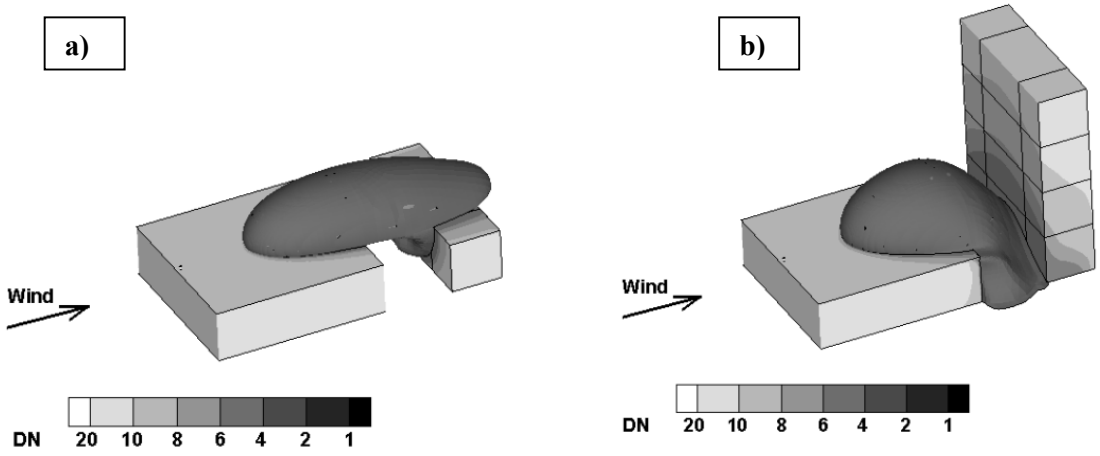

case-dh1, spacing = 0.1m (20m) case-dh4, spacing = 0.1m (20m)

Figure 7-20. Iso-surface $D_N = 6$ for case-dh1 (a) and case-dh4 (b)

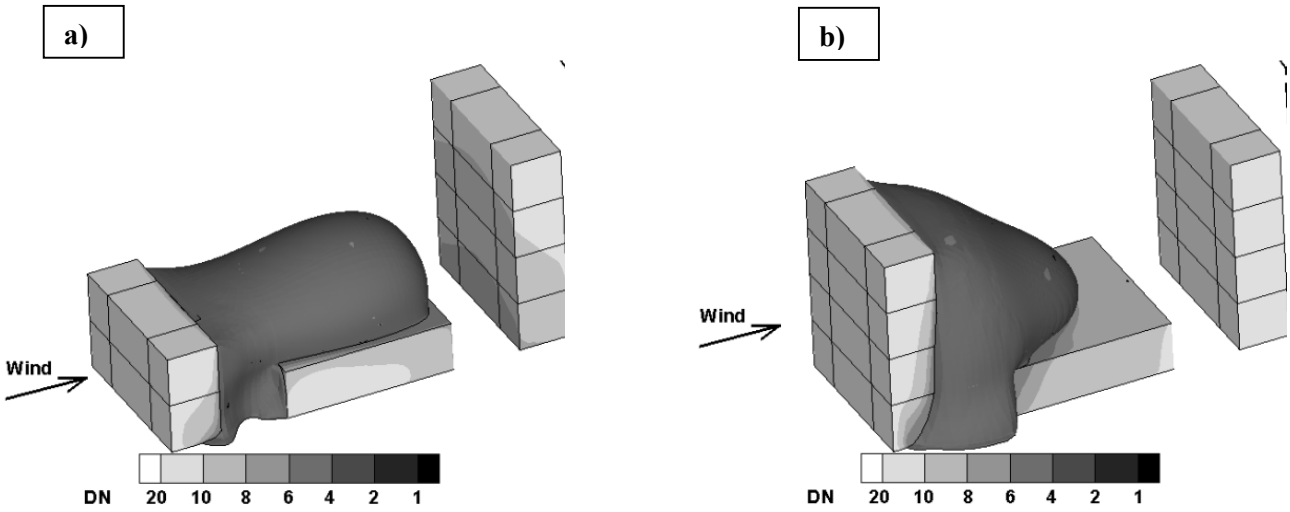

case-uh2dh4, spacing = 0.1 (20m)

case-uh4dh4, spacing = 0.1m (20m)

Figure 7-21. Iso surface $D_N = 6$ for case-uh2dh4 (a) and case-uh4-dh4 (b)

Table 7-4. Two-building configuration: effect of an UPSTREAM building

Case		Description	Suggested locations for intakes	Locations to avoid
1	Upstream building lower or same height than emitting building	-Plume is completely dragged downwind from the stack -Pollutants contaminate leeward wall of emitting building	-Any surface of the upstream building -Windward wall of emitting building -Upwind of the stack and side walls of emitting building	-Downwind from the stack -Leeward wall of emitting building
2	A medium-tall building (one storey taller than emitting building) located upstream	-Plume is partially trapped by recirculation region -Pollutants are dragged upwind and downwind of the stack	-Windward and side walls of upstream building -Lower part of leeward wall of upstream building -Side walls of emitting building	-Upper part of leeward wall of the upstream building -Entire roof of emitting building -Leeward wall of emitting building
3	A taller (two storeys or more taller than emitting building) upstream building	-Plume is completely dragged upwind the stack -Pollutants contaminate all the facades between both buildings	-Upper part of side walls of upstream and emitting building -Leeward wall of emitting building	-Leeward wall of upstream building -Windward wall and upwind edge of emitting building
4	If the spacing between buildings is large enough to ensure plume do not become trapped within the recirculation	-Plume is completely dragged downwind from the stack -Pollutants contaminate leeward of the emitting building	-Any surface of the upstream building -Side walls of emitting building -Upwind the stack if the upstream is medium tall	- Downwind from the stack for medium-tall upstream building -The entire roof of the emitting building for a tall upstream building
5	A wider and medium-tall building (one storey taller than emitting building) located upstream	-Same as case 2	-Windward, side walls and side edges of upstream building -Side walls of emitting building	-Vertical center of leeward wall of the upstream building -Windward wall ,upwind edge and roof of emitting building

Table 7-5. Two-building configuration : effect of a DOWNSTREAM building

Case		Description	Suggested locations for intakes	Locations to avoid
6	Downstream building lower or same height than emitting building	-Plume is dragged downwind from the stack -Pollutants are partially trapped between both buildings	-Side walls of downstream building -Windward and side walls of emitting building -Upwind from the stack of the emitting building	-Downwind from the stack of emitting building -Any surface between both buildings -Roof of downstream building
7	A medium-tall building (one storey taller than emitting building) located downstream	-Plume is completely trapped between both buildings -Pollutants scape from sides of and top of the downstream building	-Upper part of side walls of downstream building -Leeward wall of downstream building -Windward and side walls of emitting building -Upwind from the stack of the emitting building	-Same as case 6
8	A taller (two storeys or more taller than emitting building) downstream building	-Plume is completely trapped between both buildings -Downwash flow from upper part of downstream building keeps pollutant in the lower part between both buildings	-Same as case 7 -Upper part of leeward of downstream building	-Downwind from the stack of emitting building -Lower part of leeward wall of downstream building -Leeward wall of emitting building
9	Increased width or length of downstream building	-same as case 7	-Same as case 7	-Same as case 7

Table 7-6. Three-building configuration

Case		Description	Suggested locations for intakes	Locations to avoid
10	A medium-tall building located upstream and a taller building located downstream	-Plume is trapped by recirculation region created by the upstream building -Pollutants do not affect the downstream building	-Any surface of the downstream building -Leeward and side walls of emitting building -Windward of the upstream building	-Leeward wall of upstream building -Windward wall and roof of emitting building
11	A taller (two storeys or more taller than emitting building) upstream building	-Same as case 10	-Any surface of the downstream building -Leeward and side walls of emitting building -Windward of the upstream building	-Leeward wall of upstream building -Windward wall and upwind edge of emitting building

7.7 Summary

This chapter presented a parametric study based on numerical simulations for flow and dispersion for various non-isolated building configurations. The objective was to determinate the range of influence of adjacent building geometry on dilution distribution at the roof of the emitting building, b1. Three cases were considered: (a) a building upstream of b1, (b) a building downstream of b1 and (c) b1 between two tall buildings. The geometric parameters analysed were: the height, the length and the width of the adjacent building. The major findings were the following:

- Dilution field is mainly affected by the upstream building height. As the plume is trapped by the recirculation zone, pollutants are dragged towards the upstream building decreasing and increasing dilution upwind and downwind the stack respectively.

- A building located downstream of b1 did not affect dilution distribution at b1 roof. D_N prediction remains very similar to the isolated building case. The leeward wall of b1 showed a relative lowest D_N value for case-dh2.

- In a three building configuration dilution is mainly affected by the building located upstream. The presence of a third building downstream of b1 did no change significantly D_N distribution.

At the end of the chapter, and based on the previous findings, a guideline for safe placement of intakes on buildings facades for all configurations seen in this study is presented.

8. SUMMARY, CONCLUSIONS, CONTRIBUTIONS AND FUTURE WORK

8.1 Summary and Conclusions

The present thesis establishes a reliable method to analyse flow and dispersion of pollutants in urban areas using the Computational Fluid Dynamics (CFD) approach. The goal of the study is to better understand pollution aerodynamics within a small urban layout and evaluate the pollutant re-ingestion potential of various building configurations and geometries.

In order to define the computational approach that was used during the study, a performance evaluation of steady and unsteady CFD techniques was carried out. The numerical approach evaluation included a systematic comparison of wind tunnel data as validation process. For steady simulation technique, named as Reynolds-Averaged-Navier-Stokes (RANS), fundamental numerical considerations were reviewed such as computational domain, meshing characteristics, boundary conditions definition, stopping criterion, turbulence model and turbulent Schmidt number (Sc_t). It was confirmed that RANS tends to underestimate dilution prediction especially in the wake of buildings. This underestimation is due to the inherent incapability of RANS of capturing flow unsteadiness: Three unsteady approaches were tested: unsteady Reynolds-Averaged Navier-Stokes (URANS), Large Eddy Simulation (LES) and Detached Eddy Simulation (DES) and the results compared with wind tunnel data. In this study, DES showed the best agreement with experimental data compared with other models.

A parametric study of building configuration and geometry of the adjacent buildings was carried out to evaluate the impact on pollutants dispersion in the near-field. Almost all the numerical results are presented in terms of normalised dilution, iso-contours and streamlines. This detailed information is crucial to better understand of three-dimensional behaviour of pollutants around buildings. This permits to avoid or at least to limit the re-ingestion of polluted air into the intakes of buildings and degrade indoor air quality. In line with these considerations, a guideline for safe placement of intakes on buildings facades for all configurations seen in this study was presented in order to offer concrete and practical recommendations for engineers and practitioners involved in urban development projects.

The main conclusions of the present study can be summarized as follows:

- In general, the results confirm that pollutant plume behaviour can be detected with acceptable accuracy using steady CFD approach. However, an underestimation of pollutant dispersion especially in regions with high turbulence activity has been observed. This is likely due to the RANS incapacity of detecting flow unsteadiness.

- Pollutant dispersion from a rooftop stack is greatly influenced by the value of turbulent Schmidt number (Sc_t). It was confirmed that low values of Sc_t may partly compensate for the underestimation of dispersion, by increasing turbulent mass diffusivity. A better agreement in terms of trend with wind tunnel data is generally observed at $Sc_t = 0.3$. The choice of a suitable Sct requires a careful assessment of vortical structures in the built environment.

- It was confirmed that for complex building configuration, as a three-building case, it seems that standard Sct (0.7) performs well independently of M used, thus no changes on Sct are needed.

- The scaled residual value analysis revealed that the criterion to stop a calculation is very important, particularly for a non-isolated building configuration. The current study established that all equations should reach a residual value of $0.4x10^{-5}$ to minimize the influence of this parameter in the final solution.

- CFD provides valuable information about scalars and velocity fields as well as about vortical structures formed in the leeward side and between buildings. Knowing how these flow characteristics interact with the surroundings is essential to improve the understanding of pollutant dispersion within an urban area.

- Unsteady RANS (URANS) methodology did not show any improvement of the CFD estimates when compared to the RANS approach, as opposed to the DES and LES approach, which does improve the CFD predictions, albeit at a high computational cost.

- Performing numerical simulation over complexes geometries and multiple-building layout has a valuable potential for re-ingestion of pollutant control in urban areas. The proposed guideline in this thesis is helps practitioners to define safer locations for intake of buildings.

8.2 Contributions

The most relevant contributions of this research can be summarized as follows:

1) Concerning the extant literature on urban wind field, this research establishes a computational approach to study dispersion of pollutants (and potential re-ingestion) for non-isolated building configurations, which, as mentioned, is lacking in previous research.

2) Concerning CFD approach, this research contributes both to steady and unsteady approaches by validating or invalidating current measures and models, and proposing methodological recommendations:

   2.1.) Concerning steady CFD approach;

      i. It was verified that turbulent Schmidt number reduction improves agreement with experimental data for cases with high flow variability, however for flow with more homogeneous turbulence (less variability) the standard $Sc_t = 0.7$ performs well and no "calibration" is needed. It is thus suggested that further research should acknowledge this significant difference.

      ii. Inadequate stopping criterion can be a source of important error. In this study it is suggested to residual values to be less than the standard 10^{-5}, in particular for non-isolated building configurations.

      iii. Among the three turbulence models; SKE, RNG and RLZ, it was confirmed the superiority of RLZ. This observation is valid for the two-building configuration analysed.

   2.2.) Concerning unsteady CFD approach:

      iv. Unsteady RANS using Realizable k-ε turbulence model failed capturing large unsteadiness in the wake. It is however suggested for future research to try k-ω turbulence for unsteady RANS.

v. DES and LES performed well capturing the flow unsteadiness within the wake, but with a considerable computing time.

vi. The vortex generator model at the inlet significantly improves agreement with experimental data.

3) Concerning urban development projects, the parametric study developed in this research leads to quantification of the effect of adjacent buildings for different geometric and relative locations parameters.

i. The upstream building height and width revealed to be critical parameters for dispersion in the near-field.

ii. The proposed guideline is a valuable contribution to avoid re-ingestion of pollutants in small urban layout.

8.3 Recommendations for future research

- The natural follow-up step of the thesis would be to extend the present research to include more complex configurations with realistic geometries in order to improve the understanding of pollutant aerodynamics in actual industrial neighbourhoods or critical part of cities. Such research could be valuable information for authorities and risk managers to better cope accidental or non-accidental hazardous material release.

- The current research is based on gas dispersion simulation; however most of pollutants in urban areas are particles. Therefore, it is suggested to extend this study and explore a biphasic approach (e.g. dispersion of droplets) for pollutant dispersion simulations. The particle transport simulation based on the Lagrangian discrete particle transport model which incorporates inertia and gravity effects of particle seems to be an interesting continuity of this research. The pertinence of such research is founded on the recent Legionnaire's outbreak in Quebec City that killed 13 people (Desbiens, 2012).

- It was observed that DES performed well in capturing unsteadiness. That makes this approach an interesting alternative to LES due its advantages in terms of computing costs. More tests are needed in order to optimize the size of meshing without losing accuracy.

- The current study explored URANS using Realizable turbulence model without success. New tests are needed but using SST k-ω turbulence model based on suggestions proposed by Tominaga (2014).

REFERENCES

ASHRAE 2007. Chapter 14, Laboratories. ASHRAE Applications Handbook, American Society of Heating, Refrig. And Air-Cond. Eng., Inc., Atlanta, USA.

ASHRAE 2011. Chapter 45, Building Air Intake and Exhaust Design. ASHRAE Applications Handbook, American Society of Heating, Refrig. And Air-Cond. Eng., Inc., Atlanta, USA.

Bahloul, A. Stathopoulos, T., Chavez, M., Hajra, B. (2014). The impact of adjacent buildings on the dispersion of emissions from buildings: A numerical (CFD) and experimental approach in a wind tunnel. Report 0099-7590(b), IRSST, (http://www.irsst.qc.ca/en/-project-the-impact-of-adjacent-buildings-on-the-dispersion-of-emissions-from-buildings-a-numerical-cfd-and-experimental-approach-in-a-wind-tunnel-0099-7590.html).

Blocken, B., Stathopoulos, T., Carmeliet, J., 2007. CFD simulation of the atmospheric boundary layer: wall function problems. Atmos. Environ. 41, 238-252.

Blocken, B., Stathopoulos, T., Saathoff, P., Wang, X., 2008. Numerical evaluation of pollutant dispersion in the built environment: comparisons between models and experiments. Journal of Wind Engineering and Industrial Aerodynamics, 96, 1817- 1831.

Britter, R.E., Hanna, S.R. 2003. Flow and dispersion in urban areas. Annual review of fluid mechanics, 35, 469-496.

Brzoska M., Stock D., Lamb B., 1997. Determination of plume capture by the building wake. Journal of Wind Engineering and Industrial Aerodynamics, 67/68, 909-922.

Canepa, E., 2004.An Overview of downwash effects on dispersion of airborne pollutants. Environmental modeling and software, 19, 1077-1087.

Castro I.P., 2003. CFD for External Aerodynamics in the Built Environment. The QNET-CFD Network Newsletter, Vol. 2 No. 2, 4-7.

Cermak, J.E., Davenport, A.G., Plate, E.J., Viegas D.X., 1995. Wind Climate in Cities. Kluwer Academic Publishers, NATO ASI Series E vol. 277, The Netherlands.

Chavez, M., Hajra, B., Stathopoulos, T., Bahloul, A., 2011. Near-field pollutant dispersion in the built environment by CFD and wind tunnel simulations. Journal of Wind Engineering and Industrial Aerodynamics, 99 (4), 330-339.

Chavez, M., Hajra, B., Stathopoulos, T., Bahloul, A., 2012. Assessment of near-field pollutant dispersion: Effect of upstream buildings. Journal of Wind Engineering and Industrial Aerodynamics, 104/106, 509-515.

Cheng Y., Lien F.S.,Yee E., Sinclair R., 2003. A comparison of large Eddy simulations with a standard k-ε Reynolds-averaged Navier Stokes model for the prediction of a fully developed turbulent flow over a matrix of cubes. Journal of Wind Engineering and Industrial Aerodynamics, 91, 1301-1328.

Cheung, J.C.K., Melbourne, W.H., 1995. Building downwash of plume and plume interactions. Journal of Wind Engineering and Industrial Aerodynamics, 54, 543-548.

Davidson, L., 2003. An Introduction to turbulence models. Department of Thermo and Fluid Dynamics, Publication 97/2, Chalmers University of Technology, Sweden. (http://www.fem.unicamp.br/~im450/palestras&artigos/kompendium_turb.pdf).

Desbiens, F., 2012. Éclosion de légionellose dans la ville de Québec, Québec, Canada, été 2012 - Rapport du directeur de santé publique Direction régionale de santé publique, Agence de la santé et des services sociaux de la Capitale-Nationale. 145 p. (http://www.dspq.qc.ca/documents/RapportLegionellose05122012.pdf).

Di Sabatino, S., Buccolieri, R., Pulvirenti, B., Britter, R., 2007. Simulations of pollutant dispersion within idealised urban-type geometries with CFD and integral models. Atmospheric Environment, 41, 8316-8329.

Dyer, A.J., Bradley, E. F., 1982. An alternative analysis of flux-gradient relationships at the 1976 ITCE. Boundary Layer Meteorology, 22, 3-19.

Flesch, T. K., Prueger, J. H., Hatfield, J. L., 2002. Turbulent Schmidt number from a tracer experiment. Agriculture and Forest Meteorology, 111, 299-307.

Flowe, A.C., Kumar, A., 2000. Analysis of velocity fields and dispersive cavity parameters as a function of building width to building height ratio using a 3-D computer model for squat buildings. Journal of Wind Engineering and Industrial Aerodynamics, 86, 87-122.

Fluent User Guide, 2009, Volumes 1–4. Fluent Inc., Lebanon. (https://www.sharcnet.ca/Software/Fluent6/index.htm).

Frohlich, J. von Terzi, D., 2008. Hybrid LES/RANS Methods for the Simulation of Turbulent Flow. Progress in Aerospace Science, 44, 349-377.

Franke, J., Hellsten, A., Schunzen, H., Carissimo, B., 2007. Best practice guideline for the CFD simulation of flows in the urban environment. Cost Action, 732 (Quality assurance and improvement of micro scale meteorological models). Distributed by University of Hamburg Meteorological Institute Centre for Marine and Atmospheric Sciences, Hamburg, Germany. 52pp.

Gouseau, P., Blocken, B., van Heijst, G.J.F., 2012. Large-Eddy Simulation of pollutant dispersion around a cubical building: Analysis of the turbulent mass transport mechanism by unsteady concentration and velocity statistics. Environmental Pollution, 167, 47-57.

Gousseau, P., Blocken, B., Stathopoulos, T., van Heijst, G.J.F., 2011. CFD simulation of near-field pollutant dispersion on a high-resolution grid: A case study by LES and RANS for a building group in downtown Montreal. Atmospheric Environment, 45, 428-438.

Guenther, A., Lamb, B., Peterson, R., 1989. Modeling of plume downwash and enhanced diffusion near buildings: Comparisons to wind tunnel observations for an arctic industrial site. American Meteorological Society, 28, 343-353.

Hajra B, Stathopoulos T, Bahloul A., 2010. Assessment of pollutant dispersion from rooftop stacks: ASHRAE, ADMS and Wind Tunnel simulation. Journal of Building and Environment, 45, 2768-2777.

Hajra, B., Stathopoulos, T., Bahloul, A. 2011. The effect of upstream buildings on near-field pollutant dispersion in the built environment. Journal of Atmospheric Environment, 45, 4930-4940.

Hajra, B., 2012. A Comprehensive Experimental Study of the Effects of Adjacent Buildings on Near-Field Pollutant Dispersion. PhD Thesis at Concordia University, Montreal, Canada.

Hanna, S. R., G. A. Briggs, R. P. Hosker, 1982. Handbook on Atmospheric Diffusion. DOE/TIC-11223. U. S. Department of Energy, Oak Ridge, TN. 110 pp.

Hargreaves, D., Wright, N., 2007. On the use of the k-ε model in commercial CFD software to model the neutral at-mospheric boundary layer. Wind Engineering and Industrial Aerodynamics. 95, 355-369.

Hasse, C., Sohm., Wetzel, N., Durst, B., 2009. Hybrid URANS/LES Turbulence Simulation of Vortex Shedding Behind a Triangular Flameholder. Flow Turbulence and Combustion, 83, 1-20.

Hefny M., Ooka R., 2009. CFD analysis of pollutant dispersion around buildings: effect of cell geometry. Building and Environment; 44(8), 1699-1706.

Hogstrom, U., 1996. Review of some basic characteristics of the atmospheric surface layer. Boundary Layer Meteorology, 78, 215-246.

Iaccarino, G., Ooi, A., Durbin, P.A., Behnia, M., 2003. Reynolds averaged simulation of unsteady separated flow. International Journal of Heat and Fluid Flow, 24, 147-156.

Khan, I.J., Simons, R.R., Grass, A.J., 2005. Upstream turbulence effect on pollution dispersion. Environmental Fluid Mechanics, 5, 393-413.

Koeltzsch, K., 2000. The height dependence of the turbulent Schmidt number within the boundary layer. Atmospheric Environment, 34, 1147-1151.

Koga, D.J, Way, J.L., 1979. Effects of Stack height and position on pollutant dispersion in building wakes. Proceedings of the fifth International Conference on Wind Engineering, Colorado state University, USA, 1003-1017.

Lateb, M., 2013. Numerical study of near-field pollutant dispersion around a building complex emitted from a rooftop stack. Thèse de doctorat, École de technologie supérieure, Montreal, 190 pp.

Lateb, M., Masson, C., Stathopoulos, T., Bédard, C., 2010. Numerical simulation of pollutant dispersion around a building complex. Building and Environment 45,1788-1798.

Li, W., Meroney, R.M., 1983. Gas dispersion near a cubical model building—Part I. Mean concentration measurements. Journal of Wind Engineering and Industrial Aerodynamics, 12, 15–33.

Liu, C., Ahmadi, G., 2006. Transport and deposition of particles near a building model. Building and Environment, 41, 828-836.

Meroney, R.N., 2004. Wind tunnel and numerical simulation of pollution dispersion: a hybrid approach. Working paper, Croucher Advanced Study Institute on Wind Tunnel Modeling, Hong Kong University of Science and Technology, 66 pp.

Meroney, R.N., 2006. CFD prediction of cooling tower drift. Journal of Wind Engineering and Industrial Aerodynamics, 94 (6), 463-490.

Meroney, R.N., 2008. Protocol for CFD prediction of cooling tower drift in an urban environment. Journal of Wind Engineering and Industrial Aerodynamics, 96 (10-11), 1789-1804.

Meroney, R.N., Leitl, B.M., Rafailidis, S., Schatzmann, M., 1999. Wind –tunnel and numerical modeling of flow and dispersion about several building shapes. Journal of Wind Engineering and Industrial Aerodynamics, 81, 333-345.

Murakami S., 1993. Comparison of various turbulence models applied to a bluff body. Journal of Wind Engineering and Industrial Aerodynamics, 46/47, 21-36.

Murakami, S., Mochida, A., 1988. 3-D numerical simulation of airflow around a cubic model by means of the k-ε model. Journal of Wind Engineering and Industrial Aerodynamics, 31, 283-303.

Murakami, S., Mochida, A., 1989. Three-dimensional numerical simulation of turbulent flow around buildings using the k-ε turbulence model. Building and Environment, 24 (1), 51-64.

Norris, S.E., Richards, P.J., 2010. Appropriate boundary conditions for computational wind engineering models re-visited. In: Proceedings of the Fifth International Symposium on Computational Wind Engineering (CWE2010) Chapel Hill, North Carolina, USA, May 23-27, 1-8.

Olvera, H.A., Choudhuri, A.R. and Li, W.W., 2008. Effects of plume buoyancy and momentum on the near-wake flow structure and dispersion behind an idealized building. Journal of Wind Engineering and Industrial Aerodynamics, 96,209-228.

Panagiotou, I., Neophytou, M.K.A.; Hamlyn, D., Britter, R.E., 2013. City breathability as quantified by the exchange velocity and its spatial variation in real inhomogeneous urban geometries: An example from central London urban area. Science of the Total Environment, 442, 466-477.

Parente, A., Gorlé, C., van Beeck, J., Benocci, C., 2011a. Improved k-ε model and wall function formulation for the RANS simulation of ABL flows. Wind Engineering and Industrial Aerodynamics, 99, 267-278.

Parente, A., Gorlé, C., van Beeck, J., Benocci, C., 2011b. A Comprehensive modelling approach for the neutral atmospheric boundary layer: Consistent inflow conditions, wall function and turbulence model. Boundary Layer Meteorology, 140, 411-428.

Petersen, R.L., Cochran B.C., Carter J.J. 2002. Specifying exhaust and intake systems. ASHRAE Journal, August edition.

Philips D., 2012. Modelling scalar dispersion in urban environments. PhD Thesis, Stanford, University, Mechanical Engineering Department, 186 pp.

Pruitt, W. O., Morgan, D. L., Lourence, F. J., 1973. Momentum and mass transfer in the surface boundary layer. Quarterly Journal of Royal Meteorological Society ,99, 370-386.

Ramponi, R. and Blocken, B.J.E., 2012. CFD simulation of cross-ventilation for a generic isolated building : impact of computational parameters. Building and Environment, 53, 34-48.

Ramsdell, J.V Fosmire, C.J., 1998. Estimating Concentrations in plumes released in the vicinity of buildings: Model development. Atmospheric Environment, 32, No.10, 1663-1677.

Richardson, L.F., 1927. The deferred approach to the limit, Transaction of the Royal Society London, Ser. A, 226, 229-361.

Roache, P.J., 1994. Perspective: A Method for Uniform Reporting of Grid Refinement Studies. Journal of Fluids Engineering, 116, 405-413.

Rodi, W., 1995. Introduction to numerical simulation approaches in wind engineering. Wind Climate in Cities, NATO ASI Series, Kluwer Academic Publishers Volume 277, 633-647.

Rotta, J.C., 1964. Temperaturverteilungen in der turbulenten grenzschicht an der ebenen platte. International Journal of Heat and Mass Transfer, 7, 215-228.

Saathoff, P., Gupta, A., Stathopoulos, T., Lazure, L. 2009. Contamination of Fresh Air Intakes Due to Downwash from a Rooftop Structure. Air & Waste Management Association. 59, 343–353.

Schulman, L., Scire J.S., 1993. Building downwash screening modeling for the downwind circulation cavity. Journal of the Air Waste Management Association, 43, 1122-1127.

Sergent, E. 2002. Vers une méthodologie de couplage entre la simulation des grandes échelles et les modèles statistiques. PhD thesis, L'Ecole Centrale de Lyon, Lyon, France, 2002.

Simiu, E., Scanlan, R.H., 1996. Wind effects on structures: fundamentals and applications to design. 3rd Edition, Wiley Interscience Publication, USA, 704 pp.

Snyder, W. H., 1981. Guidelines for fluid modeling of atmospheric diffusion. EPA office of air quality, planning and standards, Research Triangle Park, NC, EPA-600/8-81-009, 199 pp.

Spalding, D.B. 1971. Concentration Fluctuations in a Round Turbulent Free Jet. Chemical Engineering Science, 26, 95–107.

Stathopoulos, T., Lazure, L., Saathoff, P., Gupta, A., 2004. The effect of stack height, stack location, and rooftop structures on air intake contamination: A laboratory and full scale study. Research report R-392, Institut de recherche Robert-Sauvé en santé et en sécurité du travail, Montreal, Canada. Available online at http://www.irsst.qc.ca/media/documents/PubIRSST/R-392.pdf, 181 pp.

Stathopoulos, T., Hajra, B., Bahloul, A., 2008. Analytical evaluation of dispersion of exhaust from rooftop stacks on buildings. Research report R-576, Institut de recherche Robert- Sauvé en santé et en sécurité du travail, Montreal, Canada. Available online at http://www.irsst.qc.ca/media/documents/PubIRSST/R-576.pdf, 103 pp.

Stathopoulos, T., Bahloul, A., Chavez, M., Hajra, B. 2014. A Wind Tunnel Study of the Effect of Adjacent Buildings on Near-Field Pollutant Dispersion from Rooftop Emissions. Report 0099-7590(a), IRSST.

Tominaga Y., 2014. CFD simulation of flow field around a high-rise building: model evaluation of URANS. Niigata Institute of Technology, Department of Architecture and Building Engineering, Kashiwazaki, Japan. Poster presented at CWE2014 in June 2014, Hamburg .

Tominaga Y., Stathopoulos, T., 2009. Numerical simulation of dispersion around an isolated cubic building: Comparison of various types of k-ε models. Atmospheric Environment 43, 3200-3210.

Tominaga, Y., Stathopoulos, T., 2007. Turbulent Schmidt numbers for CFD analysis with various types of flowfield. Atmospheric Environment, 41, 8091-8099.

van Hooff, T., Blocken, B., 2010. On the effect of wind direction and urban surroundings on natural ventilation of a large semi-enclosed stadium. Computers & Fluids, 39, 1146-1155.

Wilson D.J., 1979. Flow patterns over a flat roofed buildings and application to exhaust stack design. ASHRAE Transactions 85, part 2, 284-295.

Wilson, D.J., Chui, E., 1987. Effect of turbulence from upwind buildings on dilution of exhaust gases. ASHRAE Transaction, 93 (2), 2186-2197.

Wilson, D.J., Fabris, I., Chen, J., Ackerman, M., 1998. Adjacent building effects on laboratory fume hood exhaust stack design. ASHRAE Research Report 897, American Society of Heating and Refrigerating and Air-conditioning Engineers, Atlanta, USA.

Wong, E., Ratcliff, M., 2003. Fume Hood Exhaust Stack Design: Exhaust Criterion. RWDI, Labs 21 Conference, San Antonio.

World Health Organization, 2013. Outdoor air pollution leading environmental cause of cancer deaths. Press release No 221, (http://www.iarc.fr/en/media-centre/iarcnews/pdf/pr221_E.pdf).

APPENDIX A: ADDITIONAL RESULTS FOR STACK PLACED AT THE FRONT EDGE OF THE EMITTING BUILDING

Additional comparisons for D_N between wind tunnel data and CFD when the stack is located near the front edge of the emitting building (Figure A-1) are presented in this appendix. All the cases correspond to a stack 0.005m high (actual wind tunnel scale) and M=1.7.

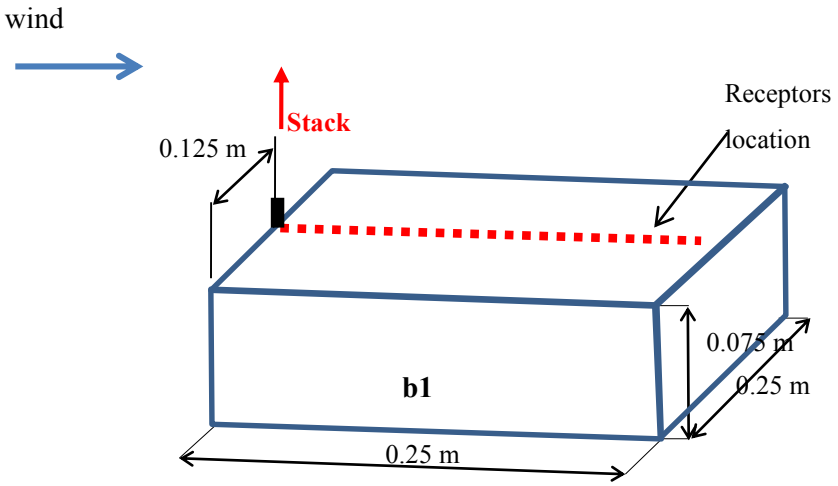

A-1. Emitting building (b1) whit stack located in the front edge.

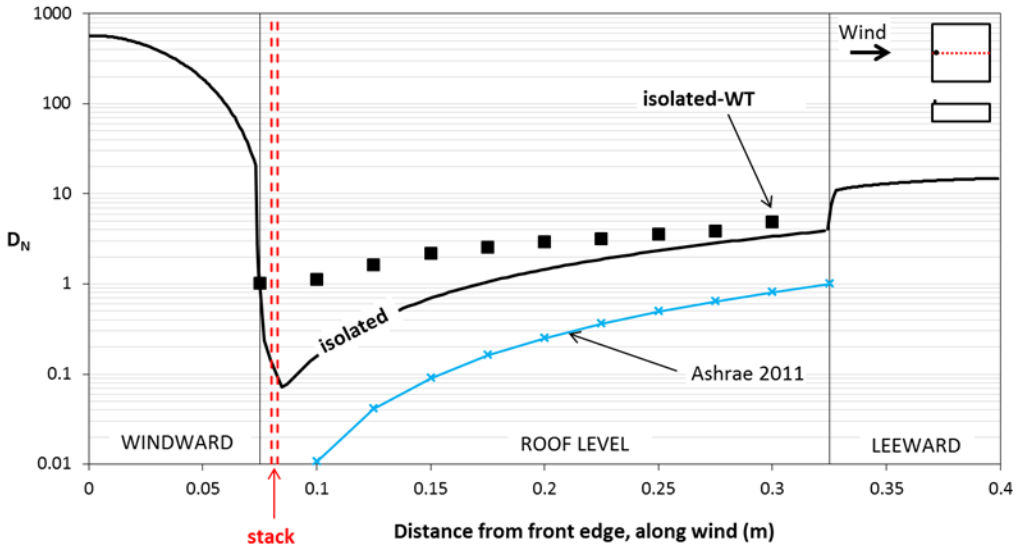

A-2. D_N for an isolated emitting building with the stack on the edge of the roof.

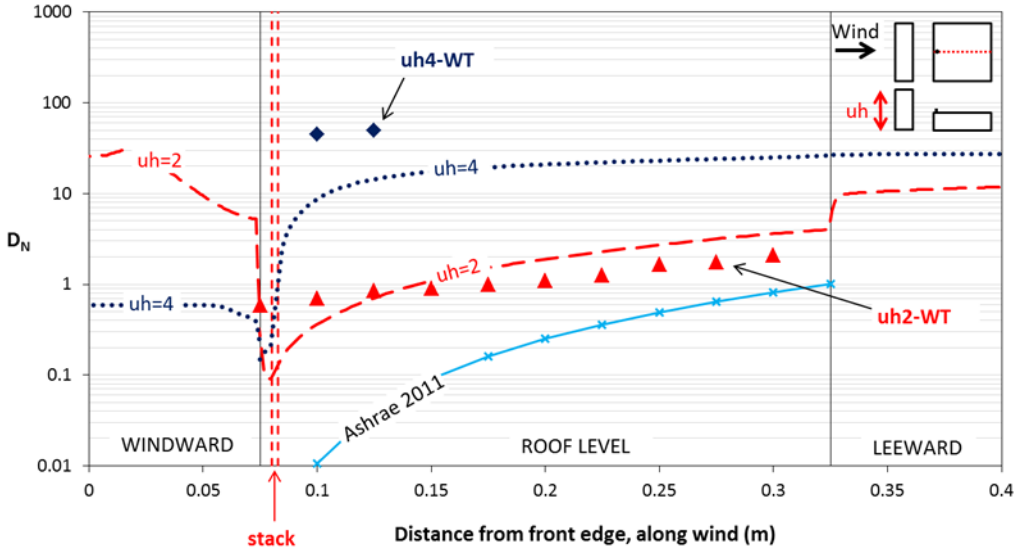

A-3. D_N when a building is located upstream of the emitting building with the stack on the edge of the roof. Buildings uh2 and uh4 have twice and four times the height of the emitting building.

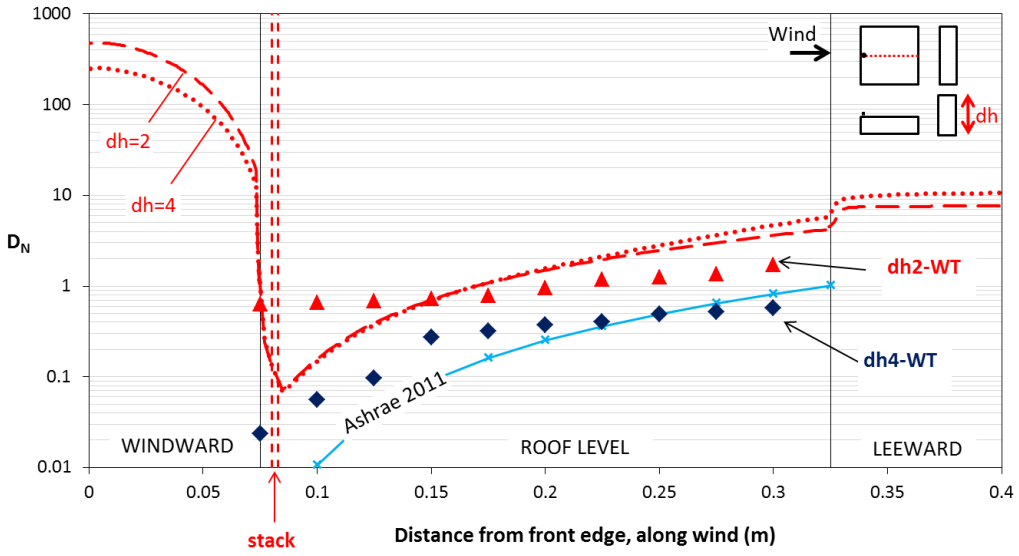

A-4. D_N when a building is located downstream of the emitting building with the stack on the edge of the roof. Buildings dh2 and dh4 have twice and four times the height of the emitting building.

APPENDIX B: VELOCITY MAGNITUDE CONTOURS FOR A TWO-BUILDING CONFIGURATION FOR DIFFERENT TURBULENCE MODELS (SKE, RNG, RLZ AND RSM).

B1) SKE

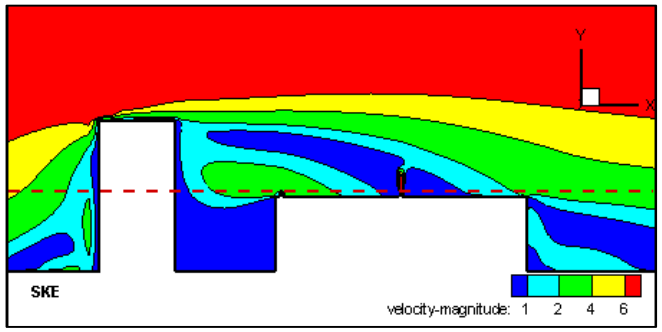

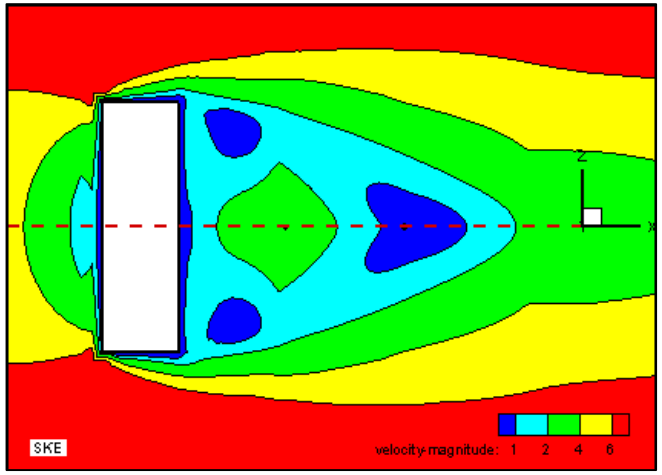

B2) RNG

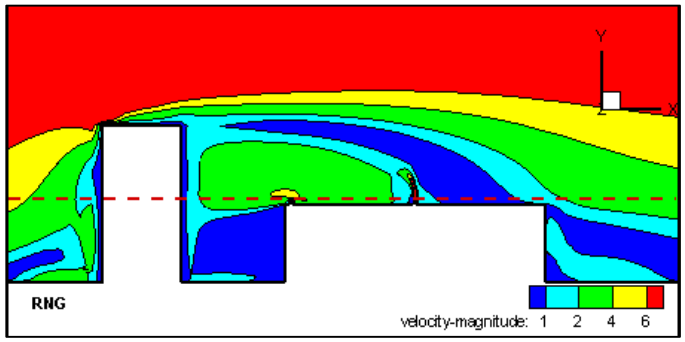

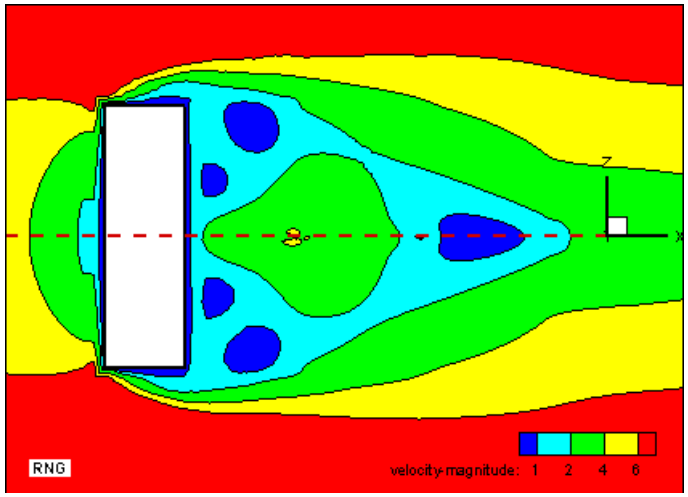

B3) RLZ

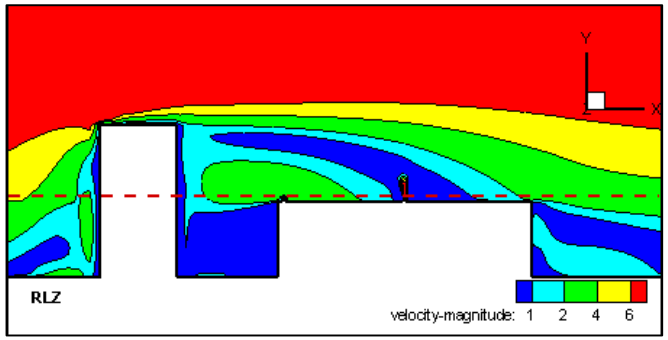
Y
X
RLZ
velocity-magnitude: 1 2 4 6

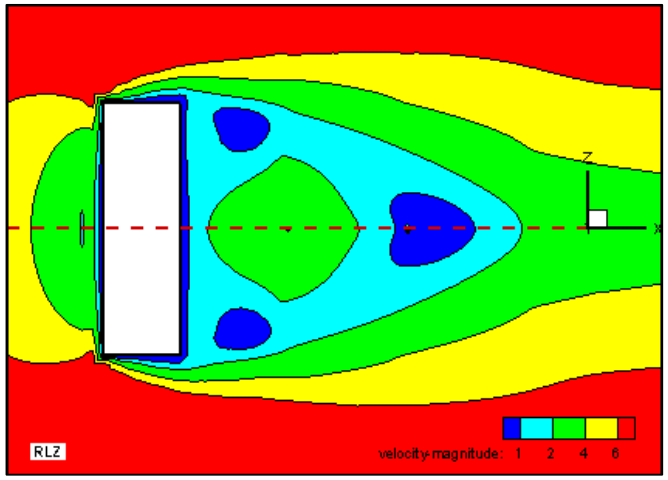
Z
X
RLZ
velocity-magnitude: 1 2 4 6

B4) RSM

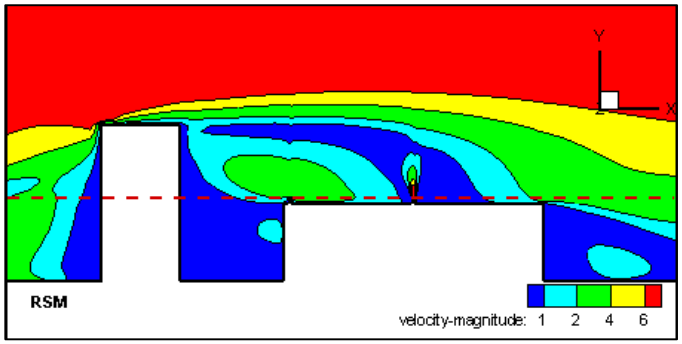
Y
X
RSM
velocity-magnitude: 1 2 4 6

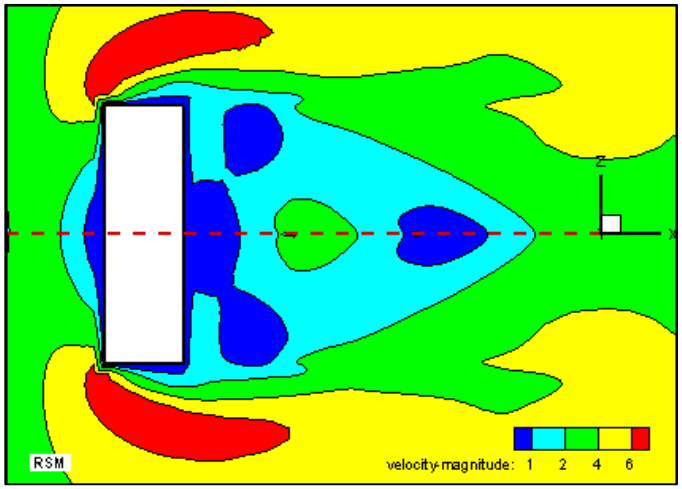
Z
X
RSM
velocity-magnitude: 1 2 4 6

APPENDIX C: TURBULENT KINETIC ENERGY CONTOURS FOR A TWO-BUILDING CONFIGURATION FOR DIFFERENT TURBULENCE MODELS (SKE, RNG, RLZ AND RSM).

C1) SKE

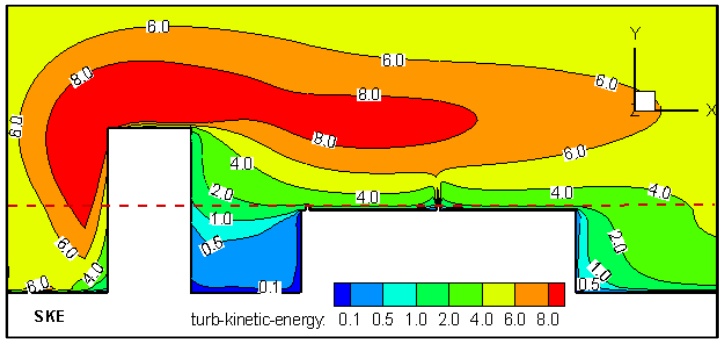

C2) RNG

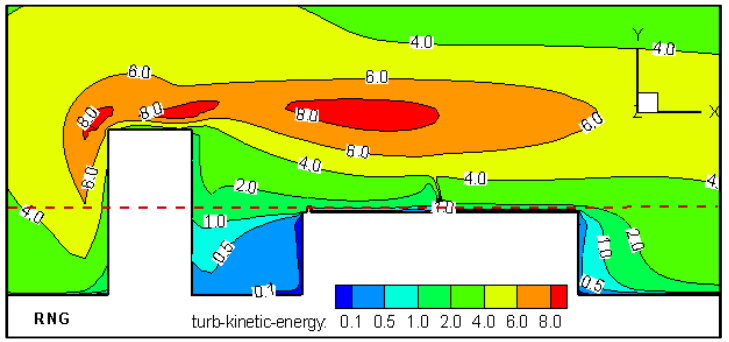

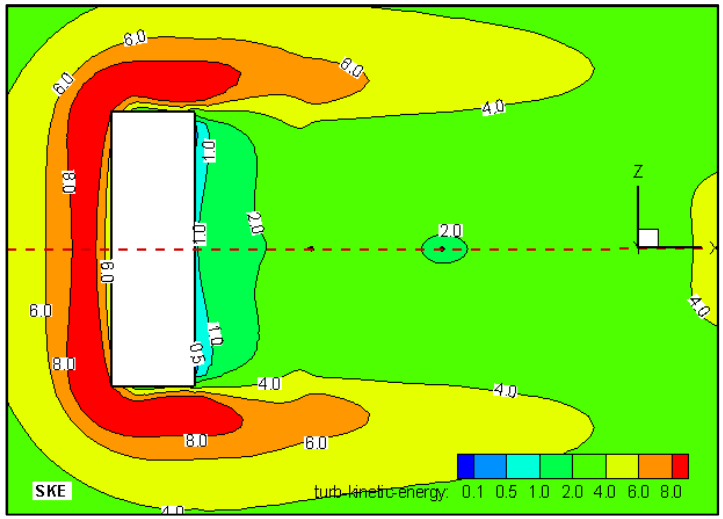

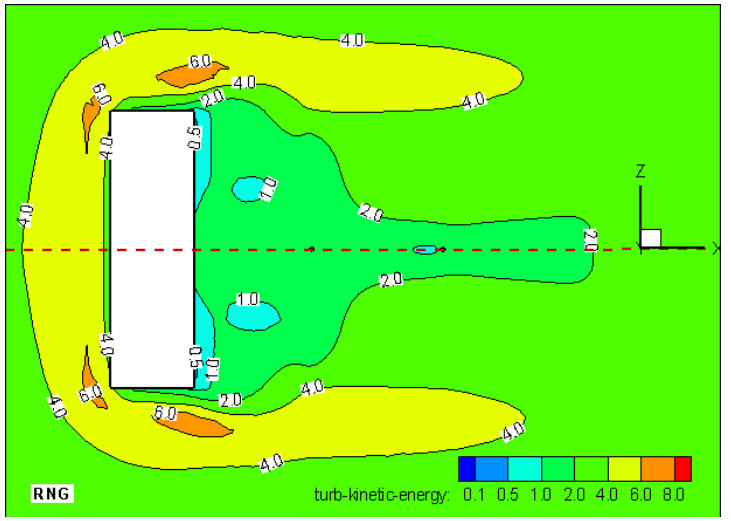

C3) RLZ

C4) RSM

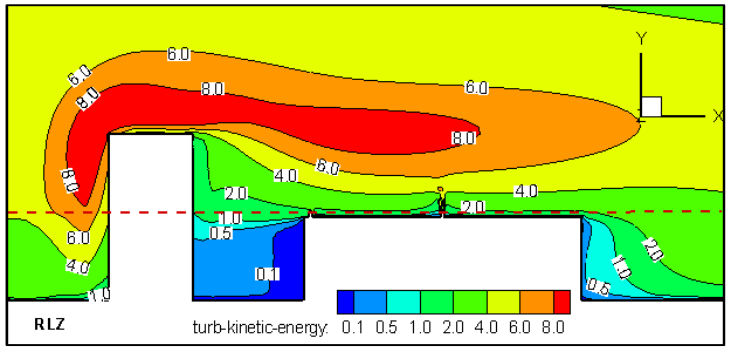
RLZ
turb-kinetic-energy: 0.1 0.5 1.0 2.0 4.0 6.0 8.0

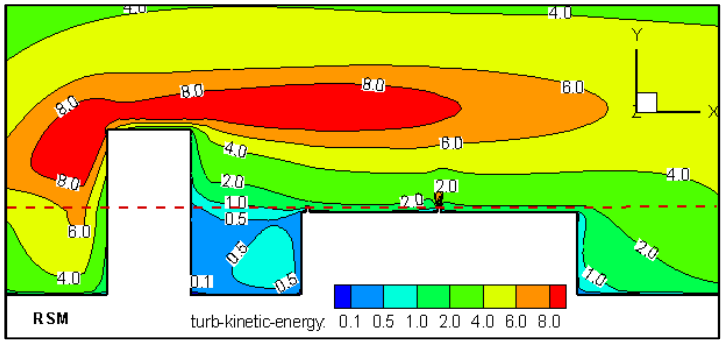
RSM
turb-kinetic-energy: 0.1 0.5 1.0 2.0 4.0 6.0 8.0

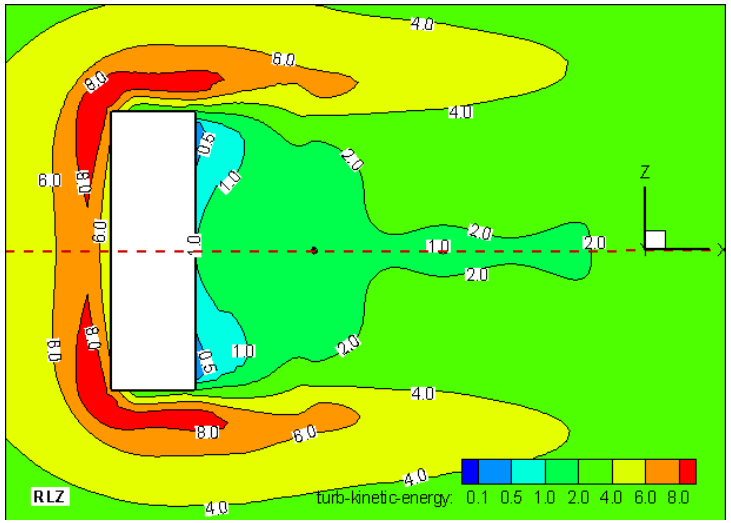
RLZ
turb-kinetic-energy: 0.1 0.5 1.0 2.0 4.0 6.0 8.0

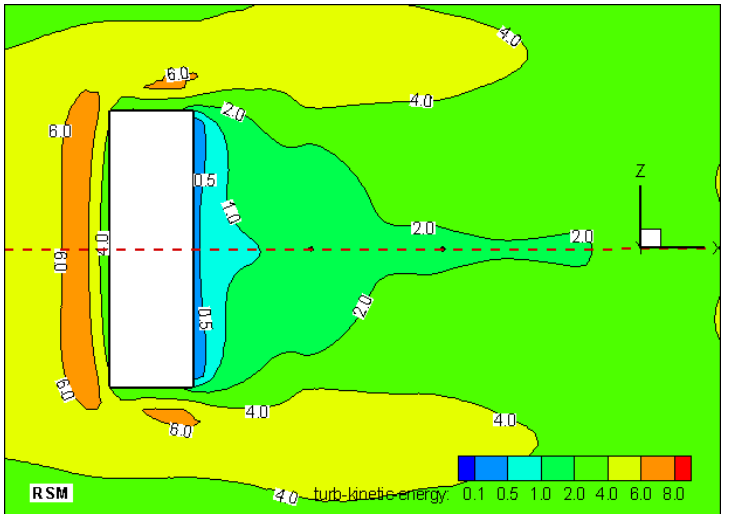
RSM
turb-kinetic-energy: 0.1 0.5 1.0 2.0 4.0 6.0 8.0

APPENDIX D: TURBULENT VISCOSITY CONTOURS FOR A TWO-BUILDING CONFIGURATION FOR DIFFERENT TURBULENCE MODELS (SKE, RNG, RLZ AND RSM).

D1) SKE

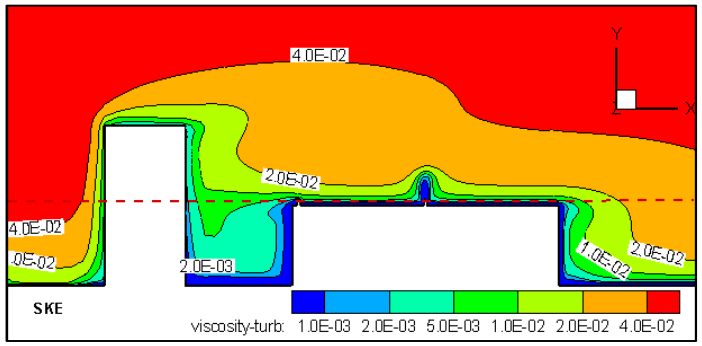

D2) RNG

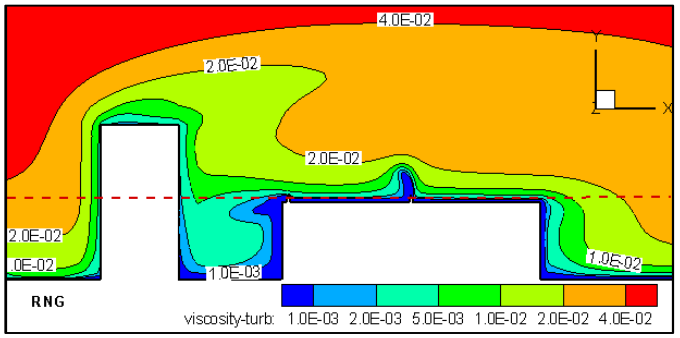

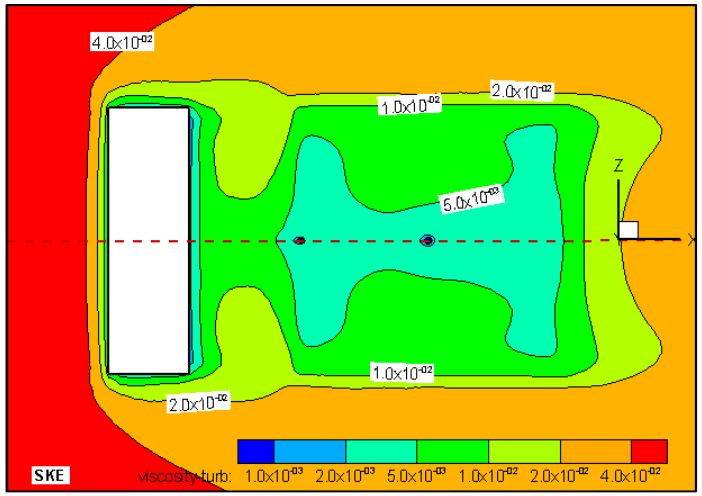

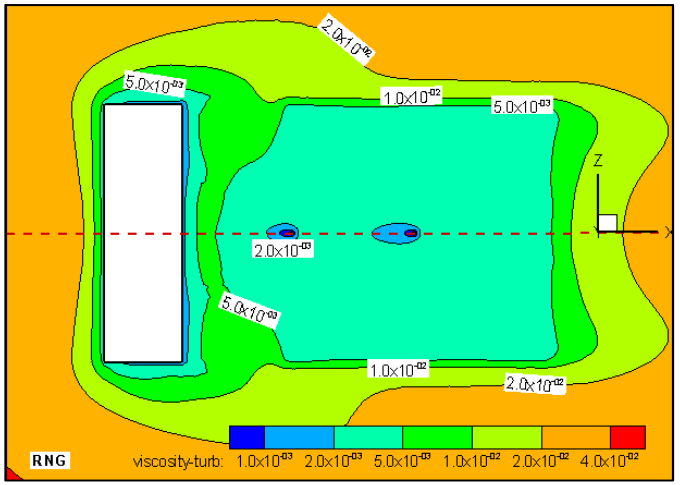

D3) RLZ

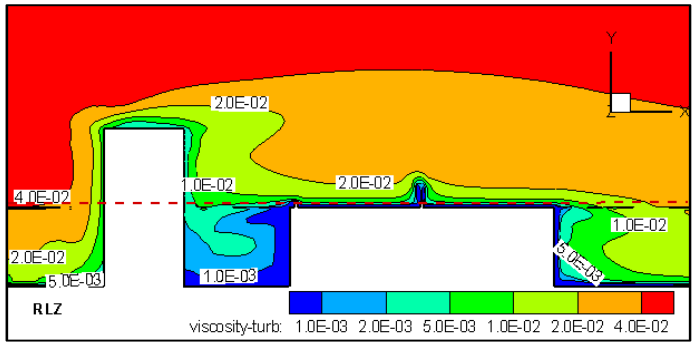
Y
X
2.0E-02
4.0E-02
1.0E-02
2.0E-02
1.0E-02
2.0E-02
5.0E-03
1.0E-03
5.0E-03
1.0E-02
RLZ
viscosity-turb: 1.0E-03 2.0E-03 5.0E-03 1.0E-02 2.0E-02 4.0E-02

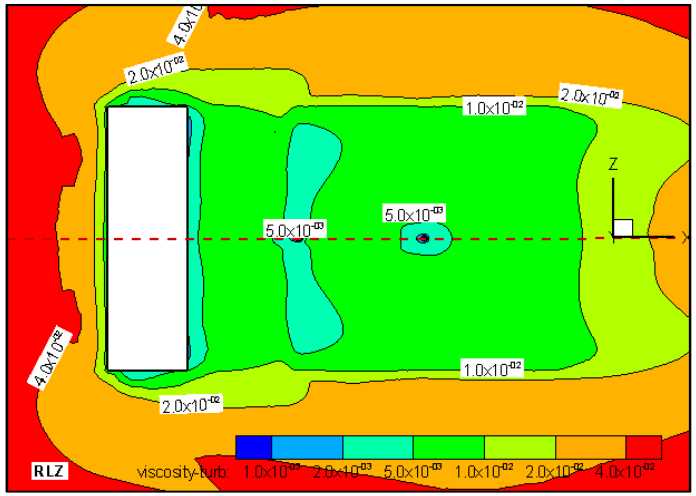
4.0x10-02
2.0x10-02
1.0x10-02
2.0x10-02
Z
X
5.0x10-03
5.0x10-03
4.0x10-02
1.0x10-02
2.0x10-02
RLZ
viscosity-turb: 1.0x10-03 2.0x10-03 5.0x10-03 1.0x10-02 2.0x10-02 4.0x10-02

D4) RSM

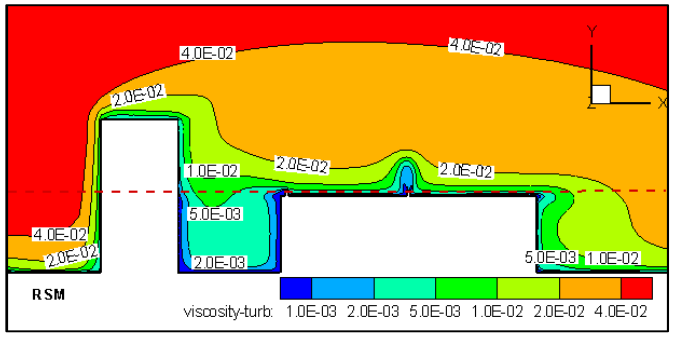
Y
X
4.0E-02
4.0E-02
2.0E-02
1.0E-02
2.0E-02
2.0E-02
5.0E-03
4.0E-02
2.0E-02
2.0E-03
5.0E-03
1.0E-02
RSM
viscosity-turb: 1.0E-03 2.0E-03 5.0E-03 1.0E-02 2.0E-02 4.0E-02

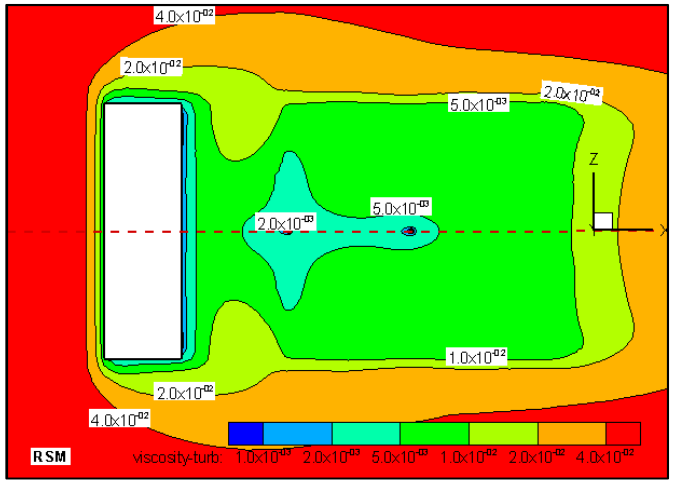
4.0x10-02
2.0x10-02
5.0x10-03
2.0x10-02
Z
X
5.0x10-03
2.0x10-03
1.0x10-02
2.0x10-02
4.0x10-02
RSM
viscosity-turb: 1.0x10-03 2.0x10-03 5.0x10-03 1.0x10-02 2.0x10-02 4.0x10-02

APPENDIX E: MEAN VELOCITY, STREAM LINES AN D_N CONTOURS RANS, URANS, DES, LES

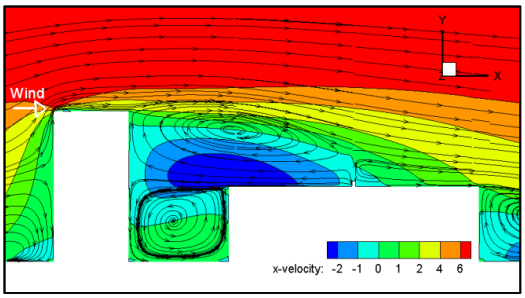

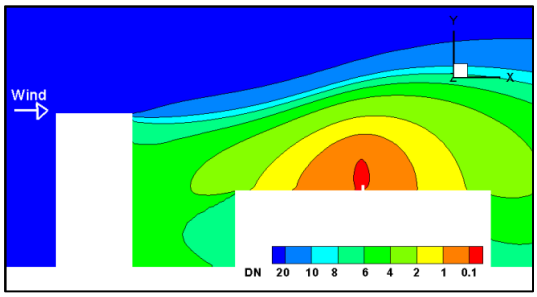

E1) RANS

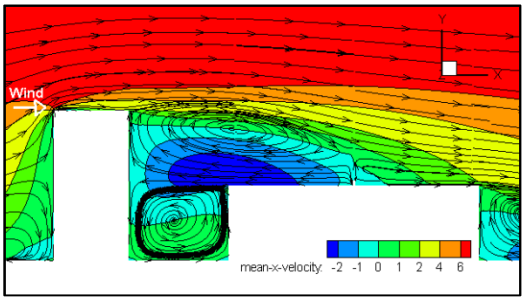

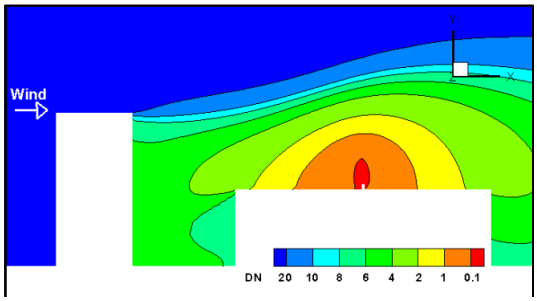

E2) URANS

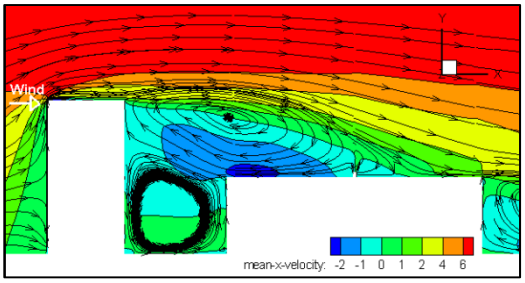

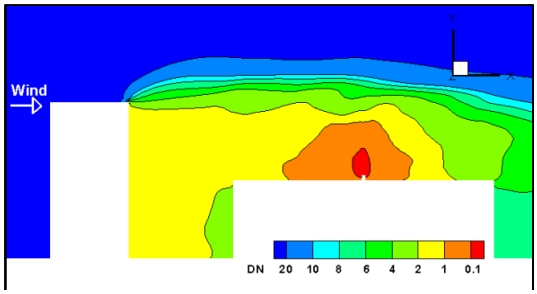

E3) DES

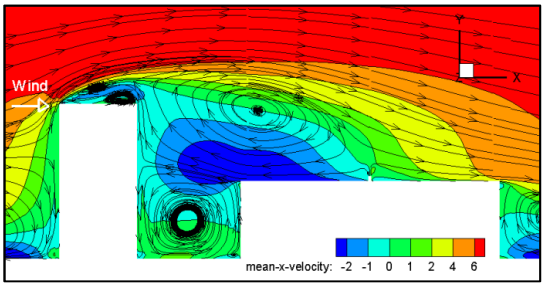

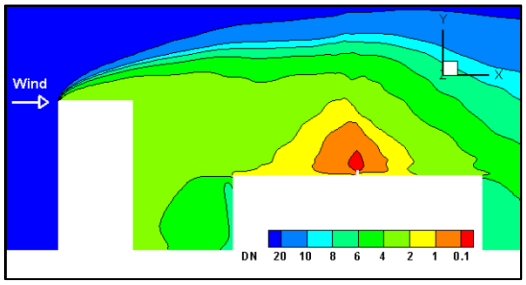

E4) LES

Mean velocity along wind (Ux), streamlines and corresponding D_N contours for RANS, URANS, DES and LES using fine mesh, time step = 0.005s and VM at the inlet for DES and LES. URANS uses RLZ turbulence mode Sct=0.3.

APPENDIX F: MEAN RMS-Ux CONTOURS DES, LES

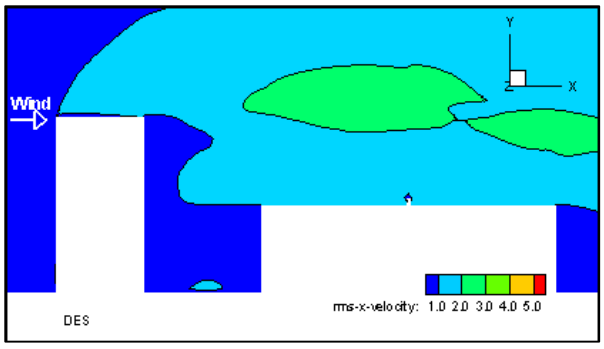

F1) DES- RMS Ux

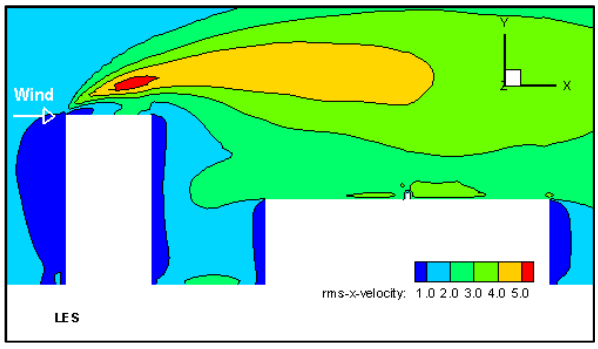

F2) LES-RMS-Ux

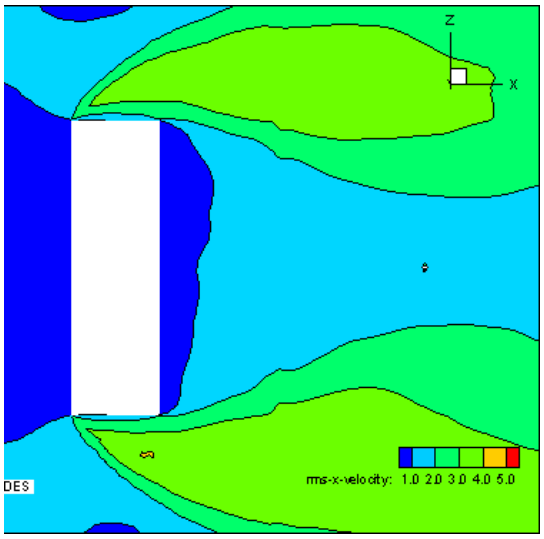

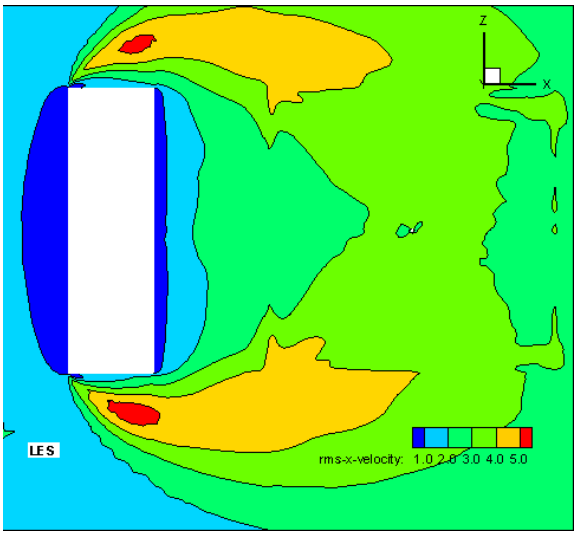

APPENDIX G: MEAN RMS-U_Y CONTOURS DES, LES

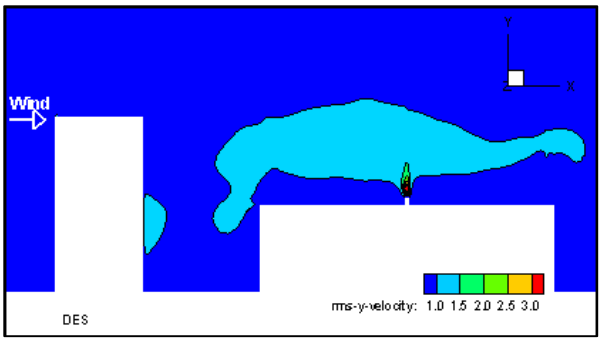

G1) DES- RMS Uy

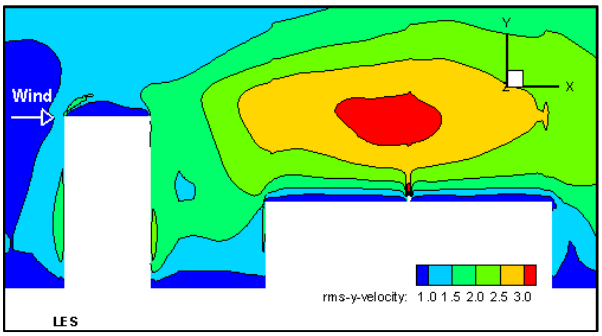

G2)LES-RMS-Uy

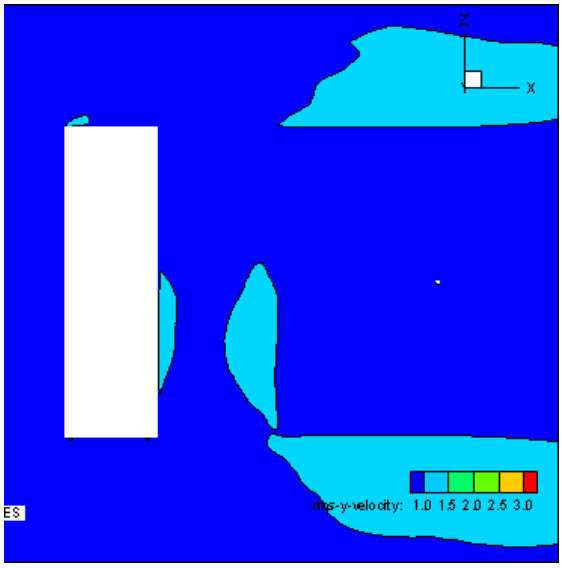

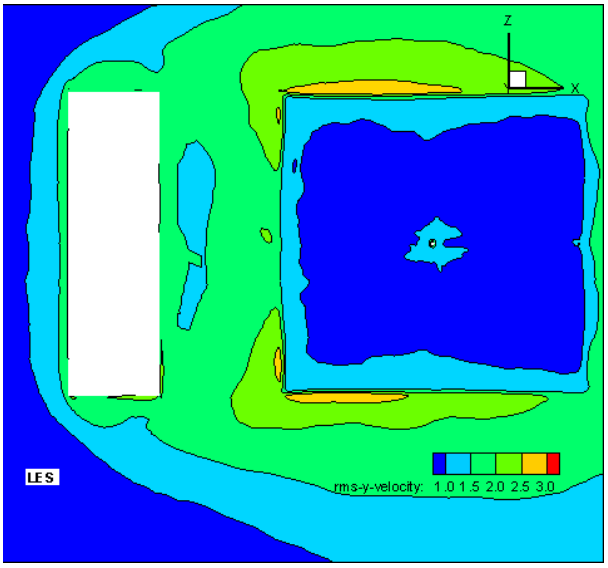

APPENDIX H: MEAN RMS-Uz CONTOURS DES, LES

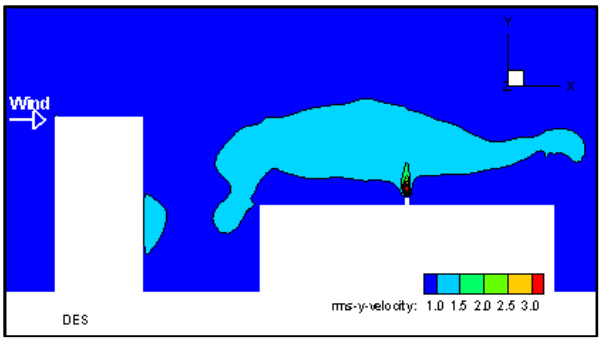

H1) DES- RMS Uy

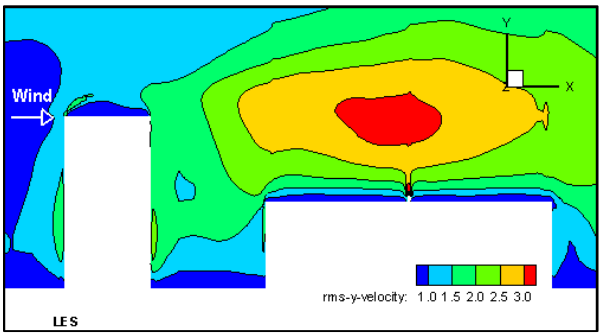

H2) LES-RMS-Uy

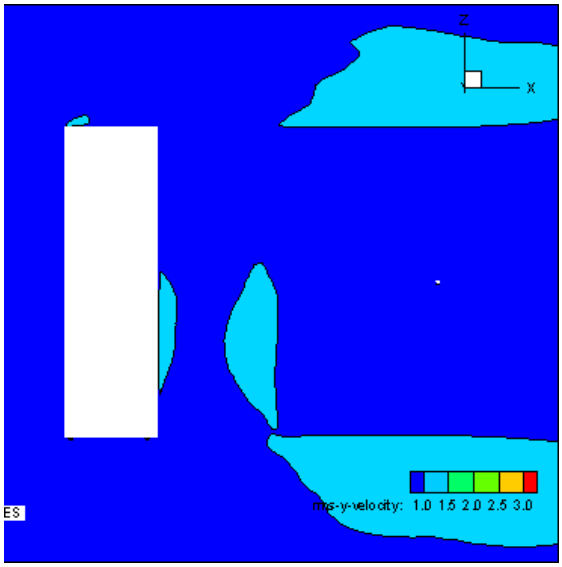

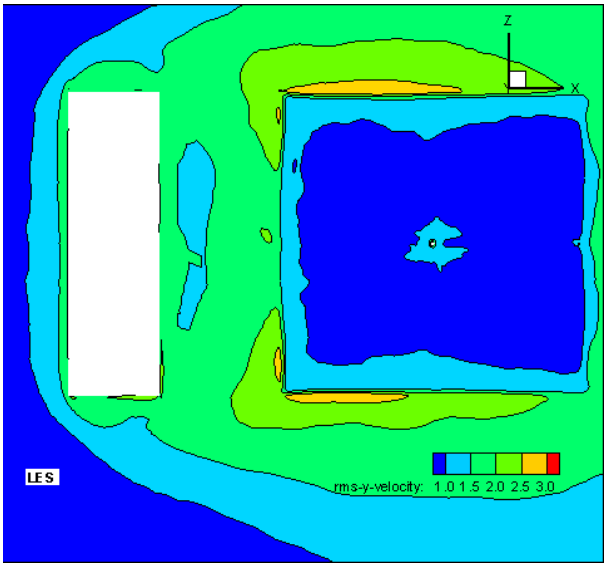

APPENDIX I: D_N CONTOURS FOR AN ISOLATED AND FOUR NON-ISOLATED BUILDING CONFIGURATIONS FROM CFD

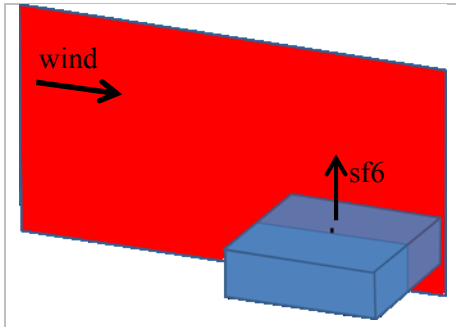

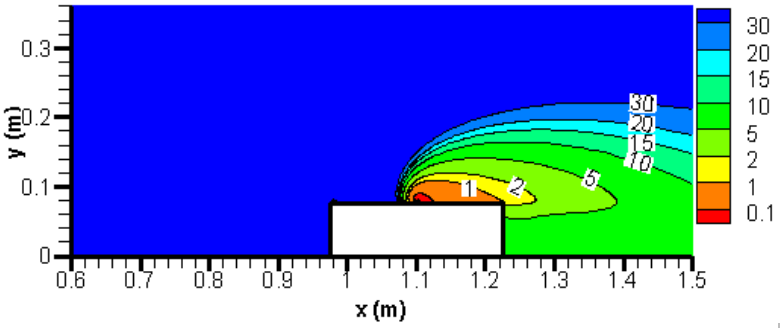

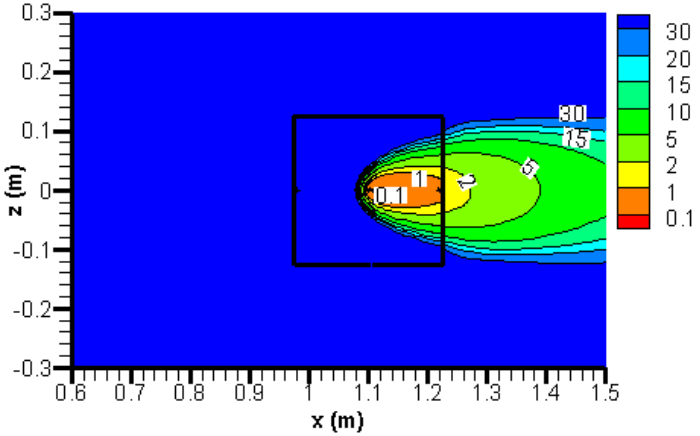

I-1(a) b1 isolated | **I-1(b) Middle elevation plane, z=0 (m)** | **I-1(c) Horizontal plane at y=0.08(m)**

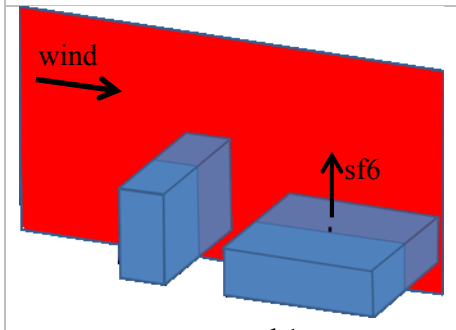

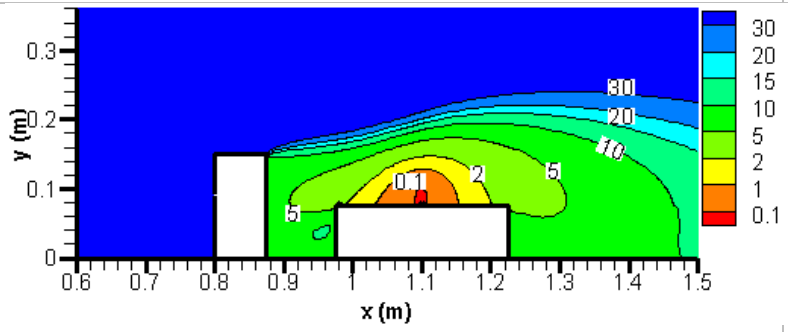

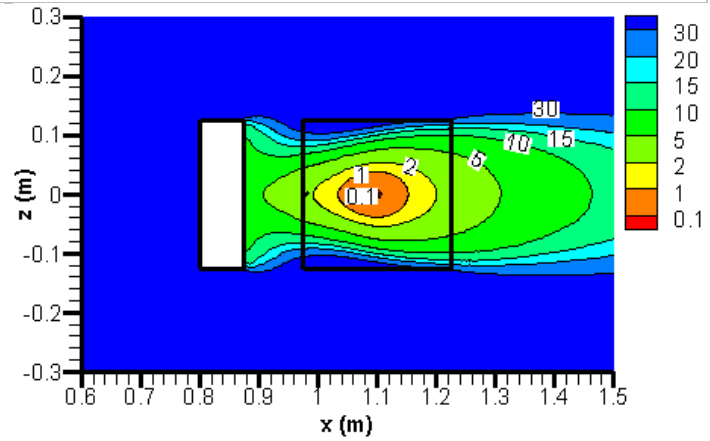

I-2(a) uh2 upstream of b1 | **I-2(b) Middle elevation plane, z=0 (m)** | **I-2(c) Horizontal plane at y=0.08(m)**

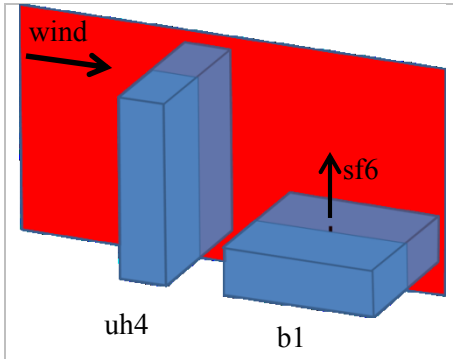

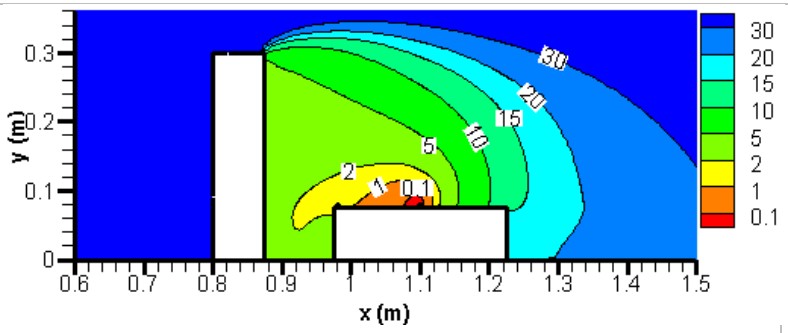

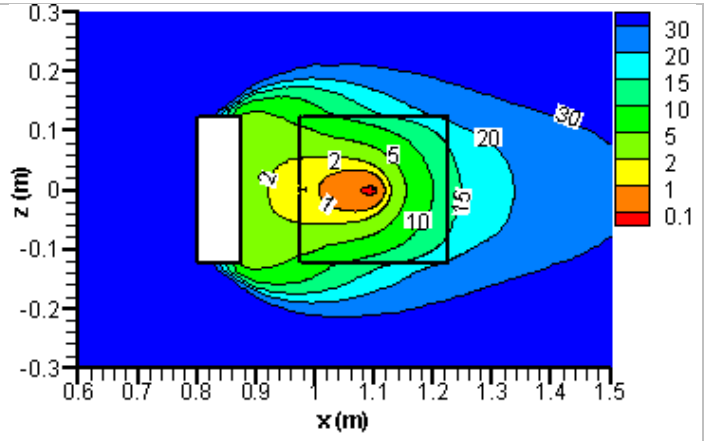

I-3(a) uh4 upstream of b1

I-3(b) Middle elevation plane, z=0 (m)

I-3(c) Horizontal plane at y=0.08(m)

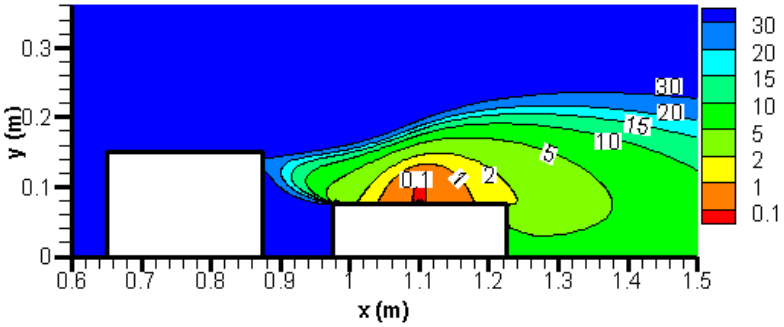

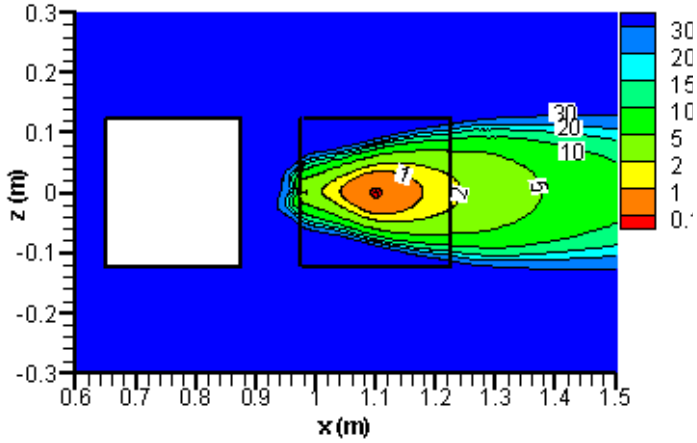

I-4(a) ul3 upstream of b1

I-4(b) Middle elevation plane, z=0 (m)

I-4(c) Horizontal plane at y=0.08(m)

	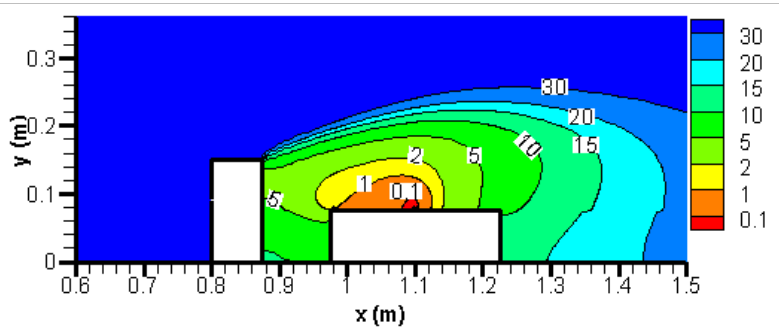	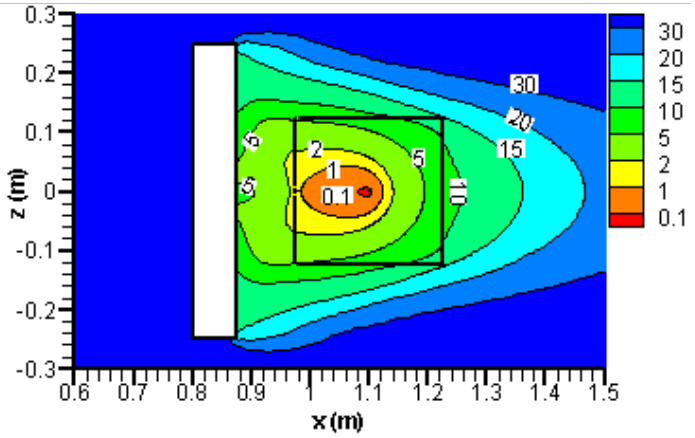
I-5 (a) uw4 upstream of b1	**I-5 (b) Middle elevation plane, z=0 (m)**	**I-5 (c) Horizontal plane at y=0.08(m)**
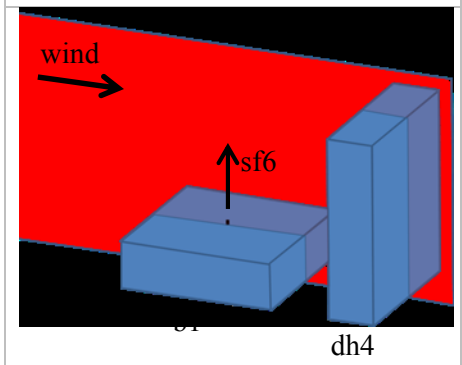	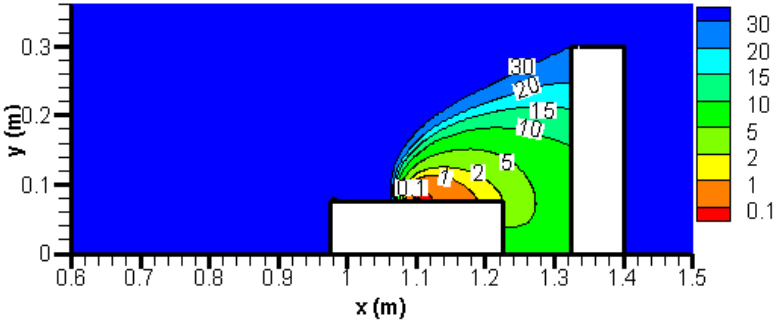	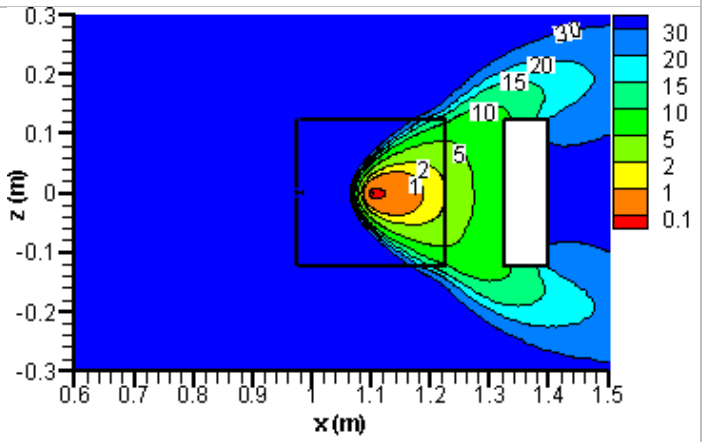
I-6 (a) dh4 downstream of **b1**	**I-6 (b)** Middle elevation plane, z=0 (m)	**I-6 (c)** Horizontal plane at y=0.08(m)

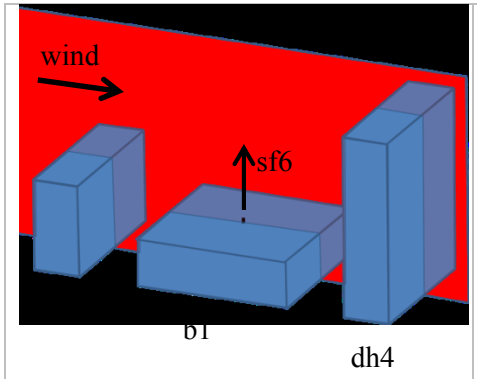

I-7 (a) uh2 upstream and dh4 downstream of b1

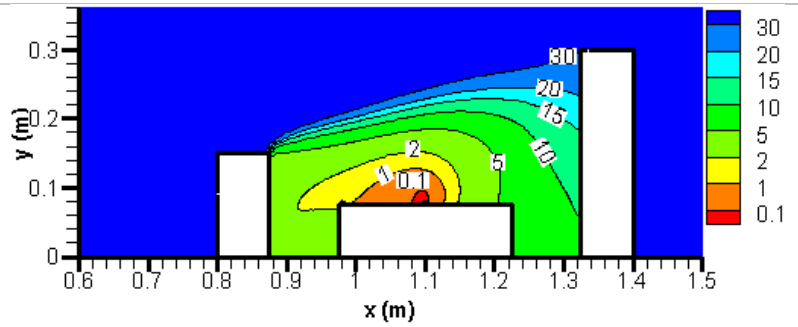

I-7 (b) Middle elevation plane, z=0 (m)

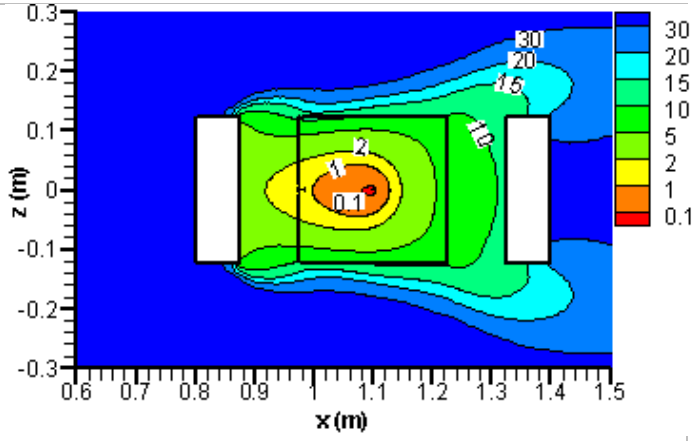

I-7 (c) Horizontal plane at y=0.08(m)

APPENDIX J: STREAMLINES FOR AN ISOLATED AND FOUR NON-ISOLATED BUILDING CONFIGURATIONS FROM CFD

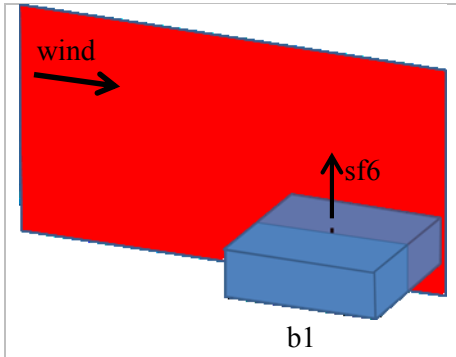

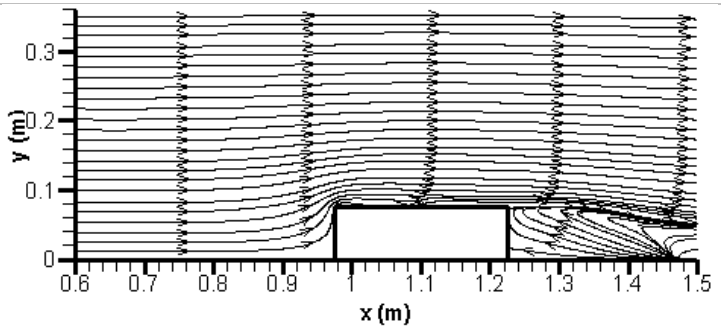

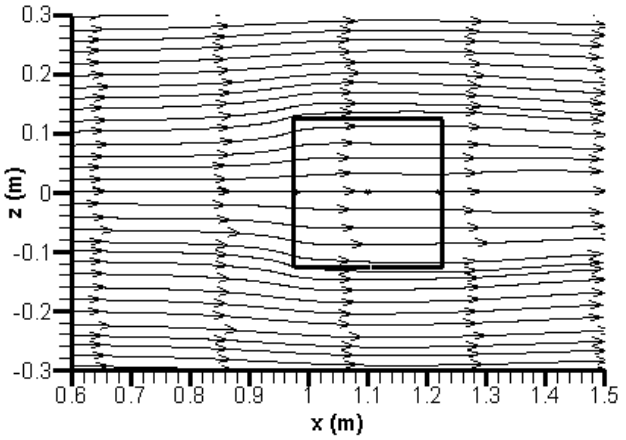

J-1(a) b1 isolated | **J-1(b) Middle elevation plane, z=0 (m)** | **J-1(c) Horizontal plane at y=0.08(m)**

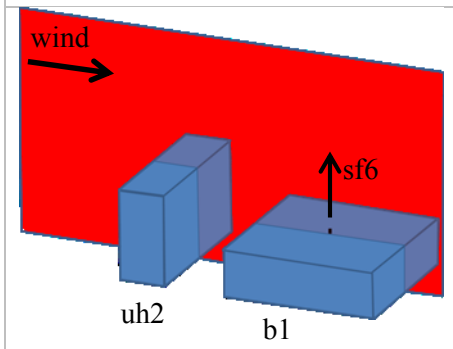

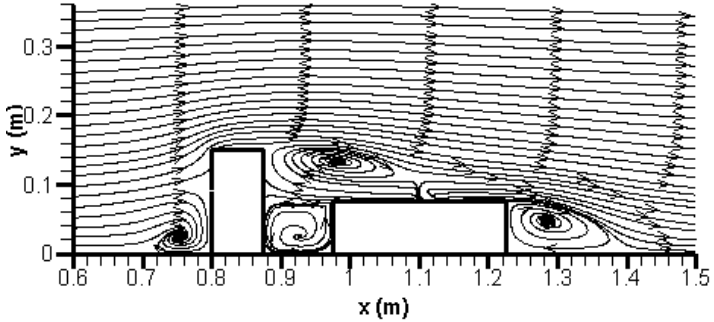

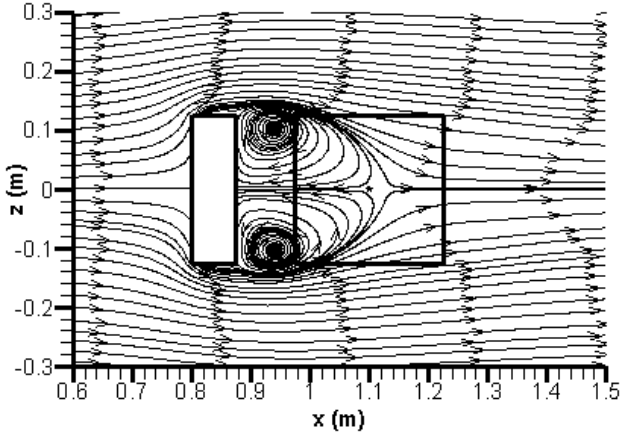

J-2(a) uh2 upstream of b1 | **J-2(b) Middle elevation plane, z=0 (m)** | **J-2(c) Horizontal plane at y=0.08(m)**

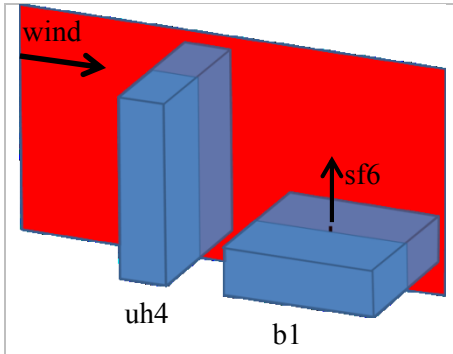

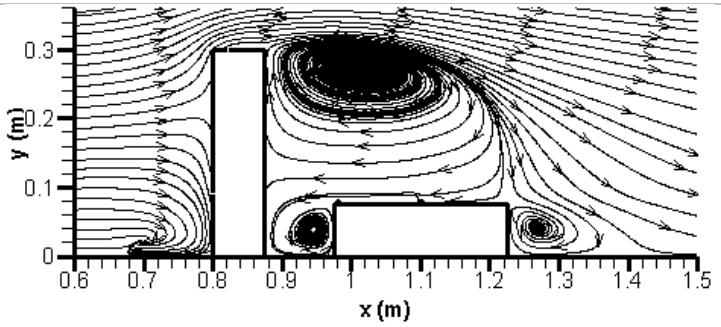

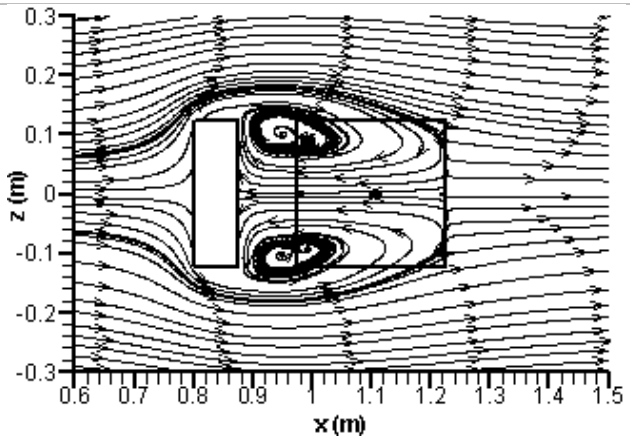

J-3(a) uh4 upstream of b1

J-3(b) Middle elevation plane, z=0 (m)

J-3(c) Horizontal plane at y=0.08(m)

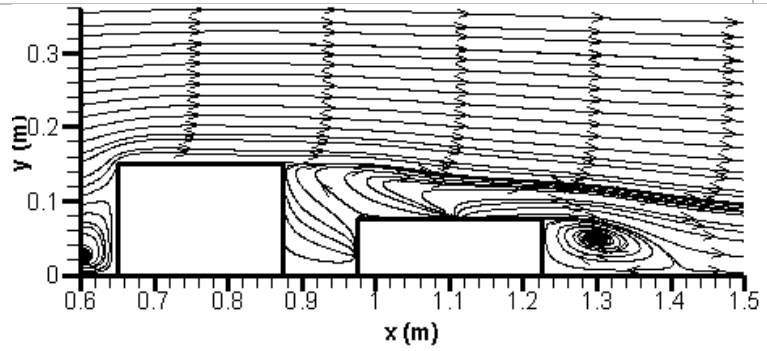

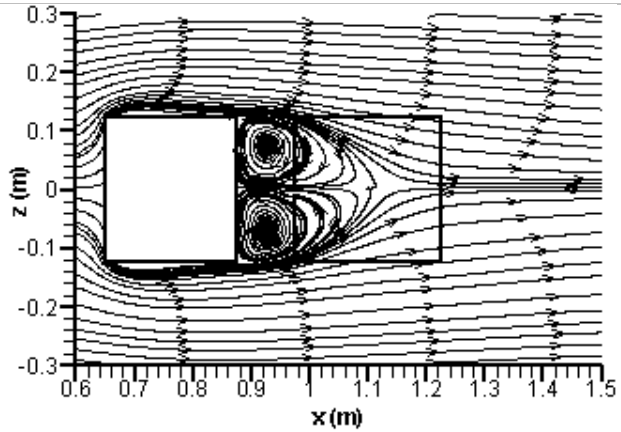

J-4(a) ul3 upstream of b1

J-4(b) Middle elevation plane, z=0 (m)

J-4(c) Horizontal plane at y=0.08(m)

	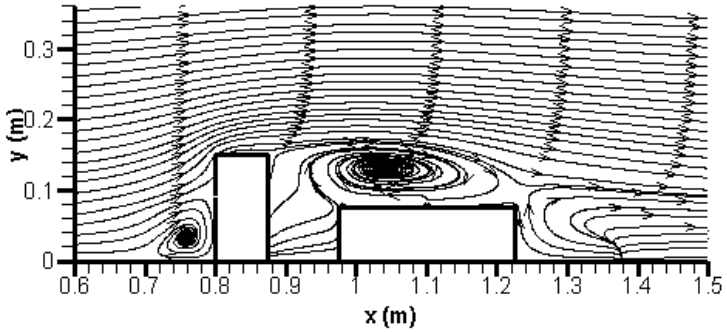	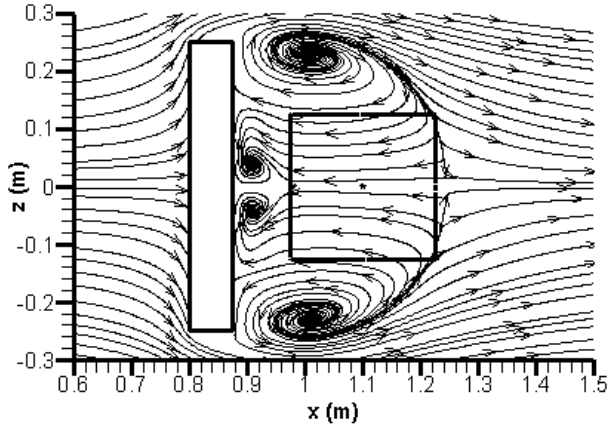
J-5 (a) uw4 upstream of b1	**J-5 (b) Middle elevation plane, z=0 (m)**	**J-5 (c) Horizontal plane at y=0.08(m)**
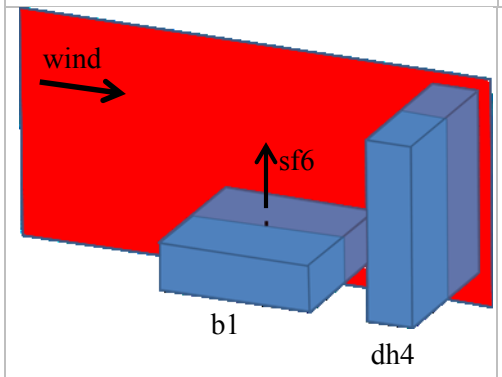	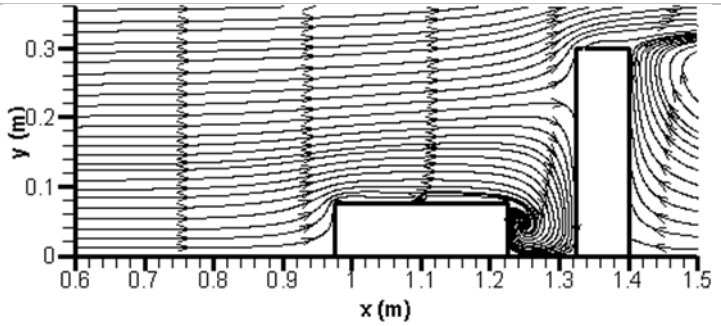	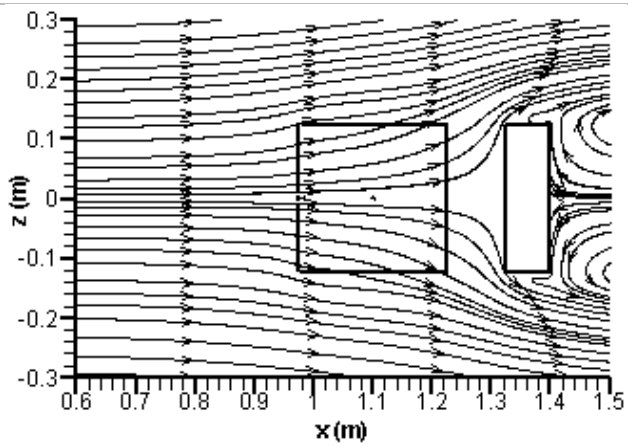
J-6 (a) dh4 downstream of b1	**J-6 (b) Middle elevation plane, z=0 (m)**	**J-6 (c) Horizontal plane at y=0.08(m)**

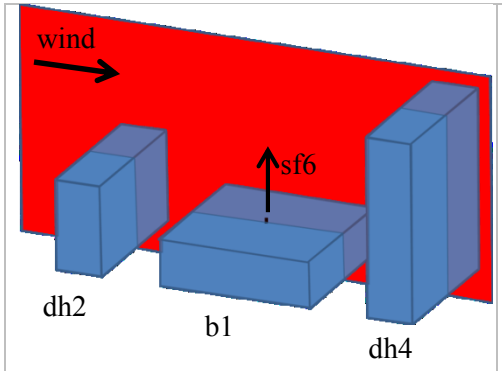

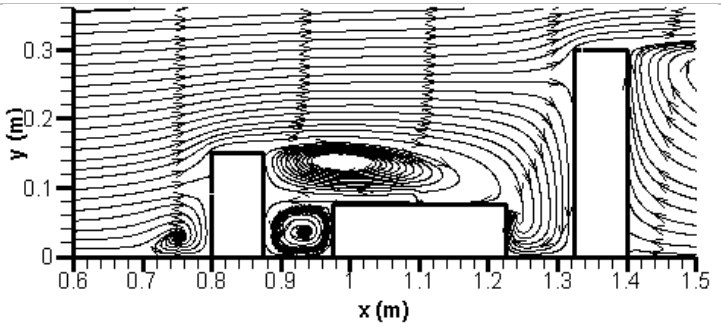

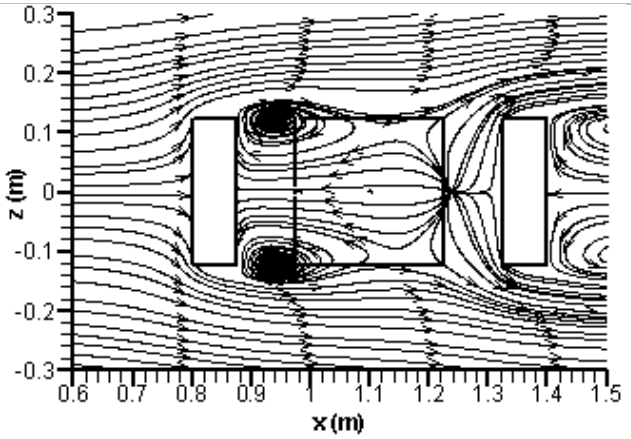

J-7 (a) uh2 upstream and dh4 downstream of b1

J-7 (b) Middle elevation plane, z=0 (m)

J-7 (c) Horizontal plane at y=0.08(m)

APPENDIX K: ISO-SURFACE OF $D_N = 6$ (EQUIVALENT TO DILUTION $D_R = 3000$)

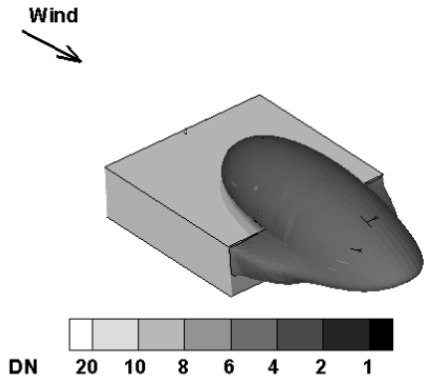

K-1. Reference case: Isolated building

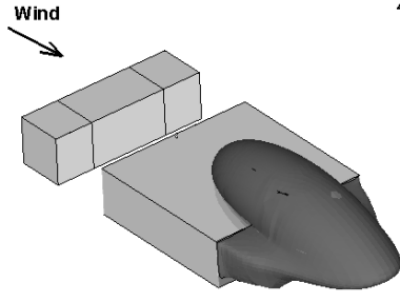

Case uh1, spacing = 0.1m (20m)

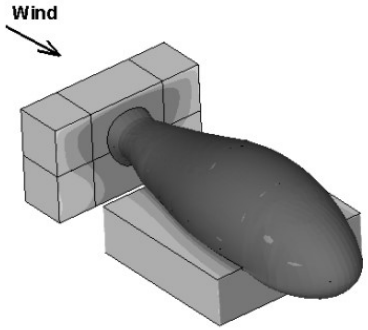

Case uh2, spacing = 0.1m (20m)

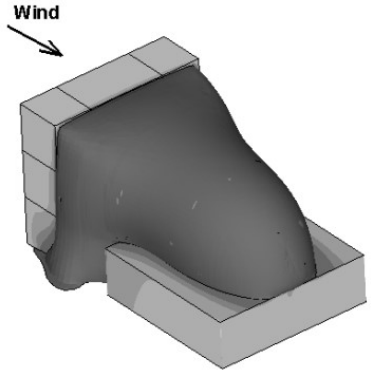

Case uh3, spacing = 0.1m (20m)

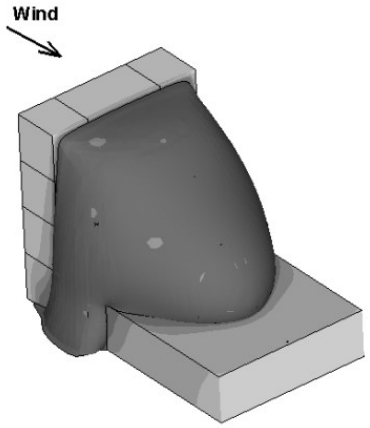

Case uh4, spacing = 0.1m (20m)

K-2. Effect of upstream building height

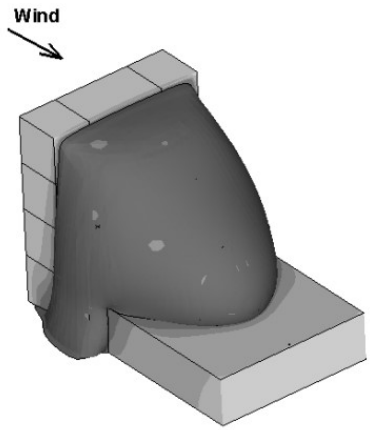

Case uh4, spacing = 0.1m (20m)

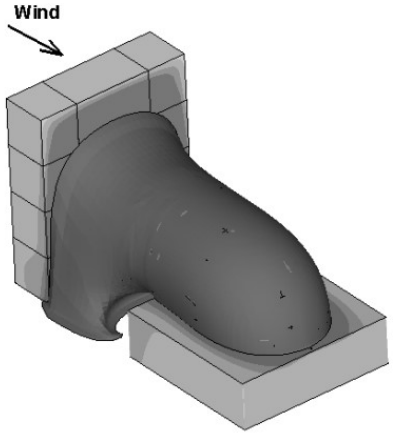

Case uh4, spacing = 0.175m (35m)

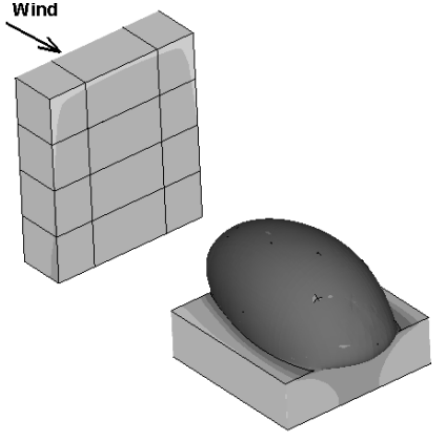

Case uh4, spacing = 0.25m (50m)

K-3. Effect of spacing between b1 and upstream building uh4

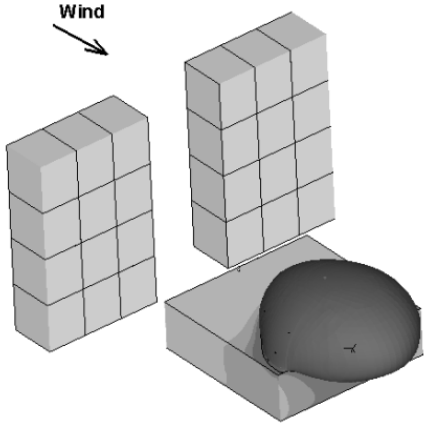

K-4. Effect of two upstream buildings of b1

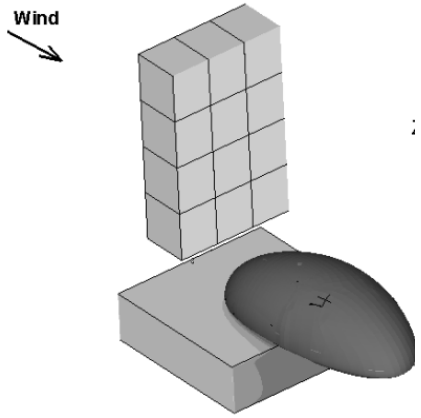

K-5. Effect of an upstream building shifted to the right

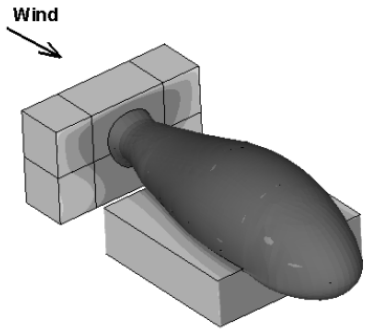

Case ul1, spacing = 0.1m (20m)

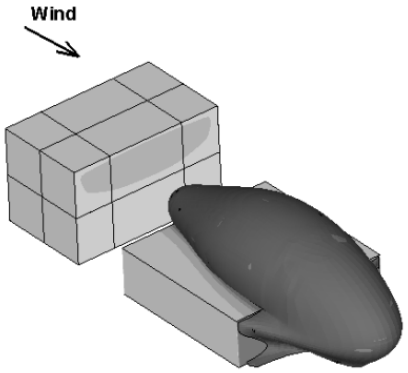

Case ul2, spacing = 0.1m (20m)

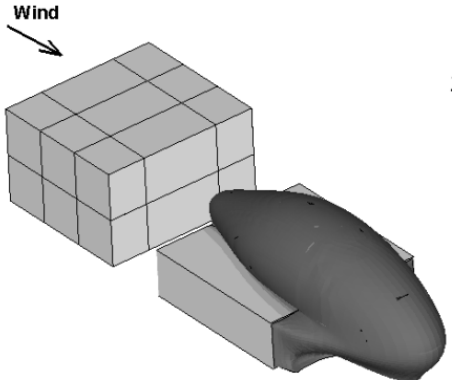

Case ul3, spacing = 0.1m (20m)

K-6. Effect of upstream building length

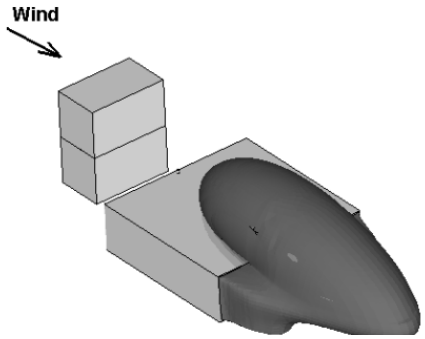

Case uw1, spacing = 0.1m (20m)

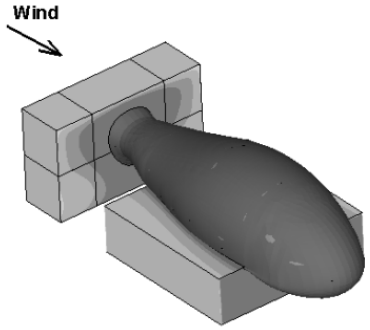

Case uw2, spacing = 0.1m (20m)

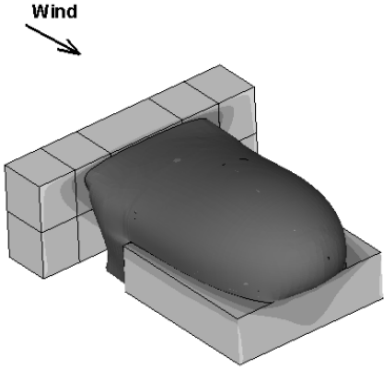

Case uw3, spacing = 0.1m (20m)

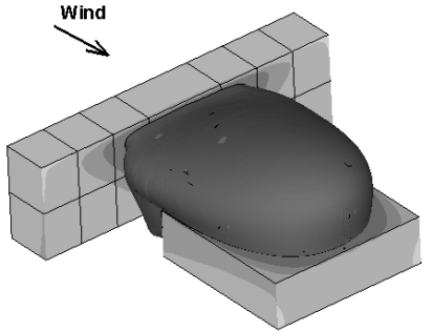

Case uw4, spacing = 0.1m (20m)

K-7. Effect of upstream building width

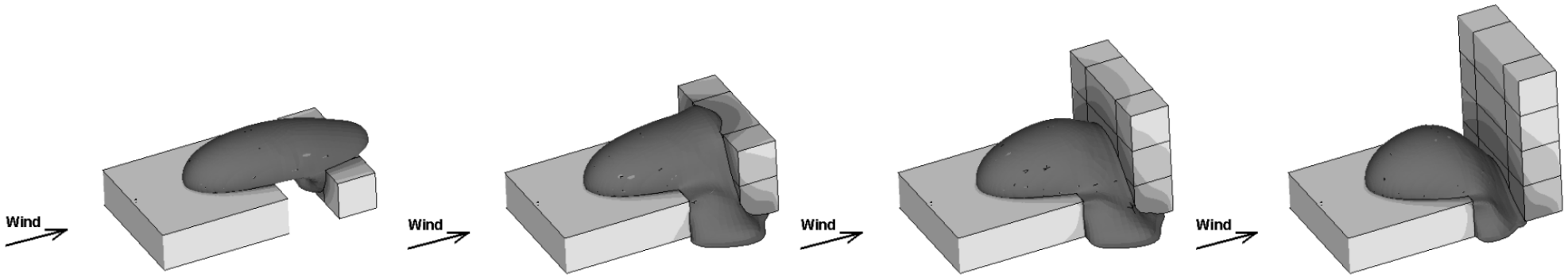

Case dh1, spacing = 0.1m (20m) Case dh2, spacing = 0.1m (20m) Case dh3, spacing = 0.1m (20m) Case dh4, spacing = 0.1m (20m)

K-8. Effect of downstream building height

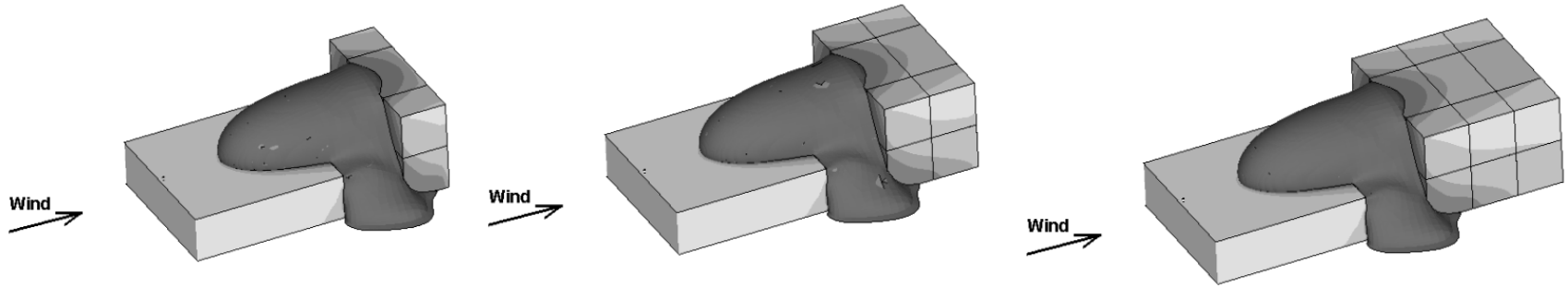

Case dl1, spacing = 0.1m (20m) Case dl2, spacing = 0.1m (20m) Case dl3, spacing = 0.1m (20m)

K-9. Effect of downstream building length

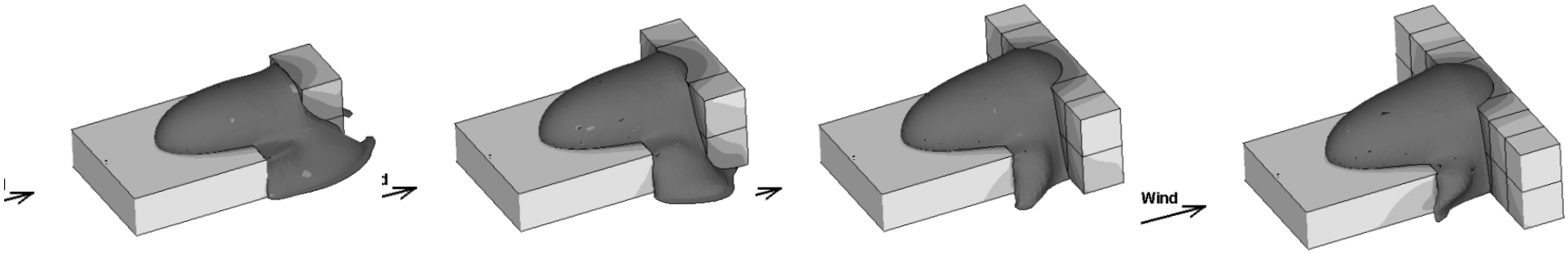

Case uw1, spacing = 0.1m (20m) Case uw2, spacing = 0.1m (20m) Case uw3, spacing = 0.1m (20m) Case uw4, spacing = 0.1m (20m)

K-10. Effect of downstream building width

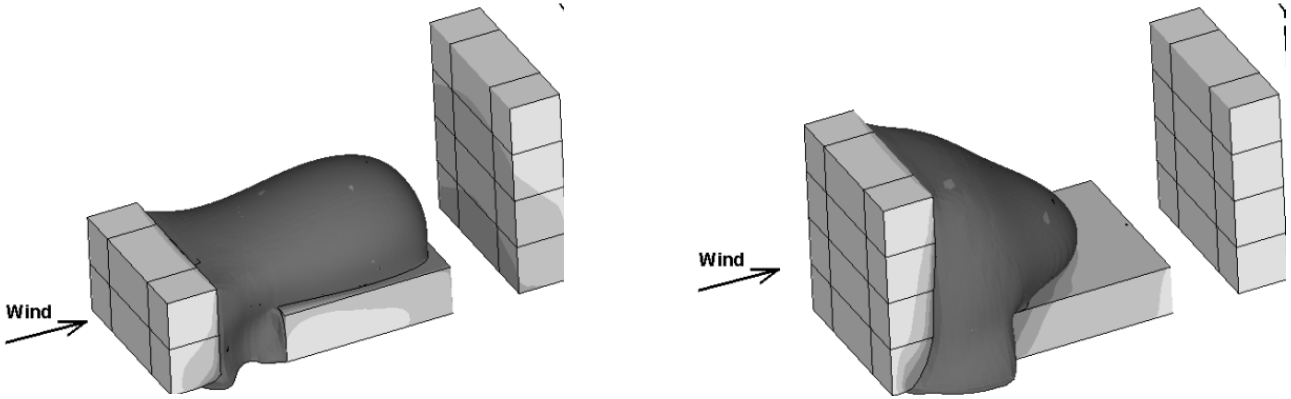

Case uh2dh4, spacing = 0.1 (20m) Case uh4dh4, spacing = 0.1m (20m)

K-11. Effect of placing b1 between two buildings